

# Patterns of Dust-borne Iron Fertilization at the Last Glacial Maximum

Master Thesis

Under the supervision of  
Prof. Martin Claußen,  
University of Hamburg and Max-Planck-Institute for Meteorology  
and  
Prof. Markus Jochum,  
Physics of Ice, Climate and Earth, Niels-Bohr-Institute, Copenhagen University

21/12/2020

**Lara Möllney**

---

lara.moellney@studium.uni-hamburg.de

M.Sc. Meteorology

Matr.-No. 6672209

Topic: Patterns of Dust-borne Iron Fertilization at the Last Glacial Maximum

Mother fountain of all the waters of the world.

*Hamlet's Mill: An Essay Investigating the Origins of Human Knowledge and Its Transmission Through Myth, Giorgio de Santillana and Hertha Von Dechend*

# Abstract

Dust-borne iron fertilization of the glacial ocean has been proposed as one key factor to explain the 80 to 100 ppm lower atmospheric CO<sub>2</sub> concentration at the Last Glacial Maximum (LGM) compared to the late Holocene. This thesis studies the underlying biogeochemical and physical mechanisms in the glacial ocean that determine regionally diverse response patterns to increased atmospheric deposition of iron, especially in light of uncertain LGM dust fluxes. While the complexity of implemented marine biogeochemistry increased, previous modelling studies have failed to take an integrated Earth system view, simplifying or fully neglecting atmosphere and land components. Furthermore, the vast majority of studies that consider uncertainties in dust-borne iron, concentrate on the Southern Ocean (SO) only.

Shifting from an ocean-only modelling perspective and extending the evaluation of the SO's iron sensitivity to the global ocean, this thesis employs the fully coupled biogeochemistry-enabled Community Earth System Model (CESM) and compares the standard LGM simulation (LGMstd) with a sensitivity experiment where aeolian dust fluxes are quintupled globally (LGM5i).

Elevated atmospheric iron deposition in LGM5i further enhances export production in the SO, leading to nutrient trapping and transfer of nutrients to the deep ocean. As a consequence, macro-nutrients are lacking in the global upper ocean north of 30 °S and let marine productivity decrease, most markedly in the North Atlantic. Elevated phytoplankton activity in the SO and in generally macro-nutrient rich regions of the Pacific Ocean outweigh declining export production elsewhere, increasing global carbon export by ~5%. However, nutrient deficiencies in large areas of the global ocean indicate an upper bound to the effect of iron fertilization on glacial CO<sub>2</sub> drawdown.

The crucial role of the SO as a major nutrient provider to the global ocean does not only challenge the idea of large-scale ocean fertilization as a remedy to anthropogenic climate change but can also have serious implications on future trends of marine productivity resulting from global warming induced changes to SO export production.

# Table of Contents

<b>1</b>	<b>Introduction</b>	<b>1</b>
<b>2</b>	<b>Theoretical Background</b>	<b>4</b>
2.1	Marine Biogeochemistry & Oceanic Circulation in the Global Ocean . . .	4
2.1.1	The Soft Tissue Pump . . . . .	4
2.1.2	Biogeochemical Nutrient Cycles . . . . .	5
2.1.3	Global Ocean Circulation and Macro-Nutrient Patterns . . . . .	8
2.1.4	Marine Iron Biogeochemistry . . . . .	11
2.2	The Last Glacial Maximum . . . . .	12
2.2.1	Changes to Ocean Circulation and the Soft Tissue Pump . . .	13
2.2.2	Iron Fertilization during the LGM . . . . .	14
<b>3</b>	<b>Methods</b>	<b>20</b>
3.1	Model Description . . . . .	20
3.1.1	The Community Earth System Model . . . . .	20
3.1.2	The Ocean Biogeochemistry Module . . . . .	21
3.2	Experimental Setup . . . . .	24
3.2.1	The Pre-Industrial Control Simulation . . . . .	24
3.2.2	The Standard LGM Simulation . . . . .	25
3.2.3	LGM Sensitivity Analysis: Imposing Increased Iron . . . . .	25
<b>4</b>	<b>Results</b>	<b>28</b>
4.1	Global Export Production and Iron Limitation . . . . .	29
4.2	Global Subsurface Macro-Nutrient Patterns . . . . .	33
4.3	Zonal Depth Transects of Macro-Nutrients . . . . .	38
4.4	Nutrient Distributions per Ocean Basin . . . . .	40
4.5	Limiting Nutrient and Population Shifts under Enhanced Iron Fluxes	43
<b>5</b>	<b>Discussion</b>	<b>46</b>
5.1	Comparison with Other Model Studies . . . . .	46
5.2	Comparison with Reconstructed Marine Productivity . . . . .	49
5.3	Model Limitations . . . . .	53
5.3.1	Physical Model . . . . .	53
5.3.2	Macro-Nutrient Cycles . . . . .	54

## TABLE OF CONTENTS

---

5.3.3 Marine Iron Biogeochemistry . . . . .	56
<b>6 Conclusion</b>	<b>61</b>
<b>Appendix</b>	<b>87</b>
<b>Versicherung an Eides statt</b>	<b>99</b>

# Abbreviations

<b>AABW</b>	Antarctic Bottom Water	<b>MOC</b>	Meridional Overturning Circulation
<b>AAIW</b>	Antarctic Intermediate Water	<b>NADW</b>	North Atlantic Deep Water
<b>ACC</b>	Antarctic Circumpolar Current	<b>NPIW</b>	North Pacific Intermediate Water
<b>BEC</b>	Ocean Biogeochemistry Module	<b>NPP</b>	Net Primary Production
<b>BP</b>	before present	<b>OGCM</b>	Ocean General Circulation Model
<b>CCSM4</b>	Community Climate System Model 4	<b>OMZ</b>	Oxygen Minimum Zone
<b>CESM</b>	Community Earth System Model	<b>PAR</b>	Photosynthetically Available Radiation
<b>DIC</b>	Dissolved Inorganic Carbon	<b>PFT</b>	Plankton Functional Type
<b>DOM</b>	Dissolved Organic Matter	<b>PI</b>	pre-industrial
<b>EP</b>	Carbon Export at 100 m Depth	<b>POC</b>	Particulate Organic Carbon
<b>ESM</b>	Earth System Model	<b>POM</b>	Particulate Organic Matter
<b>HNLC</b>	High-Nutrient Low-Chlorophyll	<b>POP</b>	Parallel Ocean Program
<b>LGM</b>	Last Glacial Maximum	<b>PRE</b>	pre-industrial CESM simulation
<b>LGMstd</b>	standard LGM simulation	<b>SAMW</b>	Subantarctic Mode Water
<b>LGM5i</b>	LGM simulation with 5x aeolian dust	<b>SO</b>	Southern Ocean
<b>MARBL</b>	Marine Biogeochemistry Library	<b>SST</b>	Sea Surface Temperature

# List of Figures

2.1	Schematic of the global overturning circulation. . . . .	9
2.2	Schematics of the structure of the global MOC in the LGM and modern times. . . . .	14
4.1	Timeseries of global EP in LGM5i and LGMstd. . . . .	30
4.2	Global map of EP in LGMstd and LGM5i in the 3680s. . . . .	30
4.3	Global map of EP anomaly (dEP) in the 3010s and 3680s. . . . .	31
4.4	Global map of diatom Fe limitation immediately before and 10 years after increase in dust flux. . . . .	31
4.5	Difference dEP(3680s)-dEP(3010s) globally and zonally integrated. . . . .	32
4.6	Global map of dEP and macro-nutrient thermocline concentration anomalies in the 3000s, and difference of 3100s and 3200s to 3000s. . . . .	34
4.7	Global map of mean upper ocean diazotrophic C fixation from NO <sub>3</sub> . Difference between LGM5i 3000s and 3100s to LGMstd 2990s. . . . .	37
4.8	Zonal mean PO <sub>4</sub> concentration in LGM5i, in the 3000s, and difference of 3100s and 3200s to 3000s. Mean PO <sub>4</sub> in the SO and in the Deep Ocean north of the SO. . . . .	39
4.9	Percentage changes in PO <sub>4</sub> concentration in LGM5i in different depths. Relative change between 3300s and 3000s per ocean basin. . . . .	41
4.10	PO <sub>4</sub> concentration in depth transects of the Atlantic, Southern and Pacific Ocean. LGM5i results in the 3000s, difference of 3200s and 3680s to 3000s. . . . .	42
4.11	Most limiting nutrient to diatom growth in LGMstd and LGM5i in the 3200s. . . . .	44
5.1	Global map of simulated export production in Oka et al. (2011). . . . .	47
5.2	Global map of simulated export production in Muglia et al. (2017). . . . .	48
5.3	Reconstructions of C export in marine sediment cores, comparison of LGM to late Holocene. . . . .	50
5.4	Global map of changes in export production in LGMstd and LGM5i compared to PRE in the 3680s and multi-proxy based reconstructions. . . . .	51
A.1	Global map of diazotroph N <sub>2</sub> fixation anomaly in the 3000s, difference of 3100s and 3680s to 3000s. . . . .	87

## LIST OF FIGURES

---

A.2	Global map of mean thermocline $\text{PO}_4$ and $\text{NO}_3$ concentration anomaly in the 3100s and 3680s. . . . .	88
A.3	Global map of $\text{SiO}_3$ concentration anomaly, mean over 200 to 1000 m depth and mean over 1000 to 2000 m depth, in the 3100s and 3680s. . . . .	88
A.4	Zonal mean $\text{O}_2$ in the Pacific in LGMstd and LGM5i in the 3000s, difference of 3100s, 3200s and 3680s to 3000s. . . . .	89
A.5	Global map of phytoplankton C fixation from $\text{NO}_3$ in LGM5i in the 3000s, 3100s and 3200s. . . . .	90
A.6	Global map of diazotroph Fe limitation and $\text{N}_2$ fixation in LGM5i 3100s, difference to LGMstd 2990s. . . . .	91
A.7	Most limiting nutrient to diazotroph growth in LGMstd and LGM5i in the 3200s. . . . .	91
A.8	Most limiting nutrient to small phytoplankton growth in LGMstd and LGM5i in the 3200s. . . . .	91
A.9	Zonal mean $\text{PO}_4$ concentration in LGMstd and LGM5i, in the 3000s and difference of 3100s, 3200s and 3680s to 3000s. . . . .	92
A.10	Zonal mean $\text{NO}_3$ concentration in LGM5i in the 3000s and difference of 3100s, 3200s and 3680s to 3000s. . . . .	93
A.11	Zonal mean $\text{SiO}_3$ concentration in LGM5i in the 3000s and difference of 3100s, 3200s and 3680s to 3000s. . . . .	94
A.12	Zonal mean $\text{NO}_3$ concentrations in depth transects of the Atlantic, Southern and Pacific Ocean. LGM5i results in the 3000s, difference of 3200s and 3680s to 3000s. . . . .	95
A.13	Zonal mean $\text{SiO}_3$ concentrations in depth transects of the Atlantic, Southern and Pacific Ocean. LGM5i results in the 3000s, difference of 3200s and 3680s to 3000s. . . . .	96
A.14	Global map of PAR in LGMstd and LGM5i in the 3100s. . . . .	96
A.15	Global map of phytoplankton biomass anomaly in the 3000s, 3100s and 3680s. . . . .	97
A.16	Global map of phytoplankton C fixation from $\text{NO}_3$ in the 3680s. Difference of LGMstd and LGM5i to PRE. . . . .	98
A.17	Global map of diazotrophic N fixation in the 3680s. Difference of LGMstd and LGM5i to PRE. . . . .	98

# List of Tables

2.1	Modelling studies of the iron fertilization hypothesis during the LGM.	18
3.1	BEC PFT growth factors and Redfield ratios. . . . .	22

# 1 Introduction

The Last Glacial Maximum (LGM) is the period during the most recent major glaciation when global ice sheets reached their maximum extent, peaking at around 21,000 years before present (BP) (Mix et al. 2001). Vast ice cover, decreased temperatures and a lower sea level characterise the LGM (Clark et al. 2009, Annan and Hargreaves 2013). Atmospheric carbon dioxide ( $\text{CO}_2$ ) concentrations were relatively stable at  $\sim 190$  ppm compared to 280 ppm in pre-industrial times (Schmitt et al. 2012). Since the first ice core measurements revealed this significant glacial-interglacial difference in the 1980s (Delmas et al. 1980, Neftel et al. 1982), research has centred around solving this  $\text{CO}_2$  enigma.

Martin (1990) hypothesised lower  $\text{CO}_2$  levels to be the result of relieved iron (Fe) limitation at the LGM that fuelled biological production by phytoplankton and thus  $\text{CO}_2$  sequestration. This theory was based on iron fertilization experiments in the subarctic Pacific Ocean that led to locally enhanced marine productivity (Martin and Fitzwater 1988). Besides the macro-nutrients nitrogen (N) and phosphorus (P), phytoplankton growth depends on vitamins and micro-nutrients, such as Fe (Moore et al. 2013b). In the modern ocean, N is the main limiting nutrient to phytoplankton growth, except for the SO, the subarctic North and the eastern equatorial Pacific Ocean where N and other necessary macro-nutrients are abundant but Fe deficiencies limit phytoplankton growth (Moore et al. 2013b). These so-called High-Nutrient Low-Chlorophyll (HNLC) regions with currently low Fe levels have been proposed as the key areas of additional glacial  $\text{CO}_2$  sequestration (Martin et al. 1991).

At the LGM, Fe limitation was relieved by atmospheric deposition of wind-borne mineral aerosols, hereafter referred to as dust (Martin 1990). Simultaneous with increasing evidence of 80 to 100 ppm lower atmospheric  $\text{CO}_2$  at the LGM, ice core analysis revealed substantial increases in glacial dust fluxes in Greenland and Antarctica (Hammer et al. 1985, Petit et al. 1981). While these findings were locally constrained, more recent research suggests a high correlation of interhemispheric dust fluxes, indicating climate-related changes in dust flux may have changed globally (Winckler et al. 2008). Global-scale interpolated dust fluxes were on average 4

times higher in the LGM than during the Holocene (Lambert et al. 2015), supporting the theory that glacial changes to the global Fe inventory have played a vital role in reducing atmospheric CO<sub>2</sub>.

The global magnitude of the effect, however, remains under-constrained with estimates ranging from a 40 ppm CO<sub>2</sub> drawdown (Watson et al. 2000) to only one tenth of the upper bound, 4 ppm, in Muglia et al. (2017). From early box models (e.g. Lefèvre and Watson 1999, Watson et al. 2000) to Earth System Models (ESMs) of intermediate complexity (e.g. Brovkin et al. 2007, Bouttes et al. 2011) to global ocean biogeochemistry models coupled to a single-level atmosphere (e.g. Oka et al. 2011, Lambert et al. 2015) – evolving knowledge on ocean biogeochemical cycles and the interplay of ocean dynamics and marine productivity fuelled a large body of research. Despite these efforts, uncertainties concerning the scale of atmospheric Fe deposition and its fertilization effect on regional to global scales persist. Furthermore, no published study so far has employed a coupled Earth System Model simulating the dynamic interactions of biospheric dust mobilisation, aeolian transport and ocean biogeochemical response, and its effect on atmospheric CO<sub>2</sub>.

In this thesis, simulations of the Community Earth System Model (CESM), including coupled atmosphere, land, ocean and sea ice components, are used to study the effect of marine iron fertilization at the LGM. In line with previous research (e.g. Muglia et al. 2017, Yamamoto et al. 2019), a standard LGM simulation (LGMstd) is complemented by a sensitivity simulation where aeolian dust fluxes are increased fivefold after 3000 simulation years (LGM5i). This does not only allow to study the effect of uncertainties in atmospheric deposition and Fe bioavailability on phytoplankton growth. It further permits to analyse the temporal evolution of marine productivity, i.e. the short and long-term effects, under relieved Fe stress in an idealised set-up. I will evaluate the export of Particulate Organic Carbon (POC) out of the surface ocean, also called ‘export production’, as a suitable measure for marine productivity, or rather the effect of changes in phytoplankton growth on CO<sub>2</sub> sequestration.

Based on these simulations the thesis will answer the following guiding questions:

1. What is the temporal relationship between increases in dust-borne Fe input and export production?
2. How do macro-nutrient patterns respond to changes in export production, globally and at basin-scale?
3. Which processes act to reduce/enhance export production on short and longer

---

timescales, and how do these mechanisms explain diverging spatial responses?

Understanding the underlying biogeochemical and physical processes that control marine carbon (C) uptake in the LGM ocean is crucial to constrain the magnitude of glacial iron fertilization, develop theories on future global warming induced changes to marine productivity and evaluate deliberate ocean fertilization which is regularly proposed as a means to mitigate anthropogenic climate change (Harrison 2017, Yoon et al. 2018, Emerson 2019).

The thesis commences with a description of marine biogeochemistry and its interaction with physical ocean dynamics, followed by a brief characterisation of the LGM and associated changes in the glacial ocean. The iron fertilization hypothesis is introduced and its analysis in proxy-based reconstructions and model studies is reviewed (Chapter 2). Chapter 3 summarises the methodological approach including a description of the CESM and its Ocean Biogeochemistry Module (BEC) as well as the performed simulations. Resulting modelled export production, nutrient distributions and limiting factors to phytoplankton growth are analysed (Chapter 4) and discussed against the background of recent modelling studies, marine sediment based reconstructions and model limitations (Chapter 5). The thesis concludes with a summary of the main findings and an outlook on desirable model improvements and potential future research questions (Chapter 6).

## 2 Theoretical Background

Analysing iron fertilization of phytoplankton as a means to have bound excess C during the LGM requires a sound understanding of the underlying biological, chemical and physical processes (Section 2.1). How do the biogeochemical cycles of C and nutrients interact and what role does global ocean circulation play? Section 2.2 revolves around these mechanisms against the background of an altered LGM climate with a special focus on the iron fertilization hypothesis. What evidence do palaeorecords provide for this theory (Section 2.2.2.1)? How has an increasing body of model studies advanced our knowledge of its global magnitude (Section 2.2.2.2)?

### 2.1 Marine Biogeochemistry & Oceanic Circulation in the Global Ocean

#### 2.1.1 The Soft Tissue Pump

The marine C cycle is often conceptualised as the interaction of three ‘pumps’ determining ocean C storage: the ‘solubility pump’, the ‘carbonate pump’ and the ‘soft tissue pump’ (Volk and Hoffert 1985). The solubility pump accounts for the strongly temperature dependent solubility of CO<sub>2</sub> which increases with increasing Sea Surface Temperature (SST). The carbonate pump affects C storage via the production of calcium carbonate (CaCO<sub>3</sub>) and its subsequent transport to depth. While all three mechanisms provide explanations for present-day as well as glacial marine C sequestration, it is the soft tissue pump that is of particular importance with regard to iron fertilization.

The soft tissue pump describes the process of surface ocean C fixation by phytoplankton and subsequent downward flux in the form of POC (Volk and Hoffert 1985). In the euphotic zone, i.e. the subsurface ocean receiving sufficient sunlight for photosynthesis to occur, dissolved CO<sub>2</sub> is transformed into POC via biological production by phytoplankton. Net Primary Production (NPP), i.e. photosynthetic C fixation less the respiratory release of CO<sub>2</sub>, is driven by CO<sub>2</sub>, temperature and light as well

## 2.1. MARINE BIOGEOCHEMISTRY & OCEANIC CIRCULATION IN THE GLOBAL OCEAN

---

as the availability of macro- and micro-nutrients (Finkel 2014). During photosynthesis, the colour pigment chlorophyll acts as a photoreceptor, absorbing sunlight and converting it into the energy required for growth. Chlorophyll concentration as an easily observable quantity, via remote sensing, in situ measurements and discrete sampling, is often used as a proxy for observed phytoplankton primary productivity (e.g. Felip and Catalan 2000, Huot et al. 2007). While these microorganisms exhibit an extreme diversity (Beardall et al. 2009), common classification distinguishes between larger diatoms, N-fixing diazotrophs, calcifying coccolithophores and small or pico-phytoplankton (Dutkiewicz et al. 2020).

Most of the organic C produced in the upper ocean re-enters the C cycle through heterotrophic respiration by zooplankton and bacteria. Only a small fraction of organic C fixed through NPP is exported into deeper waters where it remineralizes or – if escaping remineralization – is buried in the sediments. This flux of sinking POC, also called ‘export production’, is responsible for CO<sub>2</sub> sequestration on decadal to millennial timescales, depending on its path (Hain et al. 2014).

### 2.1.2 Biogeochemical Nutrient Cycles

As mentioned above, phytoplankton’s biological productivity in the upper ocean depends on the availability of nutrients, namely the macro-nutrients nitrogen (N), phosphorus (P) and silicon (Si) as well as various micro-nutrients, such as Fe, cobalt and manganese (Moore et al. 2013b). The distribution of these nutrients in the ocean is governed by biogeochemical as well as physical processes. Nutrients are transformed between inorganic and organic, dissolved and particulate forms via biological and chemical mechanisms. Vertical and horizontal physical transport and mixing redistribute nutrients on local to global scales (Williams and Follows 2003).

In the following, I will briefly describe the biogeochemical cycles of N, P and Si individually before summarising the main mechanisms of vertical and horizontal transport applying to all of them. The Section will be concluded by a conceptualisation of marine Fe cycling.

#### 2.1.2.1 Nitrogen

The marine N cycle is one of the most complex biogeochemical cycles due to its presence in various oxidation stages, ranging from NH<sub>4</sub><sup>+</sup> to NO<sub>3</sub><sup>-</sup>, and their multiple interactions (Zehr and Kudela 2011). The major sources of fixed N, i.e. N that is bioavailable to marine organisms, are biological nitrogen gas (N<sub>2</sub>) fixation and atmospheric deposition (Pajares and Ramos 2019). The conversion of dissolved

$\text{N}_2$  into bioavailable N by diazotrophs is the only biotic process contributing N to the ocean. In balance with the major sink processes, denitrification and anaerobic ammonium ( $\text{NH}_4$ ) oxidation, it determines to first order the bioavailable N inventory of the ocean (Gruber 2008). Retention of fixed N through nitrification, anaerobic respiratory ammonification and N assimilation transforms N species between its different oxidation states (Pajares and Ramos 2019).

Dissolved inorganic N – nitrate ( $\text{NO}_3$ ), nitrite and  $\text{NH}_4$  – is assimilated by primary producers, such as phytoplankton, algae and bacteria, and thus plays a vital role for the efficiency of the soft tissue pump (Gruber 2008). N is essential for phytoplankton growth and in the modern ocean often in short supply relative to other nutrients (Moore et al. 2013b). Photosynthetically fixed N befalls the same fate as organic C: most of it is either respired or remineralized in the euphotic zone. A smaller fraction escaping remineralization is exported into the deeper ocean where it remineralizes or is incorporated into sediments (Zehr and Kudela 2011). If transported back to the euphotic zone, remineralized inorganic N re-enters the cycle of phytoplankton growth and decay (Gruber 2008).

The majority of fixed N exists in the form of  $\text{NO}_3$ , with nitrite and  $\text{NH}_4$  making up only a tiny fraction of bioavailable N. Despite the  $\text{NH}_4$  inventory being about three orders of magnitude smaller than  $\text{NO}_3$ , it is a critical component of the upper ocean N cycle (Gruber 2008). Because of its short turn-over time of weeks to months,  $\text{NH}_4$  is not suitable for the analysis of the global distribution of fixed N in the upper and deep ocean. Instead, measurement campaigns of marine  $\text{NO}_3$  concentrations have shed light on the interaction of biogeochemical cycling and large-scale oceanic transport (see Section 2.1.3).

### 2.1.2.2 Phosphorus

Phosphorus in the form of orthophosphate ( $\text{PO}_4$ ), in the following simply referred to as phosphate, plays a key role in photosynthesis. Unlike N, P cannot be fixed from the atmosphere but is mainly transported into the ocean in its particulate and dissolved phases via rivers or deposited through aerosols, volcanic ash and dust (Paytan and McLaughlin 2007).

P occurs in both particulate and dissolved, organic and inorganic forms with the driver of biological productivity,  $\text{PO}_4$ , generally in the form of dissolved inorganic P.  $\text{PO}_4$  is assimilated by phytoplankton and, like C or N, transformed into organic compounds. Phytoplankton decay and zooplankton excretion release dissolved inorganic and organic P back to the ocean, where it either re-enters the cycle through

## 2.1. MARINE BIOGEOCHEMISTRY & OCEANIC CIRCULATION IN THE GLOBAL OCEAN

---

assimilation by phytoplankton or bacteria or adsorbs to sinking particulate organic matter. The main sink of P is the deposition and burial of its particulate forms in marine sediments (Paytan and McLaughlin 2007).

### 2.1.2.3 Silicon

Silicon has not received the same attention as N and P during the 20<sup>th</sup> century despite being strongly intertwined with their cycles as it is required for diatom growth (Tréguer and Rocha 2013). Marine input of dissolved silicic acid, ultimately supplied by chemical weathering, includes continental, aeolian, hydrothermal and marine sediment sources. In the euphotic layer, siliceous organisms, such as diatoms, use silicic acid to build shells of biogenic silica. A fraction of this so-called opal is directly recycled in the upper ocean, while the remainder is exported to the deep ocean (Tréguer and Rocha 2013). Subsequent regeneration of silicic acid from less labile biogenic silica takes place at greater depths than remineralization of Particulate Organic Matter (POM) from other major nutrients. Non-remineralized silica is permanently removed from the water column via burial in marine sediments (Rocha 2007).

The uptake of dissolved Si by phytoplankton does not only depend on the availability of silicic acid but is also very sensitive to Fe concentrations. Under conditions of Fe limitation, diatoms' consumption of silicic acid increases substantially, although at slower growth rates (Rocha et al. 2000, Leynaert et al. 2004). This close link between Si and Fe biogeochemistry is especially relevant against the background of glacial relieve of Fe limitation. Antarctic waters that are Si depleted today might have been silicic acid rich at the LGM (Brzezinski et al. 2002). Northward transport of excess silicate ( $\text{SiO}_3$ ) to lower latitudes, also termed 'silicic acid leakage', could have enhanced diatom production outside the SO at the expense of coccolithophores (Matsumoto et al. 2002). Subsequent changes in the ratio of  $\text{CaCO}_3$  to POC supply to the sea floor could have affected the burial of C in deep sea sediments via changes in ocean alkalinity (Archer and Maier-Reimer 1994). A decrease in the  $\text{CaCO}_3$ :POC rain ratio due to the relative increase of  $\text{SiO}_3$  fuelled diatom growth could have increased atmospheric  $\text{CO}_2$  sequestration by increasing seawater alkalinity (Archer and Maier-Reimer 1994, Brzezinski et al. 2002). More recent studies, however, indicate that this mechanism did not affect biological C uptake significantly (Kienast et al. 2006, Hendry et al. 2016, Hendry et al. 2020).

#### 2.1.2.4 The Redfield Ratio

Carbon and nutrient cycles are closely interwoven: changes to the distribution of bioavailable nutrients strongly influence the efficiency of the soft tissue pump, which in turn affects the export of nutrients into the deeper ocean and its subsequent transport. In his pioneering work, Alfred Redfield (1934, 1958) discovered that phytoplankton contain the three elements C, N and P in a remarkably fixed atomic ratio of  $\sim 105 : 16 : 1$  across depths and ocean basins.

In the past 80 years, this constant elemental stoichiometry has been revisited in a multitude of studies showing, i.a. that it varies by phytoplankton type or under conditions of nutrient limitation (Moreno and Martiny 2018). However, the overall consistency of the ratio as an average over the time and spatial scales of the global ocean has been confirmed (“Eighty years of Redfield” 2014). The Redfield ratio is widely used in models of marine biogeochemistry, partially refined by e.g. phenotypical differentiation or amended by other nutrients, such as Si or Fe (e.g. Moore et al. 2013a, Ilyina et al. 2013, Stock et al. 2014).

### 2.1.3 Global Ocean Circulation and Macro-Nutrient Patterns

While chemical and biological properties of the major nutrients differ, the main mechanisms of vertical and horizontal flux apply to all of them. In the euphotic zone, inorganic nutrients are consumed and converted into organic matter of which a small amount is then exported to the deeper ocean via gravitational settling of particles and subduction of Dissolved Organic Matter (DOM). As a consequence of subsequent remineralization, inorganic nutrients accumulate at depth, enriching deep waters that are essential for the physical supply of nutrients to the upper ocean (Williams and Follows 2003).

Traditionally, vertical mixing through advection, diffusion and convection has been considered the main mechanism of physical supply of nutrients. While this holds true for upwelling regions, the diapycnal diffusivity outside these regions is not high enough to explain the vertical nutrient distributions (Freilich and Mahadevan 2019). Instead, the nutrient supply is maintained by global-scale ocean circulation and smaller-scale horizontal transport (Gruber 2008) as summarised in Figure 2.1 and detailed in the following paragraphs.

The thermocline nutrient distribution is shaped by major anticyclonic gyres confined to each hemisphere and ocean basin (Gruber 2008, Letscher et al. 2016). The gyre movement is characterised by near-surface flow at the poleward outcrops which

## 2.1. MARINE BIOGEOCHEMISTRY & OCEANIC CIRCULATION IN THE GLOBAL OCEAN

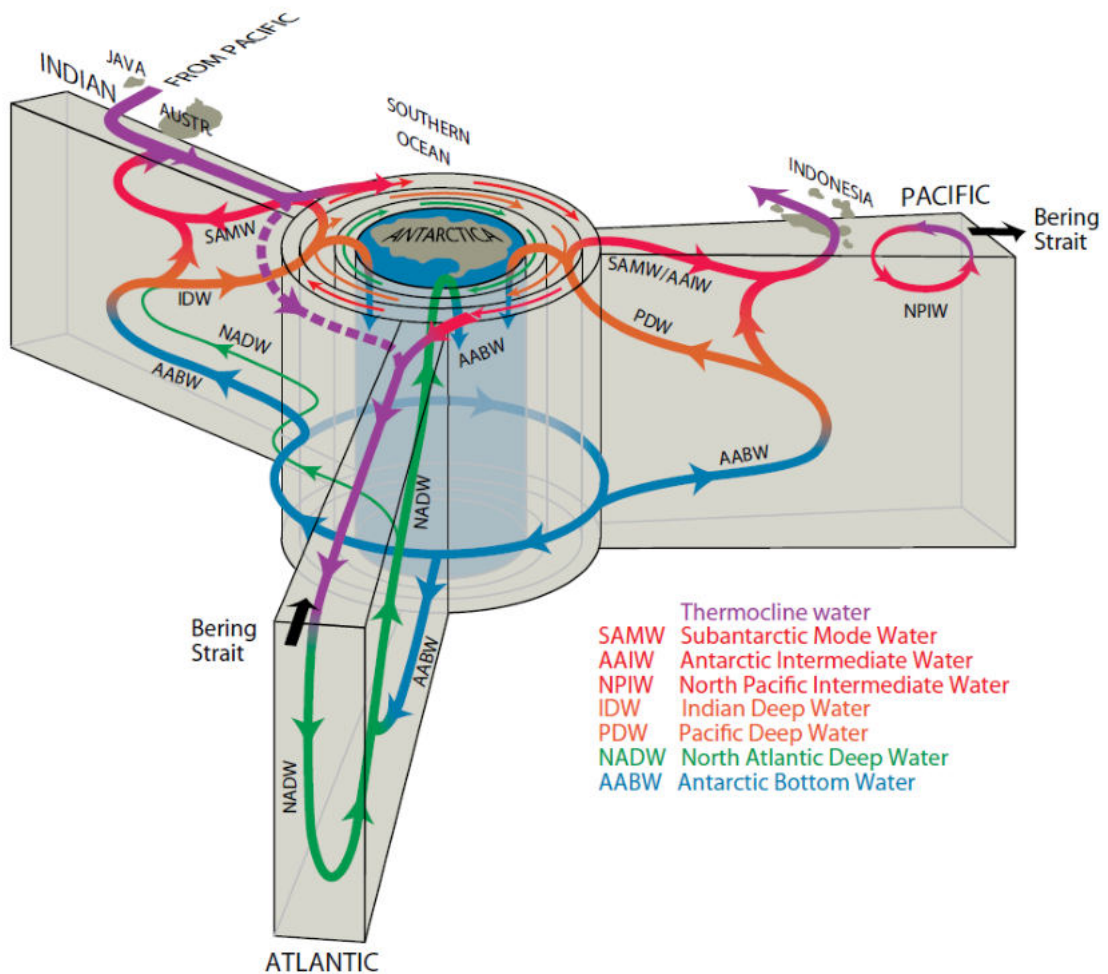


**Figure 2.1:** Schematic of the global overturning circulation from Talley (2013).

descends to depth along the eastern margin. These cold eastern boundary currents are associated with coastal upwelling systems, providing abundant nutrients to the marine ecosystem. Subsequent westward flow along the equator turns into the western boundary current at the western flank of the subtropical gyres, advecting nutrients poleward (Clayton et al. 2017). In the Southern hemisphere, the Antarctic Circumpolar Current (ACC) functions as the southern boundary to subtropical gyre flow, connecting all major ocean basins.

Deep water nutrients are determined by the lower branch of the basin overarching, global Meridional Overturning Circulation (MOC) (Williams and Follows 2003, Gruber 2008). The two major regions of newly ventilated water supply to the deep ocean are the North Atlantic and the SO. Indian and Pacific Deep Water is formed diffusively within the respective basins from inflowing deep waters (Talley 2013).

In the Atlantic, relatively warm, nutrient-poor surface water reaching the high

latitudes is transformed into colder, deep water gradually accumulating remineralized nutrients during sinking. This North Atlantic Deep Water (NADW) returns southward at depth into the SO where most of it flows across and upwells south of the ACC. Upwelled NADW mixes with local waters in the SO, increasing in density until it eventually sinks to form deep Antarctic Bottom Water (AABW) (Rahmstorf 2013). While following the strong eastward flow associated with the ACC, the SO's nutrient concentrations increase through accumulation of sinking particles and exchanges with Indian and Pacific waters (Williams and Follows 2003).

The densest water remains in the SO. Less dense AABW flows northward into all three ocean basins where it upwells into local deep waters, i.e. the North Atlantic, Indian and Pacific Deep Water. While AABW is the sole source of deep water to the Pacific and a major source to the Indian Ocean, it only plays a minor role in the Atlantic compared to its northern originated NADW. The Atlantic deep layer is mostly sourced from sea surface and hence low nutrient waters while the Pacific and Indian deep layers are almost entirely sourced from nutrient-rich upwelled bottom waters (Talley 2013). Upwelling Indian and Pacific Deep Water in the tropics and subtropics provide nutrients to the surface ocean. In the North Pacific, a comparatively weak overturning cell is associated with the formation of North Pacific Intermediate Water (NPIW) (Talley 2013). Despite its minor contribution to global-scale overturning, being mostly detached from NADW and AABW circulation, it plays a vital role for thermocline nutrient supply and maintenance of biological production in the North Pacific Ocean (Sarmiento et al. 2004, Nishioka et al. 2020).

Returning Indian and Pacific Deep Water flow back into the SO above the denser NADW, partly joining deep waters to form AABW, partly moving northward at the sea surface joining Subantarctic Mode Water (SAMW) and Antarctic Intermediate Water (AAIW) (Talley 2013). Antarctic surface water is transformed into AAIW equatorward of the Polar Front and subducts at the Subantarctic Front. SAMW is formed equatorward of AAIW formation via mixed layer deepening during the austral winter (Hartin et al. 2011). These thermocline waters characterised by enhanced nutrient concentrations circulate within the subtropical gyres of the Southern Hemisphere, eventually flowing into the North Atlantic feeding NADW, closing the circle between subsurface gyre flow and deep ocean pathways (Talley 2013). SAMW is crucial for the supply of nutrients to thermocline waters. Changes in nutrient export of SAMW source regions affect nutrient distributions on global scales (Sarmiento et al. 2004).

### 2.1.4 Marine Iron Biogeochemistry

The micro-nutrient iron assumes a central role in modulating marine productivity and thus the capacity of the ocean to act as a C sink (Tagliabue et al. 2017). Due to its relatively short residence time it is less affected by large-scale global ocean circulation but exhibits nutrient-like profiles uncharacteristic of elements with similar residence times (Johnson et al. 1997). Understanding of the Fe cycle in the ocean has advanced significantly in the past decades, painting an increasingly comprehensive picture of sources, sinks and their dynamic interactions (Boyd and Ellwood 2010, Tagliabue et al. 2017).

External Fe sources to the ocean include atmospheric dust, coastal and shallow sediments, hydrothermal activity, sea ice, riverine influx and volcanism (Boyd and Ellwood 2010). The trace metal occurs in the form of particulate and dissolved Fe, while the latter is further partitioned into soluble and colloidal phases (Wu et al. 2001). Colloids are compounds so small to operationally, by means of filtration, be part of the dissolved Fe pool despite their particle status. The following processes of removal and supply acting upon externally sourced Fe lead to the above-mentioned nutrient-like profile of dissolved Fe with relatively low concentrations in the subsurface ocean, increasing with depth (Boyd and Ellwood 2010).

Bioavailable Fe in the upper ocean is taken up by marine plankton as well as heterotrophic and autotrophic bacteria (Boyd and Ellwood 2010). Iron availability is determined both by external sources and recycling of biogenic Fe by zooplankton, viruses and heterotrophic bacteria, rapidly mobilising biogenic Fe for biological uptake. Along with Fe uptake and biological cycling, iron-binding ligands are produced, exerting control over Fe regeneration and scavenging (Tagliabue et al. 2017). Excess production of iron-complexing ligands is assumed to maintain Fe in solution and is thus a critical supply mechanism (Lauderdale et al. 2020). Despite increasing knowledge on ligand sources and cycling, considerable uncertainty concerning its dynamics remains (Tagliabue et al. 2017), leading to diverse treatment of these processes across models (e.g. Parekh et al. 2008, Moore et al. 2013a).

Removal of Fe from the upper ocean via biological uptake and subsequent sinking of particulate matter is partially balanced by remineralization, releasing Fe and organic ligands into both soluble and colloidal pools. Due to longer remineralization length scales relative to other major nutrients, Fe replenishes the deep water inventory more effectively (Tagliabue et al. 2017). In the ocean interior, scavenging of biologically degraded and transformed Fe onto lithogenic and organic particles further removes Fe. When scavenging exceeds remineralization, deep-water Fe con-

centrations do not increase progressively as is characteristic for other major nutrients (Boyd and Ellwood 2010).

Iron biogeochemistry is closely interwoven with cycles of C, N and P via biological production by phytoplankton. In the modern ocean, the micro-nutrient is the limiting growth factor in the Antarctic region, the eastern equatorial and North Pacific (Moore et al. 2013b). Before reviewing the implications of altered aeolian transport of dust, and hence iron, for glacial atmospheric CO<sub>2</sub> concentrations (see Section 2.2.2), I will briefly describe the main climatic features of the LGM as well as relevant deviations of oceanic circulation and nutrient inventories from pre-industrial times.

## 2.2 The Last Glacial Maximum

The LGM is defined as the most recent episode in Earth history when ice sheets reached their global maximum extent during the last ice age (Mix et al. 2001). Based on measurements of mean ocean water oxygen isotope ratios and glacial sea levels inferred from tropical reef and coastal sediment cores it is dated to a time frame of 24,000 to 18,000 years BP (Mix et al. 2001) with an ice volume, expressed as ice-equivalent sea-level lowering, of 118 to 135 m (Clark and Mix 2002). Despite increasing evidence for regional differences concerning the timing of maximum extent and onset of deglaciation (Clark et al. 2009, Hughes et al. 2013), the centre of the LGM has remained at around 21,000 years BP (Mix et al. 2001). Globally, ice sheets had reached their maximum volume by that time, responding to changes in external forcing, most prominently declining northern summer insolation, tropical Pacific SST and atmospheric CO<sub>2</sub> (Clark et al. 2009).

Reconstructions of mean global temperature suggest an LGM cooling of  $4.0 \pm 0.8^\circ\text{C}$  compared to pre-industrial levels (Annan and Hargreaves 2013), with mean global ocean temperatures around  $3^\circ\text{C}$  colder than today (Bereiter et al. 2018). Closely correlated to decreased temperatures, atmospheric CO<sub>2</sub> was approximately 30% lower at the peak of the Last Glacial Period than during the pre-industrial Holocene, as early ice core measurements revealed (Delmas et al. 1980, Neftel et al. 1982).

The LGM climate was colder and globally drier with an equatorward shift of climate zones compared to pre-industrial. These climatic changes together with a shifting vegetation – high-latitude treeless vegetation replaced boreal forests (Harrison and Prentice 2003, Binney et al. 2017), subtropical deserts expanded and

tropical forests were taken over by more drought-tolerant grasslands and savannas (Prentice and Jolly 2000, Marchant et al. 2009, Lu et al. 2013) – explain increased aeolian dust loading during the LGM (Harrison et al. 2001). In some regions, atmospheric dust concentrations were by an order-of-magnitude larger than during the late Holocene (Harrison et al. 2001, see Section 2.2.2.1 for more details).

### 2.2.1 Changes to Ocean Circulation and the Soft Tissue Pump

Along with these dramatic changes in LGM climate, glacial physical and biogeochemical ocean dynamics were not invariably alike modern conditions as described in Section 2.1.3. While the scientific debate is still on-going (Galbraith and Skinner 2020) and potential changes to the circulation in the Pacific Ocean remain unconstrained (Du et al. 2020), the following main features of the LGM ocean have been identified.

In the Atlantic, a weakening of the large-scale overturning circulation was accompanied by an intensification of the vertical density gradient (Adkins 2013). The boundary between the two main water masses, NADW and AABW, shoaled while reduced mixing and enhanced stratification strengthened the two-cell structure of the northern and southern source waters (Adkins 2013). Deep water formation in the North Atlantic shifted southward, potentially divided into Glacial North Atlantic Intermediate and Glacial North Atlantic Bottom Water (Howe et al. 2016, see Figure 2.2).

In the glacial North Pacific, the production of NPIW strengthened and deepened (Kim and Park 2008, Okazaki et al. 2012). Well-ventilated and nutrient-poor NPIW occupied the upper 2000 m, with less ventilated and nutrient-enriched deep water below (Okazaki et al. 2012). The transport of southern source waters into the deep Pacific decreased (Du et al. 2018) as did the export of AABW from the Weddell Sea (Huang et al. 2020). The reduction in global overturning circulation rate presumably affected both Atlantic and Southern Ocean Meridional Overturning Circulation (AMOC and SOMOC in Figure 2.2) (Du et al. 2020).

At the level of the soft tissue pump, the temperature dependency of the underlying biological processes altered phytoplankton primary productivity and export production during the LGM. Maximum phytoplankton growth rates are estimated to have been reduced by  $\sim 15\%$  at a  $3^\circ\text{C}$  cooling (Kremer et al. 2017). Respiration rates of selected species declined by a similar order of magnitude (Heine et al. 2019). How far the interplay of these counteracting processes acted to reduce or enhance export production is still under debate (Matsumoto 2007, Chikamoto et al. 2012) –

and also highly dependent on other factors, such as light and nutrient availability.

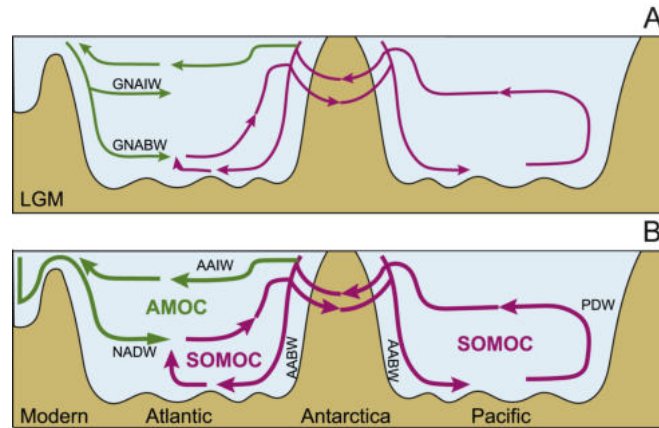


**Figure 2.2:** Schematics of the structure of the global MOC in the LGM (A) and modern times (B). (A) Pathways of Glacial North Atlantic Intermediate Water (GNAIW) and Glacial North Atlantic Bottom Water (GNABW). (B) Atlantic Meridional Overturning Circulation (AMOC) and Southern Ocean Meridional Overturning Circulation (SOMOC) with pathways of Antarctic Intermediate Water (AAIW), Antarctic Bottom Water (AABW), North Atlantic Deep Water (NADW) and Pacific Deep Water (PDW). Line thickness indicates hypothetical circulation strength. Adapted from Du et al. (2020), Figure 13.

Seasonal sea ice changes influenced phytoplankton light limitation and led to deeper mixing during winter replenishing the surface ocean with nutrient-rich deep water (Abelmann et al. 2015). Changes to the macro-nutrient inventory of the glacial ocean include, for example, a suggested increase in N on the order of 10% derived from both model studies (Schmittner and Somes 2016) and reconstructions from benthic foraminifera, a group of shelled zooplankton living in marine sediments (Glock et al. 2018). N fixation as the main source of bioavailable  $\text{NO}_3$  was likely reduced during glacial times (Ganeshram et al. 2002, Somes et al. 2017). Simultaneously, the main mechanism of N loss, denitrification in Oxygen Minimum Zones (OMZs), weakened thus counteracting or even outweighing reduced  $\text{N}_2$  fixation (Schmittner and Somes 2016, Glock et al. 2018).

One of the most prominent examples of altered nutrient distributions during the LGM is the increase of dust-borne Fe in the glacial ocean.

### 2.2.2 Iron Fertilization during the LGM

Various hypothesis have been put forward to explain the 80 to 100 ppm drawdown of atmospheric  $\text{CO}_2$  at the peak of the Last Glacial Period, ranging from well known SST dependent  $\text{CO}_2$  solubility to the highly uncertain effect of terrestrial weathering on the LGM climate (Kohfeld and Ridgwell 2009). In this field of tension of known

## 2.2. THE LAST GLACIAL MAXIMUM

---

knowns and unknown unknowns lies the iron fertilization hypothesis: while well understood in its biogeochemical mechanism, estimates of its magnitude vary widely (e.g. Lambert et al. 2015, Muglia et al. 2017).

In the 1990s, in-situ experiments of Fe enrichment in Subarctic and Antarctic waters led to substantially increased  $\text{NO}_3$  utilization and enhanced phytoplankton growth in the HNLC regions (Martin and Fitzwater 1988, Martin et al. 1990). These observations, together with evidence from ice cores of increased continental dust fluxes during the LGM (Petit et al. 1981, Royer et al. 1983, Legrand et al. 1988), gave birth to the iron fertilization hypothesis: Increased deposition of dust-borne Fe on the ocean surface in regions otherwise limited by this micro-nutrient resulted in phytoplankton fertilization and thus elevated marine productivity and enhanced  $\text{CO}_2$  sequestration during the LGM (Martin 1990). Since the early formulation of this theory, both observational studies of ice and sediment cores as well as model simulations of the LGM have explored this further.

### 2.2.2.1 Palaeorecords of Atmospheric Dust Load, Marine Deposition and Productivity

Ice core records and loess-palaeosol sequences function as archives of glacial-interglacial dust variations. Analysis of Antarctic and Greenland ice cores have continuously exhibited high atmospheric dust concentrations in times of low atmospheric  $\text{CO}_2$  (Petit et al. 1981, Steffensen 1997). Compared to Holocene values, LGM dust levels were elevated by a factor of  $\sim 20$  in Antarctica (e.g. Petit et al. 1981, Fuhrer et al. 1999, Delmonte et al. 2002), and even by a factor of 100 at several drilling sites in Greenland (e.g. Steffensen 1997, Ruth et al. 2003, Simonsen et al. 2019). Dust records from ice cores outside the polar regions covering the Last Glacial Period are rarer and paint a mixed picture of increased (Thompson et al. 1995) and decreased (Thompson et al. 1998, Wu et al. 2004) mineral aerosol concentrations in South America and China, the latter due to regionally wetter conditions and expanded snow cover.

Complementing information on past dust conditions outside glacial regions can be provided by loess-palaeosol records (Üjvári et al. 2017). Enhanced terrestrial dust accumulation is i.a. reported for Europe (Fitzsimmons et al. 2012), North America (Roberts et al. 2003) and Asia (Kohfeld and Harrison 2003). Together with ice core analysis, loess records do not only shed light on the magnitude of glacial-interglacial dust variation, but also confine dust source regions (Muhs et al. 2014). However, these palaeoproxies do not give insights into the consequences of increased aeolian

dust transport during the LGM for marine productivity and mineral utilization.

Marine sediment cores provide a unique tool to investigate this interaction between aeolian Fe deposition and biological productivity. In the past decades, multiple studies inferring export production from a variety of proxies have been performed (i.a. Kowalski and Meyers 1997, Mortlock et al. 1991, Dezileau et al. 2003, Loubere et al. 2004). The diversity of analysed proxies obscures comparison and most studies focus on one single proxy to reconstruct marine productivity. Direct flux measures of organic C or biogenic opal are a product of surface flux, lateral transport, preservation and dissolution. Indirect measures, such as radiogenic isotopes that were scavenged onto particles and are thus associated with particle flux, might be distorted by additional scavenging near continental margins or preferential adsorption to certain particles.

Considering available flux measures collectively and further normalising by constant flux proxies,  $^{230}\text{Th}$  or  $^{10}\text{Be}$ , to account for the effects of lateral sediment redistribution can remedy this (Kohfeld and Ridgwell 2009). Hence, recent research trying to answer the question of iron fertilization employs a multi-proxy approach, often in combination with reconstructions of dust deposition and the degree of  $\text{NO}_3$  consumption. Site locations cover the Southern Atlantic (Martinez-Garcia et al. 2014), the Equatorial Pacific (Costa et al. 2016) and the Subantarctic Zone around New Zealand (Durand et al. 2017). While all studies report an increased dust or Fe flux to the ocean during the LGM, regional evaluations of the iron hypothesis differ.

In the central Equatorial Pacific, Costa et al. (2016) find that the degree of  $\text{NO}_3$  consumption as well as marine productivity did not increase in the LGM despite two to three times higher dust deposition, an increase in dust load which is also supported by earlier studies (Winckler et al. 2008). Within the Subantarctic Zone around New Zealand, a lack of silicic acid is proposed to have limited diatom growth (Durand et al. 2017). Marine sediment cores in an enlarged region of the Subantarctic, with sites in the South Atlantic and South Pacific, on the contrary find increases in the degree of  $\text{NO}_3$  consumption and marine productivity (Martinez-Garcia et al. 2014). Additionally, the portion of highly bioavailable Fe in this region seems to have increased six-fold during the LGM, lending support to the iron fertilization hypothesis (Shoenfelt et al. 2018).

Despite observed increases of dust-borne Fe in all these studies, estimates of biological production differ substantially. In order to assess global-scale changes and understand the underlying dynamics of these seemingly opposing responses, a multitude of modelling studies have been undertaken.

### 2.2.2.2 Model Studies of LGM Dust Deposition and CO<sub>2</sub> Drawdown

Climate models of different complexity levels have been used to quantitatively assess glacial CO<sub>2</sub> drawdown as a consequence of iron fertilization on a global level (see Table 2.1). Early box model studies apportioned half of the glacial-interglacial CO<sub>2</sub> change to increased SO productivity (Watson et al. 2000). More complex Ocean General Circulation Models (OGCMs) including ocean biogeochemistry attribute less importance to iron fertilization, ranging from 4 to 23 ppm (Muglia et al. 2017, Nickelsen and Oschlies 2015). Earth System Models, whether of intermediate complexity (Brovkin et al. 2007, Menviel et al. 2012) or run in an ocean-only configuration, coupled to a simple atmospheric box model (Lambert et al. 2015, Heinemann et al. 2019), are within the range opened up by box models and OGCMs of <10 ppm to 37 ppm (Lambert et al. 2015, Brovkin et al. 2007, respectively).

While early studies often used LGM dust fields within a pre-industrial world (e.g. Watson et al. 2000, Parekh et al. 2008) recent research increasingly simulates the effect of observationally derived dust fluxes on glacial climate. Lambert et al. (2015) employ a sophisticated biogeochemical ocean model forced by their newly interpolated LGM dust field to estimate oceanic C export. The ocean model is coupled to a one-box atmosphere to infer atmospheric CO<sub>2</sub> sequestration on centennial timescales which amounts to less than 10 ppm. To estimate the CO<sub>2</sub> drawdown on millennial timescales, the simulated increases in export production are used to force a 50,000 year simulation of the Danish Center for Earth System Science ESM, yielding an additional ~10 ppm reduction.

Going beyond this ocean-only perspective, Muglia et al.'s (2017) biogeochemical model is coupled to a dynamical land vegetation model, but still only includes a two-dimensional single-level atmosphere. Using the same dust fields as in Lambert et al. (2015), they estimate the effect of aeolian dust fluxes on CO<sub>2</sub> drawdown to 4 ppm. Increasing LGM Fe deposition 10-fold south of 35 °S increases this value to 13 ppm.

Nickelsen and Oschlies (2015) and Heinemann et al. (2019) do not primarily aim at modelling the effect of iron fertilization from observational LGM dust fields, but focus on the effect of iron-light co-limitation and particle ballasting, respectively. However, their sensitivity experiments allow to assess the magnitude of iron fertilization in comparison to the newly parametrised processes. Coupling the ocean model to a one-box atmosphere, high deposition LGM scenarios yield a reduction in atmospheric CO<sub>2</sub> by 23 and more than 10 ppm, respectively. Iron-light co-limitation and particle ballasting play a smaller role on the orders of 4 to 5 ppm.

**Table 2.1:** Modelling studies of the iron fertilization hypothesis during the LGM, including an implementation of the Fe cycle (y=yes/n=no), boundary conditions/forcing (LGM, pre-industrial (PI) or modern), and employed atmospheric dust deposition to estimate the effect on LGM CO<sub>2</sub> drawdown  $\Delta\text{CO}_{2,\text{atm}}$ .

Authors	Model Description	Fe	Forcing	Atmospheric Dust	$\Delta\text{CO}_{2,\text{atm}}$
Lefèvre et al. 1999	PANDORA 10-box model + Fe geochemistry	y	modern <sup>1</sup>	2x ctl	10-30 ppm
Watson et al. 2000	Ocean-atmosphere C and biogeochemistry multibox model in the SO	y	modern	LGM (Vostok ice core)	40 ppm
Archer et al. 2000	Global ocean circulation and C cycle model	y	modern	LGM (Mahowald 1999)	8 ppm
Bopp et al. 2003	PISCES global ocean biogeochemistry model embedded in offline OGCM	y	LGM	LGM (Mahowald 1999)	15 ppm <sup>2</sup>
Parekh et al. 2006	MIT global ocean circulation and biogeochemistry model, coupled to atmospheric CO <sub>2</sub> reservoir	y	modern	LGM (Mahowald 1999)	8 ppm
Brovkin et al. 2007	CLIMBER-2 ESM of intermediate complexity	n	LGM	Implicit <sup>3</sup>	37 ppm
Parekh et al. 2008	Bern3D ESM of intermediate complexity + Fe cycle and biological productivity in the euphotic zone	y	PI	100x modern in the SO	10 ppm
Tagliabue et al. 2009	PISCES global ocean biogeochemistry model	y	LGM	LGM (Mahowald 2006)	11 ppm
Hain et al. 2010	CYCLOPS biogeochemical ocean-atmosphere box model + dynamical lysocline, 2 SO boxes	n	glacial	Implicit <sup>4</sup>	35 ppm
Oka et al. 2011	Biogeochemical ocean model coupled to 1-box atmosphere, forced by MIROC physical & dust fields	y	LGM	LGM (Takemura 2009) + 20x in the SO	22 ppm
Bouttes et al. 2011	CLIMBER-2 ESM of intermediate complexity	n	LGM	Implicit <sup>5</sup>	10-21 ppm
Menviel et al. 2012	Bern3D+C ESM of intermediate complexity, coupled to atmospheric Energy Balance Model	y	LGM	LGM (Dome C ice)	10 ppm
Nickelsen et al. 2015	BLING coupled global ocean biogeochemistry model, coupled to atmospheric CO <sub>2</sub> reservoir	y	PI	LGM (Mahowald 2006)	23 ppm
Lambert et al. 2015	NEMO-PISCES global ocean biogeochemistry model, coupled to atmospheric reservoir	y	PI	New interpolation of DIRTMAP database <sup>6</sup>	<10 ppm
Muglia et al. 2017	MOBI ocean biogeochemistry model coupled with University of Victoria OGCM, coupled to one-box atmosphere	y	LGM	LGM (Lambert 2015)	4 ppm <sup>7</sup>
Ganopolski et al. 2017	CLIMBER-2 ESM of intermediate complexity	n	LGM	LGM (Dome C ice)	22 ppm
Yamamoto et al. 2019	MIROC-based offline biogeochemical model, coupled to one-box atmosphere	y	LGM	LGMctl + glaciogenic dust (Mahowald 2006) <sup>8</sup>	17 ppm
Heinemann et al. 2019	MPIOM OGCM with embedded HAMOCC C cycle model, coupled to atmospheric CO <sub>2</sub> box	y	modern	LGM (Mahowald 2006)	>10 ppm

<sup>1</sup> modern circulation, glacial chemistry<sup>2</sup> 39 ppm with Fe saturated surface ocean<sup>3</sup> full PO<sub>4</sub> utilization in the Subantarctic Atlantic and Indian Ocean<sup>4</sup> more efficient nutrient consumption<sup>5</sup> more efficient nutrient consumption in the Subantarctic Atlantic and Indian Ocean<sup>6</sup> [Kohfeld and Harrison, 2001; Maher et al., 2010]<sup>7</sup> 13 ppm with 10x Fe in the SO and changes in sedimentary flux<sup>8</sup> with 3 % Fe solubility

## 2.2. THE LAST GLACIAL MAXIMUM

---

Studies in the past decade either decouple the physical and biogeochemical models (Parekh et al. 2008, Oka et al. 2011), work with ESMs of intermediate complexity (Menviel et al. 2012, Ganopolski and Brovkin 2017) or lack a full-scale atmospheric model component (Lambert et al. 2015, Muglia et al. 2017) and thus depend on external dust fields. In order to simulate the interaction of ocean biogeochemistry with land and atmospheric processes, I employ a full-scale ESM with an embedded ocean biogeochemical module and dynamic calculation of aeolian dust from terrestrial dust mobilisation and atmospheric transport. As in previous studies, an additional LGM simulation with altered dust-borne Fe fluxes is used to analyse the model sensitivity to this crucial parameter and explore possible constraints on estimates of atmospheric CO<sub>2</sub> drawdown.

## 3 Methods

This chapter introduces the ESM employed in this thesis, the Community Earth System Model (CESM) version 1.0, with a particular focus on the Ocean Biogeochemistry Module BEC. The second Section describes the experimental design of the above-mentioned LGM simulations and a simulation of the pre-industrial Holocene which is included for reference.

### 3.1 Model Description

#### 3.1.1 The Community Earth System Model

The CESM version 1.0 is a global climate model with coupled atmosphere, land, ocean and sea ice components (Hurrell et al. 2013). CESM1 supersedes the Community Climate System Model 4 (CCSM4) with new capabilities including land and ocean biogeochemical cycles, atmospheric chemistry and a dynamic ice sheet model (Hurrell et al. 2013). The model is run in its coarse resolution with an atmospheric horizontal grid of  $3.75^\circ \times 3.75^\circ$  and 26 vertical levels, and an oceanic horizontal grid with a nominal resolution of  $3^\circ$  and 60 vertical layers (Shields et al. 2012). Ocean layer thickness is 10 m in the upper 160 m and increases with depth to 250 m at around 3500 m, after which it remains constant (Danabasoglu et al. 2012). The low-resolution version is a computationally cost-efficient alternative that has proven to reproduce the mean state and overall variability of pre-industrial climate as simulated in CESM runs at higher resolution (Shields et al. 2012) and has also been widely used in palaeoclimatological studies (e.g. Pedro et al. 2018, Nielsen et al. 2019, Gu et al. 2020).

Atmospheric dynamics incorporated into the Atmospheric General Circulation Model include sources, sinks and transport of mineral aerosols (Zender et al. 2003, Hurrell et al. 2013). Dust mobilised by wind that does not fall victim to dry or wet deposition is passed to the atmospheric aerosol model which implements several transport processes: mixing within the atmospheric boundary layer, shallow and deep convective transport, and advection by large-scale eddies (Zender et al. 2003).

### 3.1. MODEL DESCRIPTION

---

Atmospheric deposition of mineral aerosols to the ocean is based on the dust climatology by Luo et al. (2003). Hence, glacial dust fields are not prescribed as in the majority of earlier model studies of iron fertilization during the LGM (see Table 2.1) but simulated dynamically. However, this also has its drawbacks which will be further elaborated upon in Section 3.2.3.

The ocean component is based on the Parallel Ocean Program (POP) (Smith et al. 2010). It is a level-coordinate model, solving the primitive equations for ocean dynamics under hydrostatic and Boussinesq approximations. For a detailed description of ocean model physics in the current version see Danabasoglu et al. (2012). Both land and ocean C models integrate biogeophysical and biogeochemical processes such as nutrient cycling and photosynthesis (Hurrell et al. 2013). The following Section describes the ocean biogeochemistry component in more detail.

#### 3.1.2 The Ocean Biogeochemistry Module

The CESM runs with the BEC module developed by Moore et al. (2002, 2004), and including changes to the N cycle (Moore and Doney 2007, Moore et al. 2013a) as well as major modifications to improve the simulation of the Fe cycle (Moore and Braucher 2008) and minor changes to parameter values (Moore et al. 2013a).

The marine ecosystem and ocean biogeochemistry module BEC follows the Nutrient Phytoplankton Zooplankton Detritus approach (Fasham et al. 1990), modelling marine ecosystem processes based on the dynamics of key Plankton Functional Types (PFTs). The PFTs included in BEC are diatoms, diazotrophs, smaller phytoplankton and coccolithophores, with the latter being simulated implicitly as a fraction of the smaller phytoplankton group, as well as one class of zooplankton. All phytoplankton have explicit pools of C, Fe and chlorophyll, diatoms also have a  $\text{SiO}_3$  pool. Detritus is accounted for in the form of DOM and sinking particulates. Interaction between these pools comprise plankton growth and decay, calcification, grazing, remineralization and sinking (Moore et al. 2004).

Limiting nutrients included in the model are  $\text{NO}_3$ ,  $\text{NH}_4$ ,  $\text{PO}_4$ , dissolved Fe and  $\text{SiO}_3$ . The plankton growth model is based on fixed C/N/P ratios for each plankton type and a fixed Fe/C ratio for zooplankton. Phytoplankton growth rates are determined by the most limiting nutrient(s) and light, allowing for co-limitation, and by SST. To account for the dynamical adjustment to changing growth conditions (Sunda and Huntsman 1997), the model implements variable Fe/C ratios for all phytoplankton types as well as a variable Si/C ratio for diatoms which increases under Fe stress. Phytoplankton biomass is thus a function of C fixation minus losses

**Table 3.1:** PFT growth factors and Redfield ratios in BEC (Moore et al. 2004).

PFT	Growth Factors	C/N/P	Fe/C [ $\mu\text{mol/mol}$ ]	Si/C [mol/mol]
Diatoms	C, N, P, Fe, Si, light, SST	117/16/1	2.5–6 <sup>3</sup>	0.0685–0.685 <sup>4</sup>
Diazotrophs	C, N <sub>2</sub> , P, Fe, light, SST	366/50/1	14–48 <sup>3</sup>	–
Small Phyto. <sup>1</sup>	C, N, P, Fe, light, SST	117/16/1	2.5–6 <sup>3</sup>	–
Zooplankton	Graze on Phytoplankton	117/16/1	2.5	

<sup>1</sup> Implicit coccolithophores with variable  $\text{CaCO}_3$  production; lower under nutrient stress/low SST

<sup>2</sup> Capable of  $\text{N}_2$  fixation: no strong N competition with diatoms & small phytoplankton

<sup>3</sup> Decrease with Fe stress

<sup>4</sup> Increase with Fe stress

through grazing, non-mortality loss e.g. respiration and aggregation (Moore et al. 2002b).

Calcification by coccolithophores is parametrised implicitly as a function of small phytoplankton primary production rate. This base calcification rate is adjusted upward under bloom of small phytoplankton, when their biomass exceeds the threshold of  $3.0 \mu\text{M C}$ , and adjusted downward under nutrient-limitation or low temperature (Moore et al. 2004).

One class of zooplankton grazes on all phytoplankton types. Zooplankton growth rates and pathways between remineralization and detrital pools vary according to food source. When grazing upon diatoms and small phytoplankton a higher fraction of the consumed organic matter goes to new zooplankton biomass than for diazotrophs. The remainder is split between remineralization, DOM and sinking particulates (the latter only for diatoms and small phytoplankton) in varying fractions for each group. Non-grazing mortality of phytoplankton and aggregation losses of diatoms and small phytoplankton are split between semilabile DOM, sinking POM and remineralization.

BEC comprises two detrital pools. DOM is divided into labile organic matter that instantly remineralizes and semi-labile matter that has a remineralization lifetime of  $\sim 100$  days. A refractory pool, characterised by a markedly longer lifetime on the order of centennials to millenniums and essential for DOM export to deep waters (Moran et al. 2016) is neglected in the model. Sinking POM is divided into a ‘free’ organic fraction that easily remineralizes and a mineral ballasted fraction remineralizing deeper in the water column or sinking to the ocean floor unaffected by degradation. The mineral ballast pool includes dust, biogenic silica, and  $\text{CaCO}_3$  (Moore et al. 2004).

This 2002, 2004 model implementation relied on several simplifying assumptions about the marine Fe cycle that have subsequently been revised to improve the rep-

### 3.1. MODEL DESCRIPTION

---

resentation of Fe sources and scavenging processes (Moore and Braucher 2008). In its current set-up, external input of Fe comes from atmospheric deposition and sedimentary release (Moore and Braucher 2008, Moore et al. 2013a). Aeolian dust contains 3.5 % Fe by weight with a constant 2 % solubility. To account for subsurface Fe dissolution, an additional 3 % of dust dissolves in the upper water column below the surface. The remaining mineral aerosols remineralize at a length scale of 40 000 m. The originally crude representation of a constant sedimentary Fe source in depths above 1100 m is now a function of the sinking POC flux, weighted by ocean bathymetry (Moore and Braucher 2008). All dissolved Fe is assumed bioavailable and phytoplankton half-saturation constants have been lowered slightly since Moore et al. (2004) to simulate more efficient Fe uptake.

According to the improved scavenging parametrisation, the fractional allocation of dissolved Fe between the sinking particulate pool and sedimentary loss is reversed, increasing the fraction of Fe scavenged onto sinking particles to 90 %. Simultaneously, the fraction of these particles reaching the ocean floor is increased slightly. The rate of scavenging is a function of the sinking particle flux, i.e. POC, biogenic silica,  $\text{CaCO}_3$  and mineral dust, and the ambient Fe concentration (Moore et al. 2004, Moore and Braucher 2008). At high Fe concentrations, the scavenging rate declines rapidly to implicitly account for iron-binding ligands. Finally, the revision now also incorporates desorption of dissolved Fe from scavenging particles, improving simulated Fe concentrations in the deep ocean (Moore and Braucher 2008).

Similarly, representation of the N cycle has been revised since BEC’s 2002 implementation. The model now includes atmospheric N deposition based on tropospheric aerosols (Lamarque et al. 2010). Phytoplankton N uptake is partitioned between  $\text{NH}_4$  and  $\text{NO}_3$ , with a strong preference for  $\text{NH}_4$  under high ambient concentrations and Fe stress (Moore et al. 2002b). Diazotrophs are capable of  $\text{N}_2$  fixation of which 30 % are exuded as dissolved organic N. In contrast to previous versions, the CESM implementation also allows for diazotrophic uptake of both  $\text{NH}_4$  and  $\text{NO}_3$  which reduces N fixation proportionately (Moore et al. 2013a). However, uptake parameters are set relatively high in comparison to the other phytoplankton types in order to avoid strong competition over these dissolved inorganic N pools.

Nitrification of  $\text{NH}_4$  is light dependent, occurring at mixed layer depth average Photosynthetically Available Radiation (PAR) values below  $4.0 \text{ W/m}^2$  (Moore et al. 2002b). Water column denitrification is a function of ambient oxygen ( $\text{O}_2$ ) concentrations taking place when  $\text{O}_2$  values fall below  $4 \mu\text{M}$  (Moore and Doney 2007). Due to CESM overestimation of OMZs this led to excessive denitrification and substantial

imbalances in the pre-industrial N cycle (Moore et al. 2013a). Thus, a constant scaling factor of  $\text{NO}_3/110$  is applied in CESM BEC simulations to reduce unrealistically high N loss (Lindsay et al. 2014).

## 3.2 Experimental Setup

Traditionally, model studies assessing the magnitude of the effect of iron fertilization on LGM climate have relied on sensitivity analysis as a powerful tool to explore the impact of uncertainties concerning atmospheric dust deposition, Fe solubility or bioavailability (e.g. Parekh et al. 2008, Muglia et al. 2017, Yamamoto et al. 2019). In this line, I investigate the iron hypothesis by comparing a standard LGM simulation (LGMstd) with an increased Fe input case (LGM5i). Most past studies have focused on the model's sensitivity regarding the extent of additional atmospheric  $\text{CO}_2$  concentration. I will concentrate not on the  $\text{CO}_2$  effect of these changes, which have already been discussed in Jochum et al. (submitted), but study the underlying dynamics hoping to contribute to a more thorough understanding of the interactions between glacial ocean physics and biogeochemistry.

The focus of this thesis will be on a comparison of both glacial simulations, LGMstd and LGM5i. However, a pre-industrial CESM simulation (PRE) is included for reference and for comparison of LGM model results to similar studies. A wide body of literature treating the question of glacial iron fertilization from both a modelling and an observational perspective often presents findings in reference to the late Holocene. In order to discuss CESM simulations against this background, LGMstd and LGM5i will be compared to PRE in Chapter 5.

### 3.2.1 The Pre-Industrial Control Simulation

Modifications to the standard CESM set-up as described in (Hurrell et al. 2013, Lindsay et al. 2014) concerning parametrisation of tidal mixing and overflow regions were necessary to account for a lack of information of their glacial representation: In CESM, overflow regions are hardcoded to present-day bathymetry (Briegleb et al. 2010) and are thus turned off for the pre-industrial and both LGM simulations. Similarly, the parametrisation of abyssal tide driven mixing from Jayne (2009) is topography dependent and tuned to best fit observed tides (Smith et al. 2010). It is replaced by an empirical diffusivity profile (Bryan and Lewis 1979).

The pre-industrial 1850 simulation PRE is based on initial conditions and forcing of its predecessor, CCSM4, as described in Gent et al. (2011) except for the

newly introduced ocean biogeochemical and the land state (Lindsay et al. 2014). The initial state of the marine biogeochemical tracers is derived from an offline, ocean-only CCSM4 simulation with these tracers added to the model, forced by a 5-year repeated high-frequency surface forcing data obtained from a coupled CCSM4 simulation (Lindsay et al. 2014). Ending conditions of this 1025 year CCSM4 run are used to initialise the coupled pre-industrial CESM simulation. Initial conditions of the land component are based on year 863 of CCSM4 (Lindsay et al. 2014).

The pre-industrial simulation is run for 4000 years, as is LGMstd. Comparison to LGM simulations focusses on the end of the run, i.e. year 3680 before LGM5i develops Dansgaard-Oeschger events.

### 3.2.2 The Standard LGM Simulation

CESM is run in its standard biogeochemistry enabled pre-industrial version (Lindsay et al. 2014), with several palaeoclimate modifications besides the above-mentioned changes to the representation of tidal mixing and removal of the overflow parametrisation.

The model calculates Earth’s orbital parameters based on Berger et al. (1993) for 21,000 years BP. Ocean bottom topography is replaced by reconstructions of ocean palaeobathymetry from Peltier et al. (2015). As a consequence of a 120 m sea level drop the ocean volume is reduced by 5.7%. Concentrations of passive tracers are increased accordingly to maintain the same total inventory. In line with phase 3 of the Palaeoclimate Modelling Intercomparison Project and similar studies (Muglia et al. 2017) a global addition of 1 PSU to salinity is applied.

Lowering the sea level requires ocean cells to be reclassified as land cells. These new cells are assigned the plant functional type of their nearest neighbour. Otherwise, land cover types remain unchanged from the model’s pre-industrial configuration. Continental palaeotopography and land ice cover are also based on the reconstruction by Peltier et al. (2015). The CESM sea ice module does not require any changes as forcing fields are the ocean grid and bathymetry and ice cover develops from a ‘no ice’ initial state. The model is run for 4000 years.

### 3.2.3 LGM Sensitivity Analysis: Imposing Increased Iron

CESM parametrisation of dust and Fe fluxes to the ocean comes with several uncertainties:

- i. In LGMstd the initial pre-industrial land cover is not changed while the dy-

dynamic vegetation model is disabled (Hurrell et al. 2013), i.e. the assigned cover type in each grid cell may change C content but not cover type. This might underestimate dust production from e.g. Eurasian expansion of treeless biomes during the LGM (Binney et al. 2017).

- ii. The parametrisation of terrestrial dust emission is empirically fitted to the current dust cycle and thus error-prone when used for past or future climates, likely underestimating larger glacial dust deposition fluxes (Kok et al. 2014).
- iii. In BEC, Fe solubility in ocean water is set to a constant value of 2%. However, the proportion of the mineral aerosol entering the oceanic pool of dissolved Fe depends on aerosol source and mineralogy (Schroth et al. 2009) as well as various atmospheric and marine processes (Baker and Croot 2010) and can thus be spatially and temporally highly variable. Recent analysis of Antarctic ice cores suggests that Fe solubility was very flexible during the LGM with 2% being on the lower limit of estimates, reaching values of up to 42% (Conway et al. 2015).
- iv. Related to Fe solubility is the question of the fraction of Fe available for biological uptake. As the model assumes all dissolved Fe to be bioavailable, this parameter is set via the assumed Fe solubility. Evidence from the Antarctic Talos Dome ice core (Spolaor et al. 2013) and subantarctic South Atlantic and South Pacific marine sediments (Shoenfelt et al. 2018) suggest that the flux of highly bioavailable Fe(II) increased by a factor of 7 to 20 during glacial times while the total Fe flux increased only two- to fivefold.

In order to confront these uncertainties, dust fluxes are increased fivefold globally after a 3000 year spin-up period in LGM5i. Given the complex nature of dust mobilisation, transport, deposition and resulting marine Fe input, this might seem a rather blunt approach but has to be seen in light of common methods and limitations of sensitivity analysis as well as previous research.

The above-mentioned model assumptions amount to a systematic underestimation of Fe deposition fluxes. Following the common approach of sensitivity analysis in climate science, varying one input factor at a time (Pianosi et al. 2016), the choice of model parameter to be perturbed should encompass all these uncertainties and distil a single value change. Increasing global aeolian dust fluxes by a factor of 5 bundles glacial changes to the dust/Fe cycle outside the ocean and is both in line with palaeoclimatological reconstructions and model studies of iron fertilization.

### 3.2. EXPERIMENTAL SETUP

---

Previous studies assessing the effect of changes in aeolian Fe fluxes on phytoplankton growth have increased dust deposition in the SO by a factor of 10 to 100 (Parekh et al. 2008, Oka et al. 2011, Muglia et al. 2017). The focus of these studies has been on the SO as one of the main HNLC regions and inspired by ice core records noting a more than 20 times higher SO dust concentration during the LGM than today (Petit et al. 1981, Lambert et al. 2008). However, it is not only the SO that has experienced increased dust deposition during the last glacial. On a global average, Lambert et al. (2015) found the LGM dust flux to have been about 4 times higher. Increasing dust deposition fivefold globally thus corresponds to recent estimates and furthermore enlarges the picture from a SO centred perspective to an assessment of global dynamics in response to plankton fertilization.

After the increase in dust fluxes, the model simulation is continued for 2000 years as it starts developing Dansgaard-Oeschger events after having crossed a critical CO<sub>2</sub> threshold (Jochum et al. submitted). As analysis of these events is not part of the thesis, model results are only considered until simulation year 3690.

## 4 Results

The CESM LGM simulation reproduces the physical LGM state realistically (Jochum et al. submitted). The model develops a glacial maximum state characterised by increased snow and sea ice cover in the high latitudes. Ocean mean temperature is around 3 °C below pre-industrial, global surface temperatures decrease markedly. The atmospheric CO<sub>2</sub> concentration is ~55 ppm lower in LGMstd. The relative increase of AABW volume in comparison to NADW is consistent with reconstructions (Adkins 2013, Oppo et al. 2018). However, an increased ventilation rate and higher O<sub>2</sub> content of the glacial ocean is not supported by observational evidence (Menviel et al. 2017, Anderson et al. 2019). For a detailed description of LGMstd characteristics, the distribution of Dissolved Inorganic Carbon (DIC) in the glacial ocean and a thorough discussion of the seemingly contradictory deep sea ventilation and O<sub>2</sub> content see Jochum et al. (submitted).

The following analysis focuses on a comparison between the standard LGM simulation (LGMstd) and the LGM simulation with five times aeolian dust (LGM5i). The difference or ‘anomaly’ between these two, i.e. LGM5i minus LGMstd, is denoted with a ‘d’ in front of the variable considered. The time frame comprises the simulation years 2990 to 3690. Simulations continued beyond this time horizon will not be analysed here as LGM5i develops Dansgaard-Oeschger events. All variables represent 10 year averages. For qualitative visualisation in the global maps and depth transects, variables have been regridded onto an equirectangular plate carrée projection using nearest neighbour remapping. Quantitative evaluation (such as in Figures 4.1 & 4.5 right panel) is based on the original POP grid.

I will use the terms ‘marine productivity’ or ‘biological production’ and ‘export production’ synonymously although marine productivity more universally refers to the production of organic matter by phytoplankton (Sigman and Hain 2012) and export production refers to the export of organic matter, or in this thesis POC, out of the surface ocean. However, export production is a valuable measure for the effectiveness of marine productivity in sequestering atmospheric CO<sub>2</sub> and thus the effect of iron fertilization on glacial CO<sub>2</sub> drawdown. In line with similar model

studies, export production out of the surface ocean is defined as the POC flux at 100 m depth and abbreviated as EP.

Increasing dust fluxes fivefold yields an additional  $\sim 15$  ppm reduction in atmospheric  $\text{CO}_2$  at the end of the considered time period that can be attributed to effects of iron fertilization (Jochum et al. submitted). However, the evolution of marine export production leading to the observed increased C sequestration is neither temporally nor spatially uniform. The following Sections explore the regionally diverse responses to increases in dust-borne Fe.

As a first step, the temporal relationship between atmospheric Fe deposition and export production will be examined (Section 4.1). In light of the close interplay of Fe availability, macro-nutrients and marine productivity, the following Sections will consider patterns of nutrient distributions in the subsurface ocean and zonally averaged depth transects in relation to export production and marine biogeochemical processes (Sections 4.2 & 4.3). Further disentangling basin specific responses will be the focus of Section 4.4 before concluding with the consequences of increased Fe fluxes on limiting nutrients and phytoplankton community composition (Section 4.5).

### 4.1 Global Export Production and Iron Limitation

Quintupling the dust flux globally leads to an immediate strong increase in global export production, tending towards a new equilibrium over the course of the simulation (see Figure 4.1). After the initial rapid adjustment, the curve of LGM5i export production flattens towards the end of the considered simulation period but the declining trend does not abate fully. Beyond the 3700s, LGM5i develops Dansgaard-Oeschger events after crossing a critical  $\text{CO}_2$  threshold (Jochum et al. submitted). These developments will not be discussed here as the thesis focuses on the analysis of the LGM climate in LGM5i. 690 years after the perturbation by increasing dust fluxes fivefold, LGM5i is regarded as sufficiently stable to examine the long-term effects of enhanced iron fertilization. After 700 simulation years the total marine Fe concentration is 50 % higher than in LGMstd and global export production at 100 m depth has risen to 6.5 PgC/yr compared to 6.2 PgC/yr in LGMstd.

In both LGMstd and LGM5i the major features of C export at the end of the considered simulation period are similar (see Figure 4.2). Export production is highest in the eastern equatorial Pacific and off the east coast of South Patagonia. Further regions of enhanced POC flux include the northern North Pacific, the east

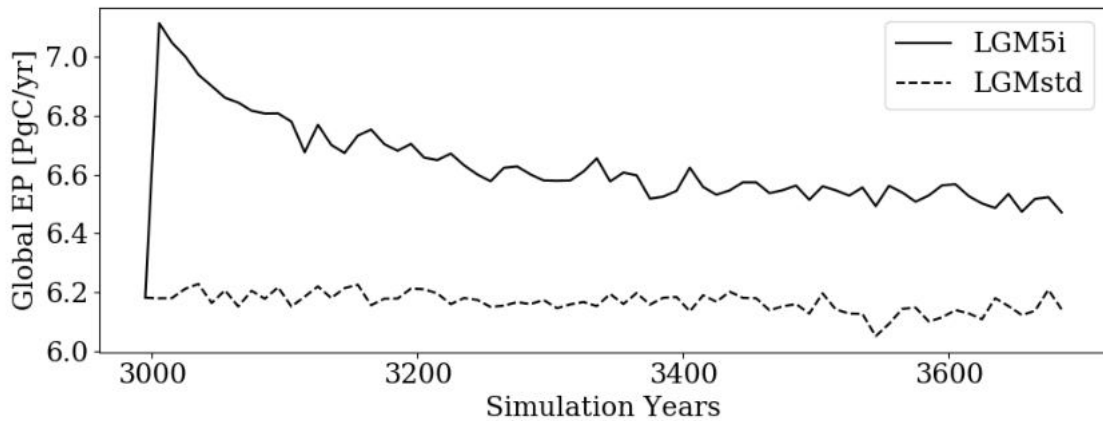


**Figure 4.1:** Timeseries of 10-year-mean global export production (EP) in LGM5i and LGMstd.

coast off modern New Zealand, the Arabian Sea and the western African coastline. In the two prominent regions of deep water formation, the SO and the North Atlantic, however, the pattern of C export is reversed. In LGMstd, the North Atlantic exhibits higher export production than most of the SO, while in LGM5i C export is enhanced in large areas of the SO opposed to a comparatively smaller POC flux in the North Atlantic.

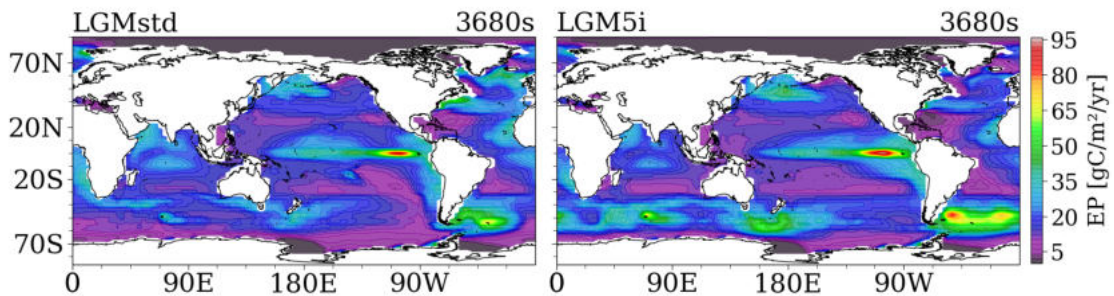


**Figure 4.2:** Global map of 10-year-mean EP in LGMstd (left) and LGM5i (right) in the 3680s.

The majority of the POC response to increased Fe occurs within the first decade after increasing dust fluxes fivefold (see Figure 4.3). Export production is considerably enhanced in the HNLC SO, northern Pacific and eastern Pacific Ocean and maintained or slightly intensified in the following 700 simulation years. The POC flux in the western Pacific, Indian Ocean and South Atlantic responds more mildly, exhibiting declining export production by the 3680s. The immediate changes, especially in regions of decreasing export production, do not fully account for the

#### 4.1. GLOBAL EXPORT PRODUCTION AND IRON LIMITATION

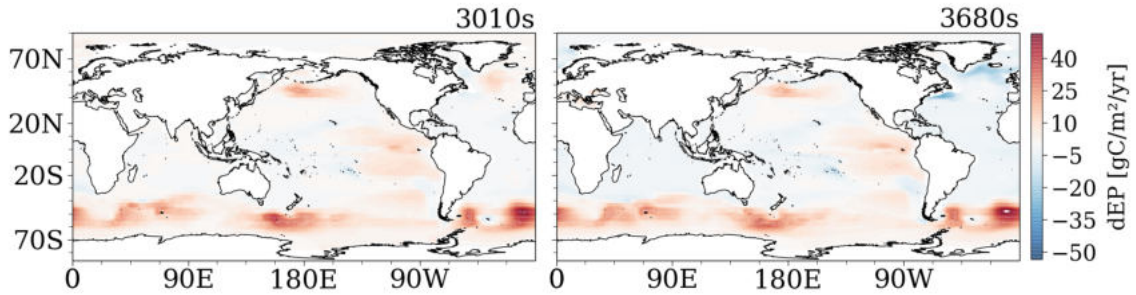


**Figure 4.3:** Global map of 10-year-mean export production anomaly (dEP) in the 3010s and 3680s.

magnitude of the response but often set the sign of the change. In the northern Atlantic, however, one can observe a pronounced sign change. A strong increase in export production dominates the picture of the 3010s while in the 3680s areas of substantial decline prevail.

The CESM allows to assess the limiting factor(s) of phytoplankton growth, varying between 0 for mean high limitation and 1 for mean low limitation. Figure 4.4 shows the Fe limitation of diatoms before and 10 years after the increase in aeolian dust fluxes. Fe limitation is reduced markedly in the SO and in the Pacific as well as in parts of the subpolar North Atlantic. The observed, immediate increases in export production in these regions thus seem to be a direct reaction to reduced Fe limitation.

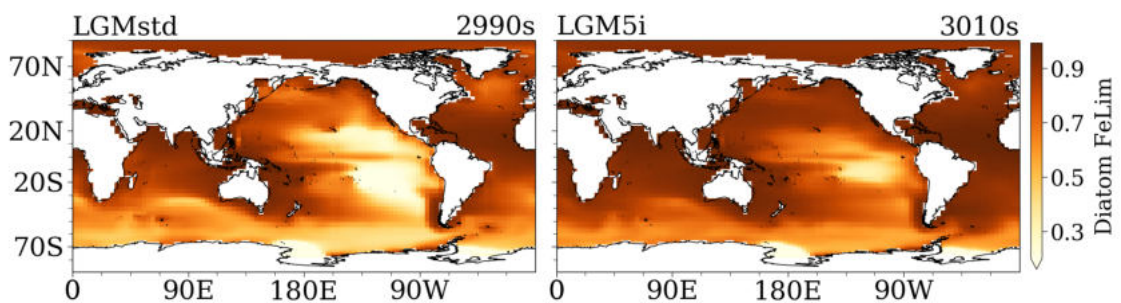


**Figure 4.4:** Global map of 10-year-mean diatom Fe limitation (FeLim) immediately before (LGMstd 2990s, left) and 10 years after increase in dust flux (LGM5i 3010s, right).

To explore the temporal evolution of export production further, Figure 4.5 depicts the global pattern and zonal integral of  $dEP(3680s) - dEP(3010s)$ . When positive, it indicates that either the initial increase in export production intensified or that the initial decrease is reduced or even reversed over time. When negative, either the initial decrease overestimates long-term decline or the initial increase is

reduced or even reversed. The difference between dEP in the 3680s and dEP in the 3010s should thus be put into the context of changes in POC flux within this period as illustrated in Figure 4.3.

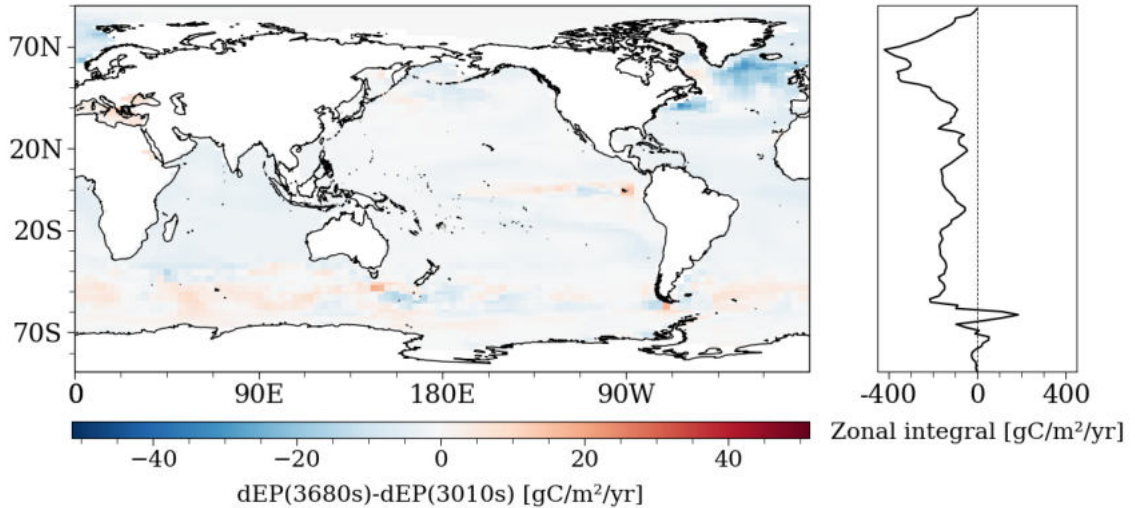


**Figure 4.5:** Difference 10-year-mean dEP(3680s)-dEP(3010s) globally (left) and zonally integrated (right) (same colourbar scaling as in Figure 4.3).

The mid-latitudes of all three ocean basins, except the eastern equatorial Pacific, undergo smaller changes from the 3010s to the 3680s. The zonal signal is dominated by regions in the Atlantic and Indian Ocean where long-term POC decrease further deepens, i.e. where the long-term effect of increased dust deposition is a decline in export production.

The SO draws a heterogeneous picture, both on the North-South and the East-West axis. Early enhanced phytoplankton growth in direct proximity of the Antarctic coast peaks off over time, reflected in a small negative zonal integral. In the subpolar South Atlantic and Indian Ocean, regions of increasing export production seem to be predominant while the subpolar Pacific is dominated by initial increases levelling out slightly. As a consequence, the sign of the zonally integrated export production in the SO oscillates on a relatively low level. Compared to the major increases in POC flux 10 years after enhanced dust deposition, these fluctuations are only minor. This supports the analysis that short-term effects, i.e. an immediate response to relieved Fe limitation, predominate in the SO.

In the northern high latitudes, especially in the Atlantic Ocean, one finds a distinct negative difference between late versus early changes in export production. The short-term response to relieved Fe limitation in this region is mostly an increase in export production, or at most a very moderate decrease. However, long-term

## 4.2. GLOBAL SUBSURFACE MACRO-NUTRIENT PATTERNS

---

effects result in a substantial decline in the POC export flux, reducing or rather reverting the initial increase.

The iron hypothesis predicts enhanced phytoplankton growth in regions where the prevailing limitation by Fe is alleviated due to increased LGM dust fluxes, but where – at least in the modern ocean – the macro-nutrients N and P are abundant, i.e. the HNLC SO and parts of the Pacific Ocean. Here, export production increases immediately as a direct response to reduced Fe limitation and stabilises over the course of the simulation. In the mid-latitude Atlantic and Indian Ocean, the impact of increased aeolian dust is negligibly small because Fe is not a limiting factor. Long-term effects lead to a slight reduction in export production in these areas after 700 simulation years. Most prominently, short-term positive or neutral responses to increased dust fluxes in the northern North Atlantic are reversed over time, leading to a pronounced decline in export production. Based on this analysis of the temporal relationship between increased dust fluxes and export production, the following Sections will further explore the long-term effects counteracting immediately enhanced marine productivity due to relieved Fe limitation.

### 4.2 Global Subsurface Macro-Nutrient Patterns

Strong fertilization and thus increased nutrient utilization in HNLC regions does not only influence regional nutrient cycling but also affects the global nutrient inventory on timescales of centennials to millenniums.

In the first 10 years after imposing increased dust fluxes, subsurface  $\text{PO}_4$  concentrations are high in HNLC regions but also in large parts of the North Indian Ocean and the North Atlantic (see Figure 4.6, B left).  $\text{NO}_3$  exhibits a very similar pattern with increased concentrations in the North, western and equatorial Pacific, the SO and the North Atlantic (see Figure 4.6, C left). Changes in  $\text{NO}_3$  are one order of magnitude higher than changes in  $\text{PO}_4$ .

In the course of 100 to 200 simulation years, this trend of similar behaviour of  $\text{PO}_4$  and  $\text{NO}_3$  continues only in certain regions: High  $\text{PO}_4$  and  $\text{NO}_3$  concentrations in the entire SO further intensify as do the negative anomalies in the South Indian Ocean and the Pacific Ocean south of  $\sim 30^\circ\text{S}$  as well as off the east coast of Patagonia. The initial decrease in nutrient concentrations is reversed over time in the central North Atlantic and in a band in the western Pacific Ocean between  $10$  to  $20^\circ\text{S}$ . North Atlantic recovery of nutrient stocks is accompanied by decreasing export production (see Figure 4.6, A right).

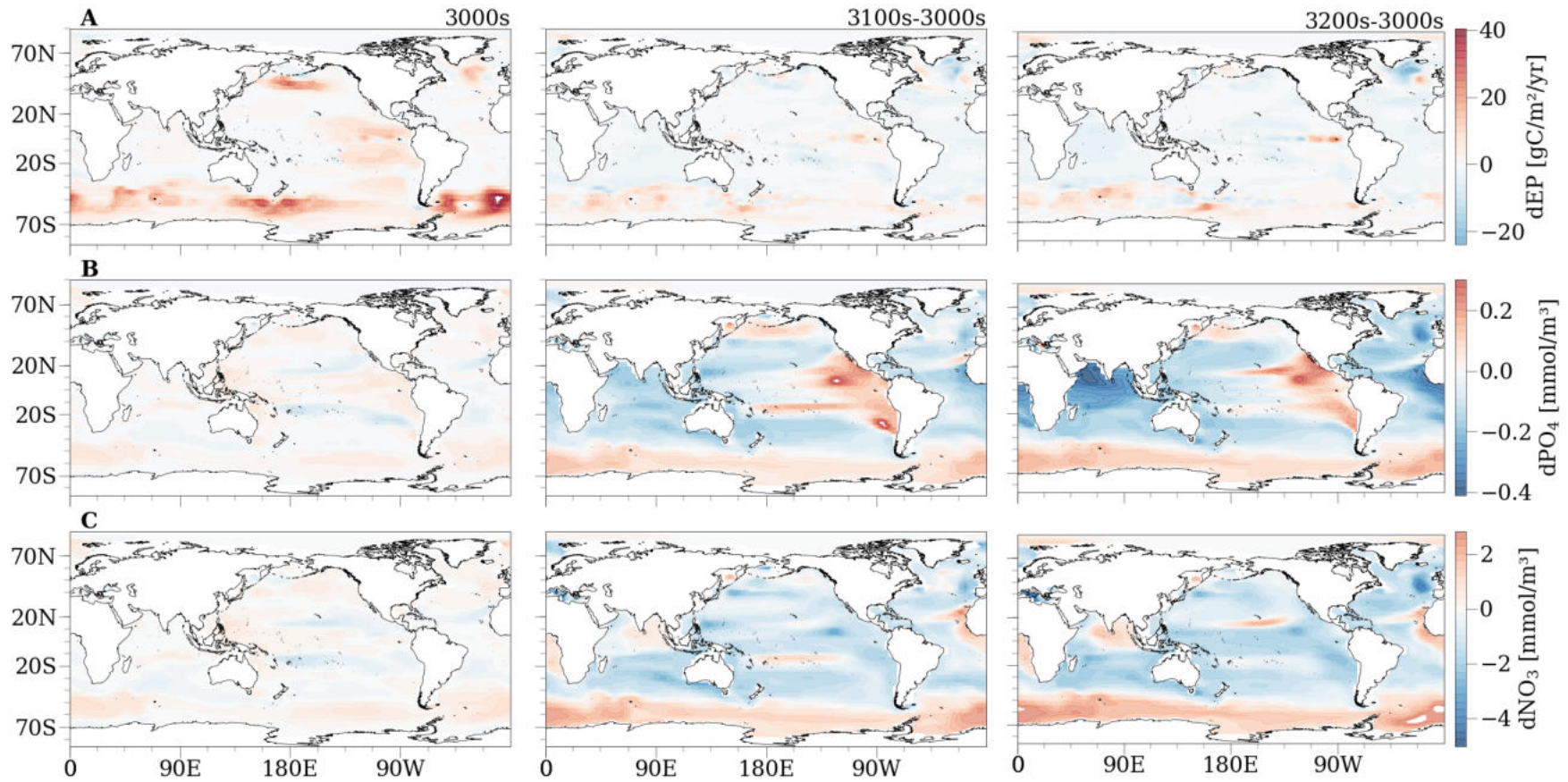


**Figure 4.6:** Global map of dEP (A) and mean thermocline concentration anomalies of PO<sub>4</sub> (B) and NO<sub>3</sub> (C) averaged over depths from 200 to 1000 m. 10-year-mean anomalies in the 3000s, and difference of 3100s and 3200s to 3000s.

## 4.2. GLOBAL SUBSURFACE MACRO-NUTRIENT PATTERNS

---

In other key regions, the distributions of both macro-nutrients evolve differently over time. North Indian Ocean and African west coast enhanced  $\text{NO}_3$  concentrations deepen while positive  $\text{PO}_4$  anomalies in these areas are reversed. Most prominently, nutrient patterns in the Pacific basin differ in the northern and eastern equatorial ocean. After 100 years, increased  $\text{PO}_4$  concentrations are further enhanced and negative anomalies reversed. The strong increase in North Pacific  $\text{NO}_3$  recedes to a small area in the north-east and positive anomalies in most parts of the Pacific Ocean are replaced by a long-term  $\text{NO}_3$  decline.

As far as the temporal relationship between increases in dust fluxes and responses of nutrient concentrations is concerned, the overall pattern of  $\text{PO}_4$  and  $\text{NO}_3$  does not change substantially between the 3100s and 3200s. Most of the key features developed in the first 100 years prevail until the 3680s (Appendix, Figure A.2). Sub-surface  $\text{PO}_4$  concentrations increase substantially in the HNLC regions of enhanced export production, but increasingly decline in the Indian and Atlantic Ocean, including receding positive anomalies in the North Atlantic.  $\text{NO}_3$  increases in the SO, the North Indian Ocean and off the African west coast. Initial rises in the North Pacific and North Atlantic are reduced or even reversed. Negative anomalies in the west Pacific Ocean deepen over time.

Different responses of thermocline  $\text{PO}_4$  and  $\text{NO}_3$  in the Pacific HNLC regions might be due to the more complex biogeochemical cycle of N compared to P. Sources and sinks include  $\text{N}_2$  fixation and (de-)nitrification, and phytoplankton are capable of the uptake of two different dissolved inorganic N forms (Moore and Doney 2007, Moore et al. 2013a).

As an external source of N to the ocean, the model implements  $\text{N}_2$  fixation by diazotrophs. This phytoplankton type has high Fe requirements, with reduced  $\text{N}_2$  fixation under Fe stress (Moore et al. 2002b). Changes in  $\text{N}_2$  fixation cannot explain reduced  $\text{NO}_3$  concentrations in the eastern equatorial Pacific as diazotrophs remain Fe limited and do not fix any  $\text{N}_2$  in both LGM simulations (Appendix, Figure A.1).

$\text{N}_2$  fixation is balanced by losses due to denitrification in oxygen-poor regions (Moore and Doney 2007). A stronger reduction in upper ocean  $\text{NO}_3$  compared to  $\text{PO}_4$  could hint at a disbalance of N sources and sinks, i.e. higher denitrification than fixation. Losses through denitrification occur below  $\text{O}_2$  concentrations of  $4 \text{ mmol/m}^3$  (Moore and Doney 2007). This is the case only in a negligibly small area in the glacial equatorial Pacific with overall unchanged or even marginally higher  $\text{O}_2$  levels in LGM5i than LGMstd and thus unchanged denitrification (Appendix, Figure A.4).  $\text{N}_2$  fixation and denitrification also remain unchanged in the North Pacific.

Nitrification, i.e. the conversion of  $\text{NH}_4$  to  $\text{NO}_3$ , depends on average mixed-layer PAR and is zero outside the polar regions where values exceed  $4.0 \text{ W/m}^2$  (Moore et al. 2002b). In the North Pacific, the extension of the minimum PAR zone in LGM5i compared to LGMstd is negligible (Appendix, Figure A.14). Hence, in both the North and equatorial Pacific, nitrification does not decrease to an extent that would explain  $\text{NO}_3$  deficiencies. However, the process of nitrification provides a link between  $\text{NO}_3$ ,  $\text{NH}_4$  and remineralization.

In BEC, remineralization is not directly included in the model equation for  $\text{NO}_3$ , only indirectly via the dependence of nitrification on  $\text{NH}_4$  which undergoes remineralization. If nitrification is unchanged between LGMstd and LGM5i, increasing  $\text{NO}_3$  uptake by phytoplankton in LGM5i diminishes the  $\text{NO}_3$  inventory without direct replenishing via remineralization. Model equations on changes to  $\text{PO}_4$ , on the contrary, directly include sources through remineralization. High  $\text{PO}_4$  concentrations in the subsurface North and east Pacific could thus be interpreted as a signal of high remineralization resulting from enhanced export production.

Another plausible explanation for different responses of thermocline  $\text{NO}_3$  and  $\text{PO}_4$  under increasing Fe fluxes could be a shift in the composition of phytoplankton populations. Diazotrophs have lower P requirements than the other PFTs with molar N/P ratios of 50/1 compared to 16/1. If phytoplankton population shifted towards more diazotrophs, less  $\text{PO}_4$  would be consumed. In regions with generally high  $\text{NO}_3$  and  $\text{NH}_4$  but low Fe concentrations, such as the equatorial Pacific, N uptake from  $\text{N}_2$  fixation and diazotroph biomass is low (Moore et al. 2013a). As a consequence of reduced Fe limitation in LGM5i, photosynthetic C fixation from  $\text{NO}_3$  shifts from diatoms and smaller phytoplankton to diazotrophs in the eastern Pacific (Appendix, Figure A.5). Still diazotroph C fixation remains two orders of magnitude smaller than fixation by the other phytoplankton classes.

If abundant, diazotrophs rely on dissolved  $\text{NH}_4$  and  $\text{NO}_3$  reducing  $\text{N}_2$  fixation proportionately (Moore et al. 2013a). In the eastern Atlantic, before increasing dust fluxes fivefold and stimulating large and small phytoplankton  $\text{NO}_3$  uptake,  $\text{NO}_3$  is sufficiently available for diazotrophs to rely on (see Figure 4.7). With increasing  $\text{NO}_3$  consumption by the other phytoplankton, diazotroph nitrate-based C fixation decreases distinctly as these  $\text{N}_2$  fixing micro-organisms do not compete with large and small phytoplankton. Simultaneously, diazotrophs temporarily increase N fixation to fulfil their N requirements, benefiting from reduced Fe limitation (Appendix, Figure A.6).

Diverging patterns in other regions, i.e. increases in  $\text{NO}_3$  in the Arabian Sea

## 4.2. GLOBAL SUBSURFACE MACRO-NUTRIENT PATTERNS

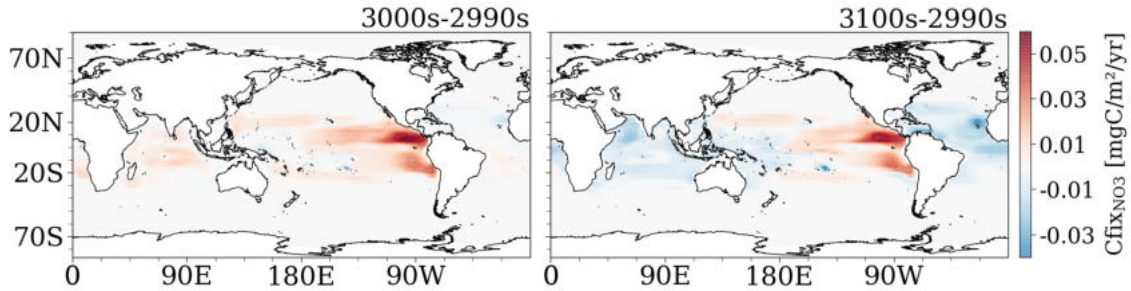


**Figure 4.7:** Global map of 10-year-mean diazotrophic C fixation from NO<sub>3</sub> (Cfix<sub>NO<sub>3</sub></sub>), averaged over upper 150 m depth. Difference between LGM5i 3000s and 3100s to LGMstd 2990s.

and off the African west coast, are highly correlated with areas of elevated surface Fe. Relieved Fe stress enhances diazotrophic N<sub>2</sub> fixation while phytoplankton NO<sub>3</sub> uptake remains unchanged or declines. Additionally, surface Fe concentrations indicate a strong aerosol source in the North Indian and equatorial Atlantic Ocean which could hint at higher atmospheric N deposition in these regions.

The global distribution of thermocline SiO<sub>3</sub> differs markedly from those of PO<sub>4</sub> and NO<sub>3</sub> (Appendix, Figure A.3). This is due to different uptake and remineralization processes of SiO<sub>3</sub>: In contrast to PO<sub>4</sub> and NO<sub>3</sub> which are consumed by all phytoplankton, SiO<sub>3</sub> is only taken up by diatoms, required to build their shells of biogenic silica. Mineral ballast associated biogenic silica remineralizes deeper in the water column than the soft POM fraction of the sinking matter flux (Moore et al. 2013a). As a consequence of different uptake and remineralization processes, changes to SiO<sub>3</sub> only reflect diatom dynamics and upper ocean SiO<sub>3</sub> depletion reaches deeper in regions of enhanced diatom productivity. When averaged over depths of 1000 to 2000 m, the pattern of SiO<sub>3</sub> corresponds more closely to subsurface PO<sub>4</sub> and NO<sub>3</sub>.

Due to the substantial differences in thermocline SiO<sub>3</sub> concentrations and the underlying dynamics, the following analysis will focus on PO<sub>4</sub> and NO<sub>3</sub>. Depth transects of SiO<sub>3</sub> are included for reference in the Appendix (Figures A.11 & A.13). With the exception of the phosphate-rich eastern equatorial Pacific and the nitrate-rich Arabian Sea and eastern South Atlantic Ocean, PO<sub>4</sub> and NO<sub>3</sub> exhibit a clear signal of increasing thermocline nutrient concentrations in the highly productive SO and declines north of 30 °S.

### 4.3 Zonal Depth Transects of Macro-Nutrients

This trend of uniformly increasing macro-nutrient concentrations in the SO and mostly decreasing molarity north of it is also visible in zonal mean  $\text{PO}_4$  and  $\text{NO}_3$  (see Figures 4.8 & A.10). As nutrient patterns and their temporal evolution are very similar for both  $\text{PO}_4$  and  $\text{NO}_3$ , I will describe depth transects of  $\text{PO}_4$  as shown in Figure 4.8 with analogous behaviour of  $\text{NO}_3$  except for initially higher concentrations in the sub-thermocline and Arctic Ocean (Appendix, Figure A.10).

The observed pattern of nutrient trapping in the Southern and Deep Ocean develops if the phytoplankton production driven downward flux of nutrients occurs north of areas where the Antarctic and Subantarctic bottom waters form, i.e. north of the Polar and Subantarctic Front. Nutrients that are stripped out of Antarctic surface waters accumulate in the SO and do not feed into intermediate water formation. As a consequence, the otherwise nutrient-rich thermocline waters providing  $\text{PO}_4$  and  $\text{NO}_3$  to all three ocean basins remain nutrient-poor and the large-scale transport of nutrients declines.

The effect is especially strong in the polar North Atlantic because surface and deep ocean waters are generally nutrient depleted. Iron fertilized phytoplankton increase the consumption of nutrients while they are still abundant, adding to the nutrient deficiencies. The particular ocean bathymetry of the Greenland-Scotland ridge hampers the exchange of water masses and thus the transfer of nutrient-richer southern waters to the Arctic Ocean. Additionally, the northern boundary of the residual MOC is at around  $60^\circ\text{N}$  (Jochum et al. submitted), further impeding water mass exchange.

Nutrient deficiency in the upper mid-latitude oceans progressively percolates into greater depths, reaching 1000 to 3500 m 200 to 300 years after increased dust deposition (see Figures 4.8 C & A.9). The decrease between  $20^\circ\text{N}$  and  $70^\circ\text{N}$  coincides with the formation and subduction regions of NADW. Its circulation transfers the nutrient-poor surface waters to greater depths while accumulating regenerated nutrients during subduction and southward flow. This gradual enrichment would, in a less nutrient depleted LGMstd North Atlantic, prevent such a strong reduction (Appendix, Figure A.9).

A northward flow of nutrient depleted surface waters compensates deep water formation and subduction in the North Atlantic. As nutrient accumulation in the Southern and Deep Ocean continues, export of  $\text{PO}_4$  and  $\text{NO}_3$  to the subtropical gyres is reduced, thus stabilising nutrient deficiencies in the upper ocean between  $50^\circ\text{S}$  and  $40^\circ\text{N}$ . Even the otherwise nutrient-rich upwelling waters at the Equator

### 4.3. ZONAL DEPTH TRANSECTS OF MACRO-NUTRIENTS

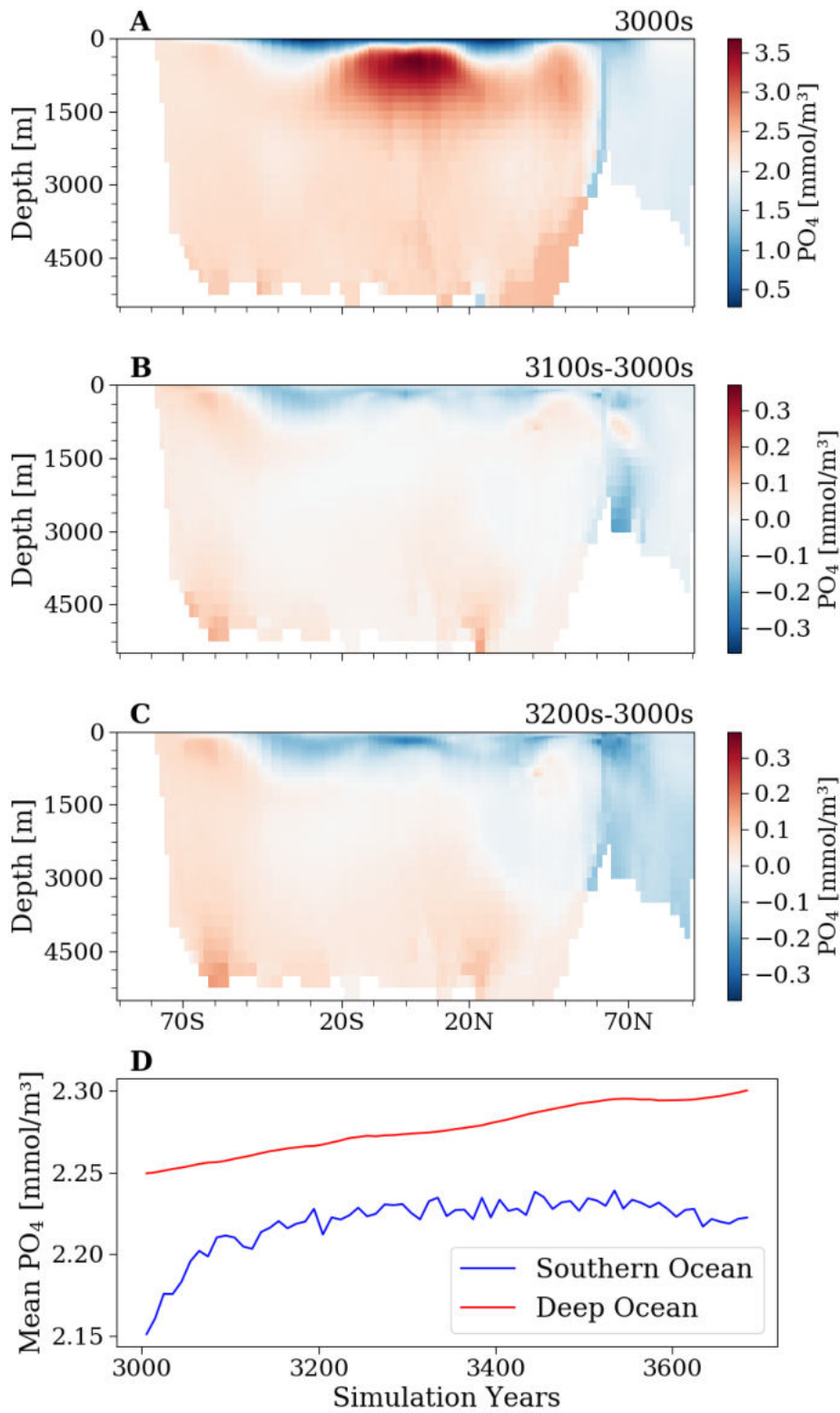


**Figure 4.8:** Zonal mean  $\text{PO}_4$  concentration in LGM5i. 10-year-mean over the 3000s (A), and difference 3100s-3000s (B) and 3200s-3000s (C). D: Timeseries of 10-year-mean  $\text{PO}_4$  in the Southern Ocean and in the Deep Ocean north of the SO.

get continuously depleted in  $\text{PO}_4$  and  $\text{NO}_3$ .

This pattern of elevated nutrient concentrations in the Southern and Deep Ocean and declines in the upper ocean north of the SO and in the subpolar North Atlantic is maintained and intensified over the complete simulation period (Appendix, Figure A.9). While SO nutrient concentrations tend to a new, higher equilibrium towards the end of the considered simulation period, deep ocean  $\text{PO}_4$  continues to rise linearly indicating that the process of deep ocean nutrient enrichment is not completed 680 years after the initial Fe increase (see Figure 4.8 D).

Nutrients accumulate in the high Antarctic latitudes and in depths below 1000 to 3500 m while declining in the subsurface and northern deeper ocean. Enhanced biological activity in the SO and parts of the Pacific Ocean progressively exports both C and nutrients into the Deep Ocean. Macro-nutrient concentrations below 1000 m increase in these regions of high export production due to direct remineralization or remineralization within the sinking matter flux. In the upper ocean north of  $40^\circ\text{S}$ , nutrient depletion reaches depths of up to 3 km (see Figure 4.8 C).

## 4.4 Nutrient Distributions per Ocean Basin

Unravelling the basin specific changes in  $\text{PO}_4$  concentration between the 3300s and 3000s in the upper ocean confirms decreasing  $\text{PO}_4$  in all ocean basins except the Antarctic (see Figure 4.9). In the subantarctic subsurface ocean (see Figure 4.9 A), changes are minor compared to all other regions where nutrient decreases range from  $-10$  to  $-40\%$ . As observed in depth transects of zonal mean  $\text{PO}_4$ , the North Atlantic is most affected by nutrient trapping in the SO. In the Indian and Pacific Ocean, both North and South basins are equally impacted, but the Pacific does not experience as strong a decline as the Indian Ocean. The large declines in nutrient concentrations of the upper Atlantic and Indian Ocean lead to the observed decreases in export production in these regions (see Figures 4.3 & 4.6).

Below 2000 m (see Figure 4.9 B), all ocean basins enrich to a small degree in  $\text{PO}_4$ , except for the subpolar North Atlantic. Here, decreases in  $\text{PO}_4$  concentration are almost as severe as in the upper ocean, amounting to  $-20\%$ . This negative trend does not show in depths below 4500 m because the subpolar North Atlantic does not have areas below this depth in the model. The relative  $\text{PO}_4$  increase is strongest in the North Indian Ocean, even 3 percentage points higher than in the Antarctic. The absolute rise, however, is by an order of magnitude smaller than in the polar SO.

#### 4.4. NUTRIENT DISTRIBUTIONS PER OCEAN BASIN

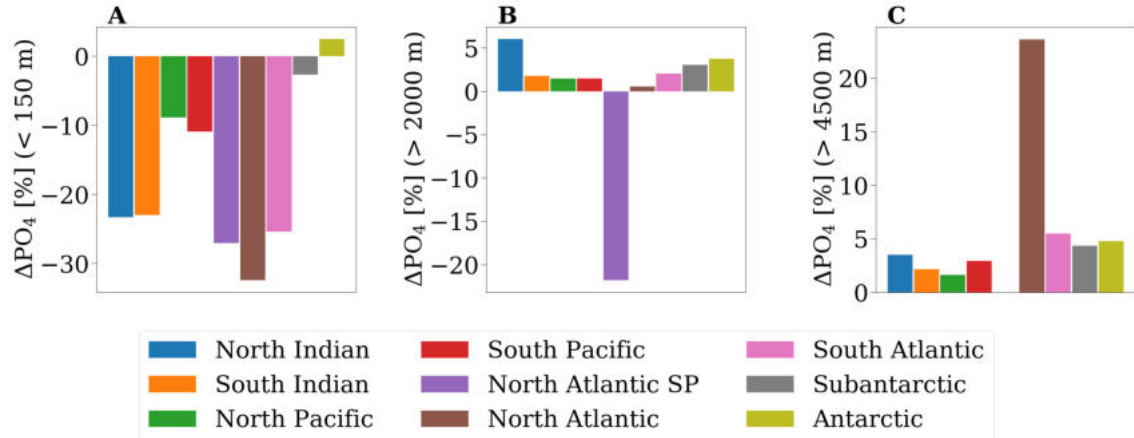


**Figure 4.9:** Percentage changes in  $\text{PO}_4$  concentration ( $\Delta\text{PO}_4$ ) in LGM5i in the upper 150 m (A), below 2000 m (B) and below 4500 m depth (C). Relative change between 10-year-mean over the 3300s and 3000s per ocean basin. ‘North Atlantic SP’ refers to the subpolar North Atlantic north of  $45^\circ\text{N}$ . The Antarctic Ocean comprises the area south of  $60^\circ\text{S}$ , the Subantarctic the area from  $38$  to  $60^\circ\text{S}$ .

In the deepest ocean (see Figure 4.9 C), the  $\text{PO}_4$  inventory is replenished in all basins 300 years after the fivefold increase in aeolian dust fluxes. The North Atlantic south of  $45^\circ\text{N}$  exhibits the strongest increase of over 20%. The relative decrease of NADW volume compared to AABW lets nutrients build up in the deep Atlantic, reflecting the increasing influence of AABW sourced Atlantic deep water.

To further disentangle basin specific responses to increased nutrient utilization in the SO,  $\text{PO}_4$  concentrations have been averaged over a zonal band in the Atlantic and Pacific as well as over a meridional band in the SO, as if on board a cruise ship from the North Atlantic to the North Pacific (see Figure 4.10). Nutrient enrichment can be observed in the Subarctic and Deep Ocean of both basins (see Figure 4.10 B, C). However, ocean-wide zonally mean  $\text{PO}_4$  concentrations as in Figure 4.8 obscure the spatially and temporally diverse responses of each ocean basin. The Atlantic Ocean is generally nutrient poor. Only the Southern Hemisphere and low-latitude subsurface ocean displays higher  $\text{PO}_4$  concentrations, typical of SO sourced nutrient-rich waters in the subtropical gyres. Phosphate values in the deep central Atlantic are also slightly higher than at mid-depth and in the northern ocean, indicating a source of nutrient-rich AABW to the deep Atlantic (see Figure 4.10 A).

In the course of 200 to 400 simulation years after the initial increase in dust fluxes, nutrient concentrations in the SO increase at all depths while the high subtropical  $\text{PO}_4$  values diminish markedly (see Figure 4.10 B, C). The Atlantic gyres are mainly fed by SAMW which forfeits nutrients due to nutrient trapping in the

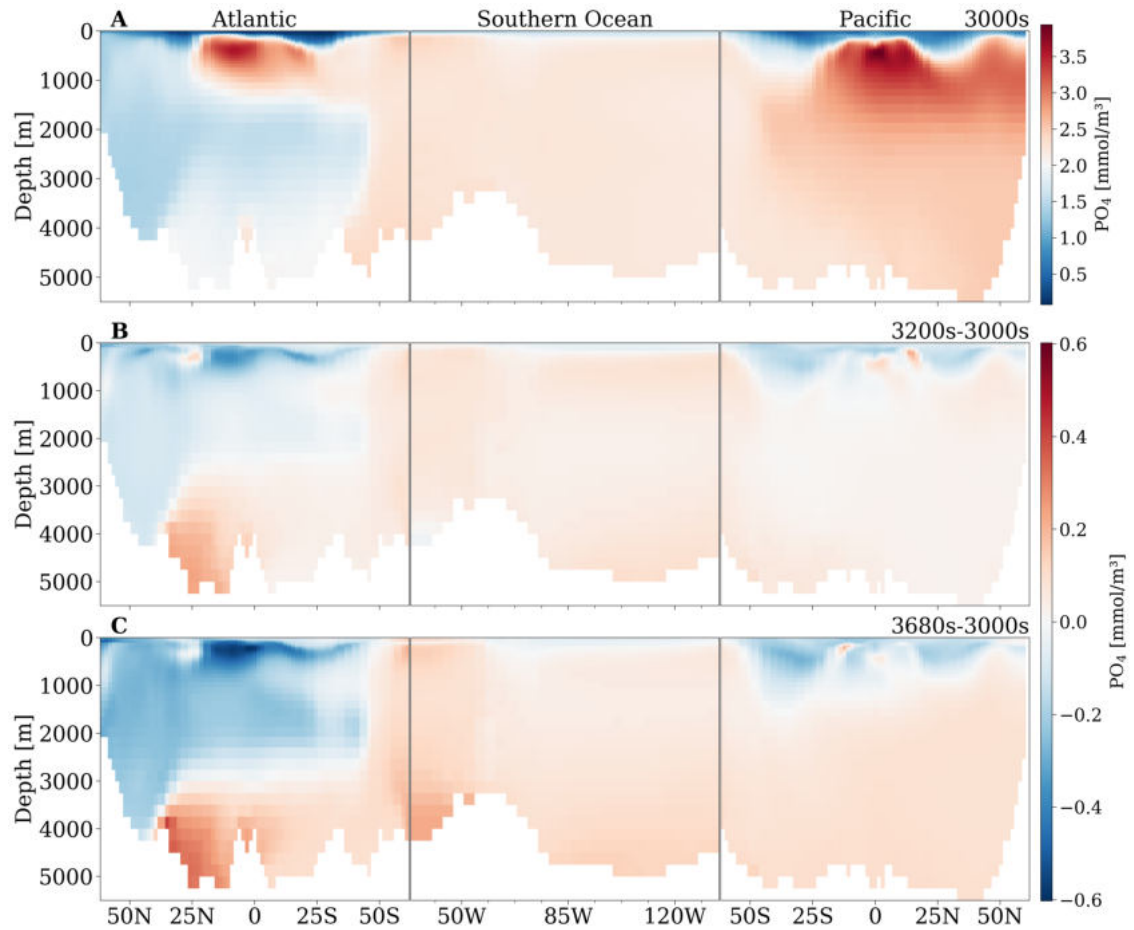


**Figure 4.10:**  $\text{PO}_4$  concentration in depth transects of the Atlantic (mean over 32–14°W), Southern (mean over 64–56°S) and Pacific Ocean (mean over 168–133°W). LGM5i 10-year-mean over the 3000s (A), difference 3200s-3000s (B), and 3680s-3000s (C).

polar Antarctic. Simultaneously, the deep Atlantic gets enriched considerably in  $\text{PO}_4$ . AABW, sourced in SO regions of increased biological productivity, accumulates nutrients and exports them to the deep ocean.  $\text{PO}_4$  concentrations in the nutrient-poor North Atlantic decline further over time as initial increases in export production due to iron fertilization strip nutrients out of the surface and subsurface ocean.

The Pacific Ocean is generally nutrient-rich, especially in proximity to the equator and north of 40°S (see Figure 4.10 A). Equatorial deep-water upwelling provides  $\text{PO}_4$  and  $\text{NO}_3$  to the surface waters where relieved Fe limitation enhances phytoplankton growth and reduces surface nutrient concentrations. In the northern Pacific, nutrient-rich NPIW and increased Fe input similarly lead to higher productivity and thus reduced surface nutrients. Nutrient depletion of the surface ocean reaches deeper at around 35°S and 25°N, in the calm cores of the subtropical gyres, following

the w-shape of the thermocline.

This  $\text{PO}_4$  distribution in the Pacific Ocean is maintained and intensified over the course of the simulation (see Figure 4.10 B, C). In contrast to the Atlantic, where the pattern of nutrient-rich upper and nutrient-poor deeper waters is reversed as a consequence of enhanced SO export production, the Pacific Ocean seems mostly unaffected by SO productivity dynamics. In the tropics, the uniformly high subsurface nutrient concentrations are broken down into smaller cells of  $\text{PO}_4$  enriched waters at the equator and around 10/15°N/S. As the depth transect is averaged over longitudes 168 to 133°W, these cells represent the westward outcrops of nutrient-rich coastal upwelling.

The observed nutrient pattern under SO nutrient trapping in the Atlantic and Pacific Ocean reflects the different supply mechanisms of nutrients in each basin. While the Atlantic subsurface ocean is mainly sourced by nutrient-deprived Antarctic thermocline waters and the North Atlantic is dominated by nutrient-poor NADW, the Pacific Ocean is characterised by upwelling of nutrient-rich bottom waters which are solely sourced by nutrient-rich AABW (Talley 2013).

As for zonal mean nutrient concentrations, very similar observations apply to the depth transects of  $\text{NO}_3$  from the North Atlantic to the North Pacific (Appendix Figure A.12). Discrepancies in the thermocline of the equatorial Pacific and coastal east Atlantic have been discussed above.

## 4.5 Limiting Nutrient and Population Shifts under Enhanced Iron Fluxes

A final look at the limiting nutrients for diatom growth in LGM5i in the 3200s confirms that, in comparison to LGMstd, Fe stress is mostly replaced by N limitation in the North and Equatorial Pacific as well as in the North Atlantic and Antarctic Ocean (see Figure 4.11). Even a fivefold increase in dust fluxes does not relieve Fe limitation in the SO and eastern equatorial Pacific to an extent that would supersede the mineral as the most limiting nutrient to phytoplankton growth because absolute concentrations of dissolved Fe remain low.

Very similar observations apply to diazotrophs and small phytoplankton which experience relieved Fe limitation in all regions but the SO and eastern equatorial Pacific (Appendix, Figures A.7 & A.8). Due to their  $\text{N}_2$  fixation capabilities diazotrophs cannot be nitrogen-limited (Moore et al. 2002b) and former Fe limitation is replaced by P constraints. Small phytoplankton N limitation expands in the North

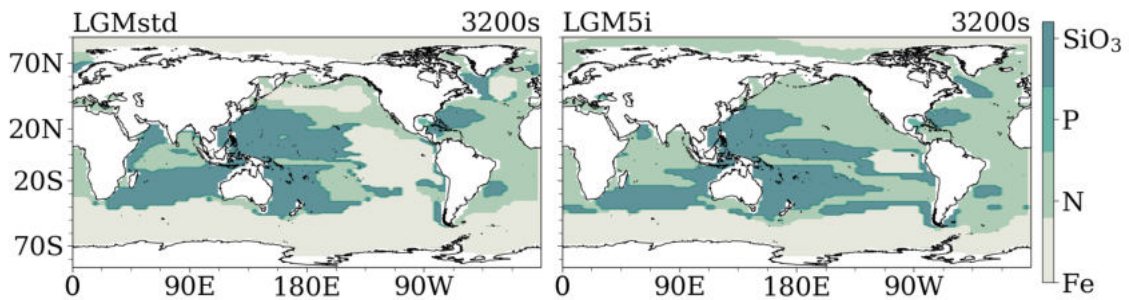


**Figure 4.11:** Most limiting nutrient to diatom growth in LGMstd (left) and LGM5i (right). 10-year-mean over the 3200s.

Atlantic and Pacific Ocean. Both diatoms and small phytoplankton do not experience stronger P than N limits. Regions that were initially most limited by N remain nitrogen-limited as both  $\text{PO}_4$  and  $\text{NO}_3$  further decline. In areas where Fe ceases to be the most limiting nutrient as a consequence of increased dust fluxes, namely the North and eastern equatorial Pacific Ocean,  $\text{PO}_4$  concentrations increase over time, making N the primary limiting factor there.

Changing nutrient patterns also influence biomass composition across all three phytoplankton types (Appendix, Figure A.15). As a response to iron fertilization in the SO, diatom biomass increases considerably in the Southern Atlantic, Indian and the west Pacific Ocean. Small phytoplankton react inversely, with biomass reductions in regions where diatoms thrive and increases in the remaining SO. The tropics and subtropics are characterised by pronounced increases in diazotroph biomass in the Pacific and decreases in the Indian and Atlantic Ocean. The relative contribution of diazotrophs to phytoplankton biomass remains small, with values by an order of magnitude lower than for diatoms and small phytoplankton. However, changes in diazotroph population affect the marine N inventory as they are the only PFT capable of  $\text{N}_2$  fixation. Nitrogen fixation drops significantly in regions of reduced diazotroph biomass and might add to the prevalence of N as the most limiting nutrient for diatom and small phytoplankton in large parts of the Indian and Atlantic Ocean.

Most of the immediate changes in phytoplankton biomass in response to iron fertilization are maintained or even intensified until the end of the considered simulation period. Diatoms outcompete small phytoplankton in large areas of the SO while diazotrophs thrive in the subtropical Pacific. The northern North Atlantic, by contrast, evolves from instantaneously enhanced diatom biomass to a pronounced reduction. Here, small phytoplankton exhibit a similar inverse relationship to di-

#### 4.5. LIMITING NUTRIENT AND POPULATION SHIFTS UNDER ENHANCED IRON FLUXES

---

atom dynamics as in the SO. As diatoms dominate the central northern Atlantic in the first decade after increased dust fluxes, small phytoplankton recede, exhibiting slight increases at the eastern and western margins where diatom biomass decreased. Reductions in diatom biomass by the 3680s are partially replaced by increases in small phytoplankton biomass. Overall, positive and negative changes to the small phytoplankton class in the North Atlantic seem balanced.

All phytoplankton exhibit mostly positive short-term responses to relieved Fe limitation as a consequence of fivefold increased dust fluxes. The SO and the Pacific Ocean are dominated by immediate increases in export production, stabilising and intensifying over time. Outside these HNLC regions, nutrient trapping in the SO reduces the northward transport of macro-nutrients to all ocean basins, resulting in receding marine productivity. How far the observed dynamics correspond with previous modelling studies and palaeoclimatological reconstructions will be topic of the following chapter.

# 5 Discussion

## 5.1 Comparison with Other Model Studies

Simulated global export production in the glacial CESM runs of 6.2 to 6.5 PgC/yr is at the lower bound of similar model studies, estimating glacial export production to 6.7 to 8.5 PgC/yr (Muglia et al. 2017, Oka et al. 2011 & Yamamoto et al. 2019). The overall pattern and magnitude of export production in both LGMstd and LGM5i (see Section 4.1, Figure 4.2) agree well with simulations by Lambert et al. (2015) and Muglia et al. (2017). They also find high productivity regions in the eastern equatorial and North Pacific, the Arabian Sea, at the west African coast, off New Zealand and east Patagonia. In the North Atlantic, their LGM simulations display high export production at the east coast of North America, with outcrops spreading to the eastern basin boundary. The most productive regions in the North Atlantic reach values of 50 to 60 gC/m<sup>2</sup>/yr (Muglia et al. 2017, Lambert et al. 2015, respectively). This is very similar to simulated export production in LGMstd, both in its spatial extent and size.

As mentioned above, sensitivity analysis is a valuable tool to assess model responses to uncertain parameters, widely used in studies on the effect of iron fertilization in the LGM. Yamamoto et al. (2019) focus on the role of increased glacial dust fluxes globally while Oka et al. (2011) and Muglia et al. (2017) constrain changes to the SO. Though experimental designs differ between these studies, as well as compared to the LGM5i simulation in this thesis, a comparison of model results sheds light on the underlying biogeochemical and physical mechanisms of glacial iron fertilization, especially concerning the role of the SO under different dust deposition and Fe solubility scenarios.

Comparing Oka et al.'s (2011) standard LGM simulation (simulation 'LGM') to an experiment with 20-fold increased dust fluxes in the SO south of 60 °S (simulation 'LGM2'), one can observe lower export production in the northern and western North Pacific, and to a smaller degree in the Arabian Sea (see Figure 5.1). Productivity increases markedly in all ocean basins between 30 to 60 °S but does not change in the

## 5.1. COMPARISON WITH OTHER MODEL STUDIES

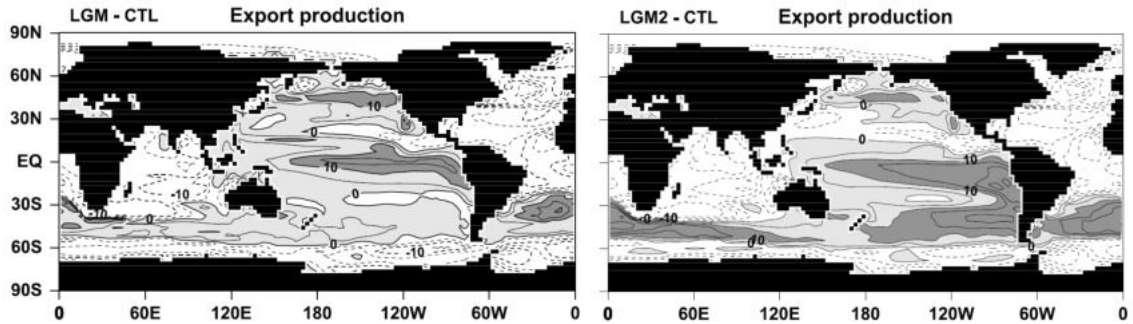


**Figure 5.1:** Global map of simulated export production in Oka et al. (2011) LGM (left) and LGM2 (right) as difference from pre-industrial control run (CTL). Contour interval is  $5 \text{ gC/m}^2/\text{yr}$ . Values larger than 0 and 10 are indicated by light and heavy shading, respectively. Adapted from Oka et al. (2011), Figures 4b & 5.

Atlantic Ocean north of  $30^\circ\text{S}$ . Increasing SO Fe input substantially enhances export production there, a finding that I share. Constraining changes in the dust flux to the SO does not relieve Fe limitation in the Pacific HNLC regions as observed in LGM5i. Oka et al. (2011) acknowledge the effect of increased SO nutrient utilization on Atlantic export production, but fail to reproduce it in their LGM sensitivity experiment. This might be due to the biogeochemical model employed that only accounts for the effect of light, Fe and P on phytoplankton growth and does not include N as a limiting nutrient. It is  $\text{NO}_3$  that is the primary limiting nutrient for larger phytoplankton in that region (see Section 4.5). Neglecting the influence of N deficiencies might thus overestimate North Atlantic productivity.

Similar to Oka et al. (2011), Muglia et al. (2017) conduct a sensitivity experiment with an elevated soluble Fe flux in the SO (simulation ‘LGM\_highFe’). Increasing glacial Fe fluxes tenfold south of  $35^\circ\text{S}$  leads to locally enhanced export production (see Figure 5.2). In the Indian and west Pacific Ocean productivity decreases slightly. Regions of high POC flux in the northern and eastern North Pacific as well as in the eastern subtropical South Pacific remain largely unchanged. Only the area of east Pacific export production does not extend as far west. In contrast to Oka et al. (2011) and in good agreement with CESM simulations of generally increased dust fluxes, the Atlantic response to SO iron fertilization is a uniform decline in productivity in the North and the western South Atlantic Ocean. The observed pattern is very similar to LGM5i, supporting the analysis that the SO response to increased Fe is crucial at setting export production north of  $30^\circ\text{S}$ , especially in the Atlantic.

In an attempt to improve simulated LGM dust deposition, Ohgaito et al. (2018) include an additional glaciogenic dust source to model-based dust generation. This

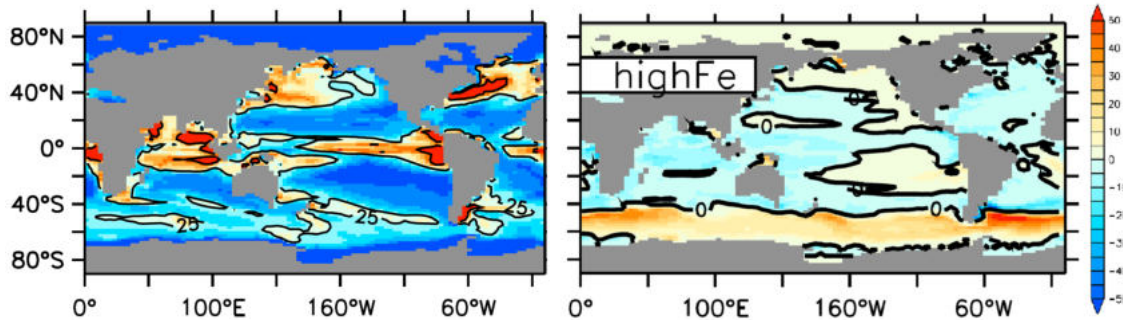


**Figure 5.2:** Global map of simulated export production in Muglia et al. (2017) default LGM simulation (left) and LGM\_highFe as difference from default LGM. Values in  $\text{gC}/\text{m}^2/\text{yr}$ . Adapted from Muglia et al. (2017), Figure 6.

improves underestimation of dust deposition in North America, Eurasia, the South Pacific, the SO and Antarctica compared to the model-only dust fluxes. Yamamoto et al. (2019) use these dust deposition experiments to study iron fertilization in the LGM by running a model-only as well as a glaciogenic dust flux case assuming 3% Fe solubility in glaciogenic dust ('LGM\_glac3%'). In the latter, Fe deposition at the ocean surface increases by up to an order of magnitude in the Arctic and the South Atlantic Ocean, and less prominently in the Indian and west Pacific Ocean south of  $30^\circ\text{S}$  (cf. Figure S3, Yamamoto et al. 2019). As a consequence of enhanced primary production in the SO, Yamamoto et al. (2019) report remarkable reductions in export production north of the iron-limited SO. The authors assign this to enhanced consumption of  $\text{NO}_3$  in the euphotic zone of the SO and subsequent transport of the negative nutrient anomaly to low latitudes.

Observed patterns of nutrient limitation in the standard versus additional glaciogenic dust scenario (cf. Figure 1, Yamamoto et al. 2019) agree well with modelled nutrient limitations in LGM5i (see Section 4.5, Figure 4.11) – despite the different approaches to increasing Fe input. In both models, macro-nutrients replace Fe as the primary limiting nutrient in the North and large parts of the east Pacific. Fe limitation is also slightly reduced in the SO. Increasing dust fluxes fivefold everywhere underestimates Patagonian sourced Fe deposition in the South Atlantic as modelled by Yamamoto et al. (2019). However, this is not reflected in patterns of nutrient limitation as this region is already more limited by N than Fe.

With the crucial role of N and P inventories in mind, it is particularly interesting to study the results of Yamamoto et al.'s (2019) additional sensitivity experiment which increases  $\text{NO}_3$  and  $\text{PO}_4$  by 15% globally ('LGM\_all'). This choice is justified by a recent model study that finds glacial dissolved P to have been 17 to 40% and

dissolved N to have been 16 % higher than pre-industrial (Wallmann et al. 2016). Enhanced nutrient availability in LGM<sub>all</sub> leads to a 10 % increase in global export production and generates an additional CO<sub>2</sub> decrease of 16 ppm. Rises in marine productivity occur from ~40 °N to 60 °S with largest increases in the Subantarctic. The northern oceans above 40 °N remain largely untouched by changes in the nutrient inventory (cf. Figure 3d, Yamamoto et al. 2019). Even if macro-nutrient concentrations in the glacial ocean were substantially higher than pre-industrial, the effect of nutrient trapping in the SO could only be mitigated slightly in the mid-latitudes and hardly in the high latitude Northern Hemisphere. This has implications for geo-engineered iron fertilization as a global warming remedy and future developments of primary productivity under a changing climate.

Moore et al. (2018) find global warming induced SO nutrient trapping in a transient CESM simulation from pre-industrial to 2300, resulting in declines of C export north of 30 °S by 41 %. In a future climate, the poleward shift of the westerlies, increasing SST and reduced sea ice cover drive marine productivity in the SO (Moore et al. 2018). As a consequence, export production declines globally north of 60 °S, except for the eastern tropical and northern North Pacific. Productivity increases in the Southern and the Pacific Ocean are outweighed by large decreases outside these HNLC regions. The authors attribute the increased eastern Pacific production to elevated Fe concentrations near the upwelling zone. Basin-scale nutrient distributions indicate that the signal of SO nutrient trapping would continue propagating northwards beyond 2300 (Moore et al. 2018). The initial North Pacific increase in export production might thus recede in the long term.

Despite the different time periods considered in this thesis and Moore et al. (2018), and thus differing physical fields and underlying mechanisms for enhanced SO productivity, the response of the global ocean to SO nutrient trapping is stunningly similar. To a certain degree, knowledge of the consequences of glacial SO iron fertilization seems transferable to future increases in SO marine productivity. On the other hand, the similarity of LGM and Anthropocene simulations might also allude to model deficiencies in the representation of glacial characteristics (see Section 5.3).

## 5.2 Comparison with Reconstructed Marine Productivity

Reconstructing export production from palaeoproxies is not trivial and prone to errors if one sole proxy is considered (see Section 2.2.2.1). Hence, the following col-

lation of observed LGM/Holocene export production ratios (see Figure 5.3) as summarised in Kohfeld et al. (2013) and extended by additional research in the equatorial Pacific (Costa et al. 2016, Durand et al. 2017), the North Atlantic (Bradtmitter et al. 2016, Demina et al. 2019) and the (Sub-)Antarctic Ocean (Martinez-Garcia et al. 2014, Thöle et al. 2019) differentiates between all reconstructions (left) and multi-proxy  $^{230}\text{Th}$  normalised evidence only (right).

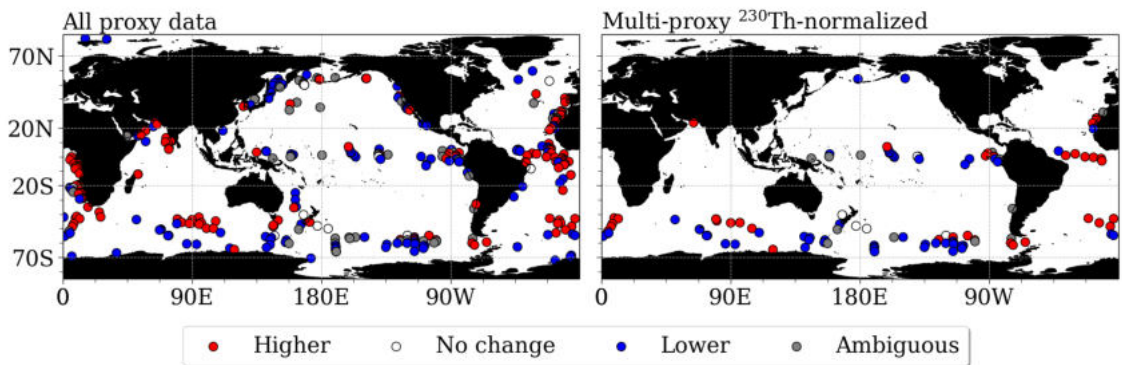


**Figure 5.3:** Reconstructions of C export in marine sediment cores, as summarised in Kohfeld et al. (2013) and derived from additional studies by Fukuda et al. (2013), Martinez-Garcia et al. (2014), Bradtmiller et al. (2016), Costa et al. (2016), Durand et al. (2017), Demina et al. (2019) and Thöle et al. (2019). Comparison of the LGM to the late Holocene for all studies (left) and  $^{230}\text{Th}$  normalised multi-proxy studies only (right).

The main unambiguous features of glacial C export in multi-proxy studies are lower values in the Antarctic Zone of the SO, the northern Pacific and large areas of the eastern equatorial Pacific Ocean. The Subantarctic Atlantic, North Indian and equatorial Atlantic Ocean are characterised by higher export production. Reconstructions from sediment cores at the eastern margin of the North Atlantic and Pacific Ocean as well as in the western equatorial Pacific are inconclusive. The uniformly increased productivity in the Subantarctic Ocean lends support to the hypothesis of nutrient trapping in the SO.

The comparison between reconstructed and simulated productivity is complicated by the differing points of reference. While reconstructions interpret C export fluxes in reference to the late Holocene, the thesis has focused on comparison of LGM simulations with different aeolian Fe scenarios. The following analysis shall close this gap by briefly discussing LGM-Holocene productivity changes in CESM in relation to reconstructions (see Figure 5.4).

The bimodal distribution of export production in the Southern Indian and Atlantic Ocean is reproduced well in LGM5i, to a lesser degree in LGMstd. In the

## 5.2. COMPARISON WITH RECONSTRUCTED MARINE PRODUCTIVITY

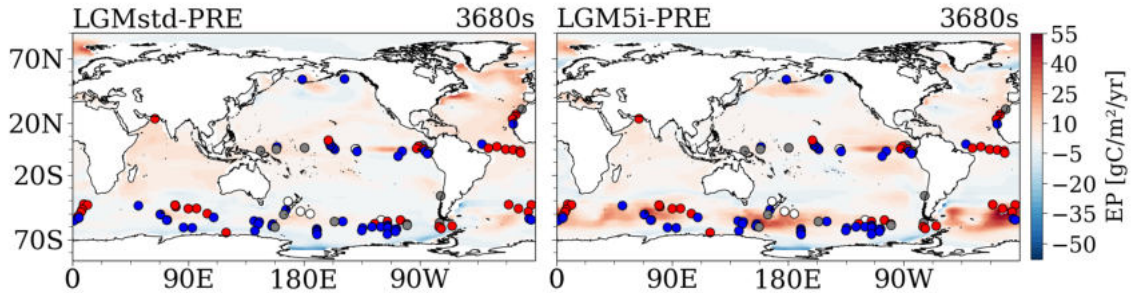


**Figure 5.4:** Global map of 10-year-mean changes in export production from LGMstd (left) and to LGM5i (right) compared to PRE in the 3680s. Circles indicate multi-proxy based reconstructions as in Figure 5.3.

Subantarctic Pacific, the zero line falls on the 60° latitude in both LGM simulations as expected from marine sediment cores.

In the equatorial Pacific, proxy studies seem to agree on (slightly) lower or unchanged productivity, aside from one core outside the upwelling zone (Costa et al. 2016), associated with unchanged  $\text{NO}_3$  consumption. Both LGM model simulations on the contrary display strong increases in export production in the equatorial Pacific. Outside the upwelling zone, LGMstd is in better agreement with reconstructions of lower productivity in the eastern Pacific, LGM5i with decreases in the central tropical Pacific.

Recent palaeoproxy studies often include further parameters besides export production to draw a broader picture of the interplay between marine productivity and glacial nutrient utilization. Martinez-Garcia et al. (2014) find that increases in dust flux and productivity are accompanied by increased  $\text{NO}_3$  consumption in the Subantarctic Atlantic. Despite overlaying effects of the potential equatorward movement of the Subantarctic Zone and an altered degree of  $\text{NO}_3$  consumption in the Antarctic Zone, this is uniquely consistent with the theory of dust-borne iron fertilization. In the Antarctic, glacial export production dropped while  $\text{NO}_3$  consumption increased, possibly due to a reduced deep-ocean supply (Studer et al. 2015).

Costa et al. (2016) hypothesise that this increased  $\text{NO}_3$  consumption in the Subantarctic SO acted to decrease nutrient export from SAMW formation regions and thus explains unchanged or lower productivity as well as an unchanged degree of  $\text{NO}_3$  consumption in the equatorial Pacific. If nutrient trapping in the SO was responsible for productivity changes in the Pacific Ocean, one would expect lower export production in the equatorial Pacific in LGM5i than LGMstd. The sensitivity experiment does find slightly decreased export production in a slim band of the

equatorial Pacific Ocean compared to LGMstd but increased productivity north and south of the equator. Depth transects of nutrient patterns in the CESM LGM5i simulation (see Section 4.4, Figure 4.10 & Appendix, Figure A.12) suggest that Costa et al.'s (2016) theory corresponds well to modelled nutrient concentrations in the Atlantic Ocean, but does not explain increasing export production and below-thermocline  $\text{PO}_4$  and  $\text{NO}_3$  enrichment in the tropical Pacific.

Nutrient trapping is not observed in LGMstd and hence could explain higher productivity than expected from reconstructions. LGM5i model simulations with increased Fe fluxes clearly display effects of nutrient trapping in the Southern and Deep Ocean and slightly lower productivity in the equatorial Pacific compared to LGMstd (see Section 4.1, Figure 4.3) but still elevated levels compared to PRE. Moreover, model results indicate that the effect of nutrient trapping is notably less relevant in the Pacific than in the Atlantic Ocean due to the underlying dynamics of lateral transport.

In CESM, levels of C fixation from  $\text{NO}_3$  by the largest phytoplankton are elevated in both glacial simulations (Appendix, Figure A.16). Diazotrophs and smaller phytoplankton reduce overall C fixation from  $\text{NO}_3$  in the tropical Pacific Ocean, but not enough to outcompete diatom increases and thus the general trend of enhanced  $\text{NO}_3$  based C fixation. While foraminifera-bound reconstructions of the degree of  $\text{NO}_3$  consumption and modelled C fixation from  $\text{NO}_3$  cannot be compared one-to-one, the overall trend of increased export production and increased  $\text{NO}_3$  based C fixation in the equatorial Pacific of both glacial simulations conflicts with proxy-based evidence of reduced marine productivity. CESM seems to have a positive bias compared to observations.

The majority of previous model studies implementing increased glacial dust fluxes are in agreement with reconstructed decreased export production in the glacial equatorial Pacific (e.g. Lambert et al. 2015, Buchanan et al. 2016, Muglia et al. 2017). CESM, however, exhibits a bias in this region. In contrast to expectations connected to a generally higher simulated  $\text{O}_2$  content compared to reconstructions (Jochum et al. submitted), this bias does not result from overestimated  $\text{N}_2$  fixation. Differences between pre-industrial and glacial diazotrophic N fixation in the equatorial Pacific are minor (Appendix, Figure A.17). However, uncertainties in modelled nutrient budgets might play a role for the bias in equatorial Pacific export production (see Section 5.3).

Both LGM simulations show distinct increases in northern North Pacific export production. Reconstructed lower LGM productivity lies outside the modelled max-

## 5.3. MODEL LIMITATIONS

---

ima. Kienast et al. (2004) argue that a highly stratified upper ocean, extensive sea ice and light limitation could be responsible for lacking evidence of iron fertilization in this HNLC region. Similarly, Gebhardt et al. (2008) hypothesise strong stratification to have inhibited the resupply of subsurface nutrients which proxies indicate to have been high in the eastern and western subarctic Pacific. LGM5i exhibits higher subsurface  $\text{PO}_4$  and  $\text{NO}_3$  concentrations in the North Pacific than LGMstd and higher export production (see Section 4.2, Figure 4.6). Either CESM underestimates stratification in the North Pacific or the choice of drilling location was unfortunate as it is not representative of the overall trend in glacial productivity.

In the Atlantic Ocean, reconstructions paint an ambiguous picture. Western margin productivity is enhanced in regions of modern coastal upwelling (Bradt Miller et al. 2016) which is equally reproduced by both LGM simulations. The equatorial region lacks a clear signal across the entire width of the ocean basin. Bradt Miller et al. (2007) argue that their results of increased marine productivity in the eastern equatorial region is in line with previous studies and admit conflicting reconstructions in the western equatorial Atlantic. LGMstd productivity in this region is slightly above pre-industrial values, LGM5i slightly below as one would expect from enhanced SO nutrient consumption and thus reduced lateral transfer to the Atlantic Ocean north of  $30^\circ\text{S}$ .

The glacial CESM simulations are in good agreement with reconstructions where multiple studies paint a coherent picture, namely the Antarctic and Subantarctic and the North Indian Ocean. In the equatorial and North Pacific as well as in large areas of the Atlantic Ocean studied proxies do not agree. These ambiguous observations become slightly clearer if only multi-proxy  $^{230}\text{Th}$  normalised studies are considered but still partially conflict with theoretical considerations on the effect of iron fertilization in the SO which is estimated to be responsible for about three-quarters of marine productivity north of  $30^\circ\text{S}$  (Sarmiento et al. 2004). On the other hand, modelled patterns of LGM productivity underlie parametrisation and modelling choices that might also introduce biases into e.g. nutrient distributions or bioavailability of Fe.

## 5.3 Model Limitations

### 5.3.1 Physical Model

The CESM version employed in this thesis originally includes a new overflow parametrisation of the Nordic Seas, i.e. the Denmark Strait and Faroe Bank Channel,

as well as of Antarctic Ross and Weddell Sea (Danabasoglu et al. 2010, Briegleb et al. 2010). This representation of density driven flows through narrow straits and channels and their subsequent injection into abyssal waters substantially reduces the shallow penetration depth bias of NADW (Danabasoglu et al. 2010). As the overflow parametrisation has not been fitted to appropriately capture palaeoceanography, it is disabled in CESM, re-introducing a strong topographic barrier in the Nordic Seas (Danabasoglu et al. 2010). This might produce an excessively strong response of northern North Atlantic nutrient concentrations with pronounced reductions in all depths north of  $60^\circ\text{N}$  because missing overflow hampers the exchange of water masses across the Greenland-Scotland ridge (see Section 4.3, Figure 4.8 & Appendix, Figure A.10).

On the other hand, several studies of the LGM physical ocean state (e.g. Rahmstorf 2013, Howe et al. 2016, Du et al. 2020) suggest a southward shift of NADW formation which would similarly result in a more self-contained Arctic Atlantic. The residual MOC in the LGM CESM simulations does not exhibit such a shift (Jochum et al. submitted). Hence, the topographically isolated subpolar North Atlantic might accurately represent the glacially confined Nordic Seas, but for the wrong reasons.

Further discrepancies between the modelled and observed glacial ocean are higher  $\text{O}_2$  contents and a higher ventilation rate of the abyssal ocean compared to pre-industrial in contrast to reconstructions (Jochum et al. submitted). The challenges of model-observation comparisons and implications of a better ventilated and oxygenated glacial ocean for DIC levels have already been discussed in Jochum et al. (submitted). Simulated  $\text{O}_2$  concentrations also interact closely with the N cycle through denitrification in oxygen-poor regions (Moore et al. 2013a). If CESM underestimated LGM OMZs, reduced denitrification would result in overestimation of N availability for phytoplankton growth. However, a larger LGM/PRE ratio of marine  $\text{O}_2$  than expected does not necessarily mean that LGM simulations are unrealistic. It could also result from the documented excessively large subsurface OMZs in PRE (Lindsay et al. 2014, Jochum et al. submitted).

### 5.3.2 Macro-Nutrient Cycles

The modern N cycle in BEC exhibits negative  $\text{NO}_3$  biases as a consequence of small imbalances of N sources and sinks (Moore et al. 2013a). Riverine N input and sedimentary losses due to denitrification and burial are not implemented in the model. The interglacial ocean loses  $\text{N}_2$  on the long-term (Moore et al. 2013a). Water column denitrification exceeds current estimates due to largely overestimated OMZs

### 5.3. MODEL LIMITATIONS

---

(Lindsay et al. 2014). In an effort to achieve a more realistic representation of the modern N cycle, Moore et al. (2013a) use a constant scaling factor which reduces denitrification by more than 50 %, allowing simulated N to nearly balance. With this parametrisation of the N cycle fitted to modern observations, caution should be exercised when studying N dynamics in the context of climate change (Moore et al. 2013a). Manually downscaling denitrification increases N concentrations. However, global macro-nutrient patterns in CESM do not hint at an overestimation of  $\text{NO}_3$  compared to  $\text{PO}_4$  at the LGM. Due to the well oxygenated glacial ocean, denitrification is confined to negligibly small areas and manual downscaling thus does not change phytoplankton N limitation.

Further modelling choices affecting global nutrient distributions are prescribed remineralization curves with a fixed length scale applied to sinking organic matter (Moore et al. 2004). This overestimates the vertical distribution of  $\text{PO}_4$  and DIC at mid-depths and underestimates it below  $\sim 1000$  m in the modern ocean (Moore et al. 2013a). If upper ocean  $\text{PO}_4$  remineralization is also overestimated in LGM simulations, this might partially explain positive upper ocean  $\text{PO}_4$  anomalies in regions of high glacial export production, namely the North and eastern subtropical and tropical Pacific.

In BEC, soft POM has one uniform remineralization length scale which depends only on ambient temperatures (Moore et al. 2004). In reality, remineralization varies by particle, with generally longer length scales for minerals compared to macro-nutrients (Boyd et al. 2017), and further depends on i.a.  $\text{O}_2$  concentrations (Laufkötter et al. 2017) and depth (Kriest and Oschlies 2008). Besides assigning a temperature and  $\text{O}_2$  dependent length scale for each nutrient, parametrisation of remineralization could be improved by implementing a depth dependent remineralization rate, i.e. a length scale increasing with depth in conjunction with size-dependent sinking speeds based on surface particle size spectra (Kriest and Oschlies 2008). A longer remineralization length scale for Fe would reduce upper ocean concentrations and thus the effect of iron fertilization. The strength of this impact, especially in view of other partially counter-acting parametrization choices of the Fe cycle (see following Section), cannot be quantified. In the modern ocean, Moore et al. (2013a) suppose that depth dependent remineralization curves would reduce positive biases in  $\text{PO}_4$  and DIC and negative biases in  $\text{O}_2$  at mid-depth. Glacial  $\text{PO}_4$  reductions would not affect iron fertilization as it is N, not  $\text{PO}_4$ , that limits phytoplankton growth.

A first step towards a more sophisticated parametrisation of remineralization was

taken in CESM2, the successor of CESM1 (Danabasoglu et al. 2020). The updated biogeochemistry module MARBL implements variable C/N/P stoichiometry of the DOM pool, allowing for variable production and remineralization rates of DOM (Letscher et al. 2015). Additionally, MARBL breaks with the constant C/N/P stoichiometry of phytoplankton in Moore et al. (2004) by introducing variable C/P ratios as a function of ambient  $\text{PO}_4$  concentration (Galbraith and Martiny 2015). Both parametrisations are based on modern marine observational data and should thus be treated with caution when applied to glacial simulations. The effect of a variable C/N/P stoichiometry on glacial  $\text{CO}_2$  sequestration, however, is non negligible. Weber and Deutsch (2010) estimate that higher C/P ratios in the glacial SO due to phytoplankton community shifts would reduce atmospheric  $\text{CO}_2$  by 15 ppm.

### 5.3.3 Marine Iron Biogeochemistry

Understanding of the Fe cycle in the ocean has advanced significantly in the past decade, painting an increasingly comprehensive picture of sources, sinks and their dynamical interactions (Tagliabue et al. 2017). Major simplifying assumptions on marine Fe biogeochemistry in the early BEC model (Moore et al. 2002b) have been revised by Moore and Braucher (2008) to include desorption of dissolved Fe, an improved scavenging parametrisation and an elaborated sedimentary source. However, the model lacks a more sophisticated representation of several critical components of the Fe cycle.

BEC implements continental margins and shelf sediments as well as atmospheric deposition as external Fe sources (Moore and Braucher 2008). While parametrisation of the former has been improved since Moore et al. (2002b), the assumption of 3.5 % Fe content by weight in mineral dust with a constant 2 % solubility has not been revisited. Moore et al. (2002, 2004) explain their choice by a global mean 2 % solubility (Jickells and Spokes 2001) and the lack of information to develop a global parametrisation (Fung et al. 2000). In recent years, such global scale datasets have been compiled (Sholkovitz et al. 2012) and improved methodologies of modelling atmospheric soluble Fe have been proposed (Hamilton et al. 2019). As the performed CESM simulations have shown, atmospheric Fe deposition plays a crucial role for the LGM climate. Besides assumptions on Fe content in dust and its solubility, this also includes the estimation of the land-atmosphere flux.

Dust mobilisation in CESM is based on a mineral aerosol entrainment and deposition module which is embedded in a chemical transport model (Zender et al. 2003). Comparison with satellite and in situ observations showed that the model

### 5.3. MODEL LIMITATIONS

---

predicts mineral aerosol distributions in the period from 1979 to 2000 well (Luo et al. 2003) and captures trends and magnitude of glacial dust deposition (Albani et al. 2016). In some regions, however, the model deviates from reconstructions by up to an order of magnitude (Albani et al. 2016). LGM dust deposition fluxes in CESM are overestimated in Antarctica and Greenland, and underestimated in the equatorial Pacific.

Atmospheric dust fluxes and Fe solubility are closely interwoven. How uncertainties in the former propagate into soluble Fe deposition depends on the underlying assumptions of the latter, e.g. assigning a constant 2% Fe solubility as in Moore et al. (2002b), implementing size dependence or modelling it as a function of total aerosol Fe load (Albani et al. 2016). Assuming a constant 2% Fe solubility, the uncertainties in dust fluxes translate into higher deposition of soluble Fe in the central and North Atlantic and lower deposition in the equatorial Pacific compared to observations (Albani et al. 2016). In the SO, CESM results are at the lower end of observationally constrained estimates. Here, excessively large dust deposition might not translate into higher soluble Fe fluxes as a 2% solubility is not representative of the LGM Antarctic and Subantarctic Ocean. Reconstructions of Fe solubility in the glacial SO found a mean LGM value of 10% (Conway et al. 2015).

The uncertainty in modelled land-atmosphere dust fluxes together with the influential assumptions on Fe solubility calls for a revision of the parametrisation of the atmospheric Fe source. A more realistic and regionally differentiated representation of dust-borne, soluble Fe would move the SO more towards the LGM5i scenario. Even if CESM currently overestimates dust fluxes in Antarctica compared to reconstructions, this effect seems to be overcompensated by a too-low solubility (Albani et al. 2016). In other key regions, it is hard to predict how an improved parametrisation of dust fluxes would interact with revised Fe solubility.

Besides dust-borne and sedimentary sourced Fe, hydrothermal activity (Tagliabue et al. 2010), riverine inflow (Rijkenberg et al. 2014, Krachler et al. 2019) and sea ice (Lannuzel et al. 2016) are important external sources on regional to global scales, not incorporated in BEC. A global ocean circulation model coupled with a biogeochemical model including hydrothermal vents assigns a minor but not insignificant role to the hydrothermal Fe source at the LGM (Muglia et al. 2017). The authors point out that model limitations and uncertain knowledge of Fe biogeochemistry do not allow a robust estimate of the role of different Fe sources in a glacial climate. This emphasises that future work is necessary to further explore the contribution of different external Fe sources to LGM ocean fertilization.

Another crucial component of the marine Fe cycle are organic ligands, exerting control over regeneration and scavenging (Boyd and Ellwood 2010). In BEC, the effect of ligands on scavenging is included implicitly: scavenging rates increase rapidly at high values of dissolved Fe, when Fe assumedly exceeds ligand concentrations, and progressively decreases at low values of dissolved Fe, accounting for reduced scavenging losses due to iron-complexing ligands (Moore and Braucher 2008). However, biogeochemical models are very sensitive to changes in ligand concentrations (Tagliabue et al. 2014). Doubling concentrations in a pre-industrial ESM simulation yields an additional 10 ppm CO<sub>2</sub> drawdown as well as a 10% higher PO<sub>4</sub> consumption in the euphotic zone (Parekh et al. 2008). Iron-binding ligands maintain the soluble Fe stock and might enhance solubility of particulate and colloidal Fe (Gledhill and Buck 2012). Explicitly including ligand dynamics in BEC would be computationally expensive but could improve simulations of the ocean Fe cycle (Moore and Braucher 2008). If standing stocks of dissolved Fe were higher due to iron-complexing ligands, this would further reduce Fe limitation in HNLC regions and enhance phytoplankton growth. Simultaneously, increasing consumption of macro-nutrients in the SO would limit marine productivity outside these regions.

Phytoplankton exhibit substantial variations in their stoichiometry, i.e. the Fe consumption relative to C or PO<sub>4</sub> (Sunda and Huntsman 1997, Twining and Baines 2013). This is partially accounted for by variable Fe/C ratios for phytoplankton depending on ambient Fe concentrations (Moore et al. 2004) but could be elaborated further by distinguishing between diatoms and small phytoplankton. Additionally, zooplankton's stoichiometry in BEC is assumed fixed. Recent studies have shown Fe quotas to decrease with increasing zooplankton size (Baines et al. 2015) or depend on food quality (Chen et al. 2014). Furthermore, the model assumes fixed Redfield ratios within phytoplankton groups and zooplankton: Variable elemental ratios in Moore et al. (2002b) were replaced by fixed C/N/P ratios in Moore et al. (2004), reducing the computational effort markedly. While it might be computationally costly to re-introduce variable elemental ratios, its role for glacial export production is non-negligible (Matsumoto et al. 2020). Allowing for flexible C/N/P stoichiometry in a glacial ESM simulation increases C export by 20% compared to the classical Redfield ratio (Matsumoto et al. 2020).

Lastly, there is growing evidence that phytoplankton are able to acquire non-dissolved Fe, especially under Fe limited conditions (Strzepek et al. 2011). While this might be less relevant for glacial simulations of a more abundant Fe inventory, it points to the relevance of Fe bioavailability for phytoplankton growth. BEC assumes

### 5.3. MODEL LIMITATIONS

---

the complete dissolved Fe pool to be bioavailable (Moore et al. 2004). Bioavailability thus directly depends on the strength of sedimentary and mineral dust sources where considerable uncertainties persist (Moore and Braucher 2008). Recent analysis of dust-borne Fe speciation in marine sediments of the Subantarctic Ocean revealed that the total Fe flux was only 3 to 5 times higher during the LGM but highly bioavailable Fe(II) increased by a factor of  $\sim 15$  to 20 (Shoenfelt et al. 2018). Higher glacial bioavailability would further fuel SO productivity but simultaneously reduce the lateral transport of macro-nutrients.

To some extent, the LGM sensitivity simulation with fivefold increased Fe fluxes corresponds better to observations and theory (Costa et al. 2016, Sarmiento et al. 2004) than the standard LGM run. Nutrient trapping does not occur in LGMstd (Appendix, Figure A.9), in contrast to increasing evidence of a glacial SO control on global nutrient distributions. As LGM5i shows, Fe deposition to the ocean plays a crucial role in modulating marine productivity and nutrient distributions. Several levers exist to improve representation of the Fe cycle in the model, some of which have already been tested with CESM (e.g. improved dust parametrisation (Albani et al. 2014), incorporation of sea ice bearing Fe (Wang et al. 2014) and atmospheric Fe processing (Hamilton et al. 2019)). Among the most important changes would be a variable Fe solubility that reflects glacial-interglacial as well as regional discrepancies, and an improved parametrisation of iron-complexing ligands.

Besides Fe, the role of other minerals acting as micro-nutrients to marine productivity receives increasing attention (Moore et al. 2013b). Enrichment experiments, as those performed by the founder of the iron fertilization theory, John H. Martin (1988, 1990), found co-limitation of Fe not only with N and P (North et al. 2007), but also with N and cobalt (Browning et al. 2017) as well as with manganese (Pausch et al. 2019). These minerals are not yet reflected in common ocean biogeochemistry models but could provide further insights into the impact of mineral elements on ocean biogeochemistry in a glacial climate. Research is only beginning to understand the multiple interactions between trace metals and vitamins concerning phytoplankton growth (Browning et al. 2018, Koch and Trimborn 2019) and thus cannot predict the role of other micro-nutrients and vitamins for glacial iron fertilization.

Despite the shortcomings discussed above, CESM1's overall pattern and magnitude of export production in response to glacial iron fertilization agree well with recent studies employing biogeochemical ocean models. The effect on atmospheric CO<sub>2</sub> drawdown of 15 ppm (Jochum et al. submitted) is in the range of estimates of 4 to

23 ppm opened up by Muglia et al. (2017) and Nickelsen and Oschlies (2015). The effect of nutrient trapping in the SO is visible in studies increasing Fe deposition only in the SO (Oka et al. 2011, Muglia et al. 2017) as well as in sensitivity experiments trying to improve the representation of glacial dust fluxes globally (Yamamoto et al. 2019). SO nutrient trapping is a robust finding across models and dust flux representations but remains limited to sensitivity tests. This calls for improved parametrisation of the glacial Fe cycle and nutrient dynamics in ESMs.

## 6 Conclusion

The coupled, biogeochemistry-enabled Community Earth System Model (CESM) version 1.0 has been employed to study the effect of glacial iron fertilization by airborne dust as one possible explanation for increased binding of atmospheric CO<sub>2</sub> at the Last Glacial Maximum (LGM). A standard LGM simulation (LGMstd) was compared to a sensitivity run with globally fivefold increased aeolian dust fluxes (LGM5i).

Analysis of the temporal relationship between increases in dust-borne iron (Fe) and marine export production reveal a dichotomous response between High-Nutrient Low-Chlorophyll (HNLC) regions and the rest of the global ocean. Export production increases in large areas during the first 10 years after quintupling dust fluxes, especially in the Southern Ocean (SO), the eastern and North Pacific as well as in the North Atlantic Ocean. Within the following centennials, however, immediately enhanced marine productivity recedes or reverses outside HNLC regions and areas with neutral or negative responses exhibit further declines.

Over the course of the simulation, macro-nutrients enrich in the Southern and Deep Ocean and decrease in the upper ocean north of the SO. Upper ocean declines are most pronounced in the Atlantic Ocean, followed by the Indian Ocean and to a lesser degree by the Pacific Ocean. In the subpolar North Atlantic decreased nutrient concentrations reach well below 2000 m, while all other ocean basins exhibit increasing macro-nutrients with depth.

On short timescales, relieved Fe limitation due to increased aeolian dust fluxes stimulate marine productivity in large areas of the LGM ocean. Iron fertilization in the nutrient-rich SO continues to enhance export production in the following centennials. Resulting higher consumption of macro-nutrients in the Subantarctic Ocean has major implications for export production north of 30°S, transferring phosphate (PO<sub>4</sub>) and nitrate (NO<sub>3</sub>) to the deep ocean and reducing the lateral transport of these macro-nutrients in all ocean basins. The SO's crucial role as a nutrient provider to the global ocean weakens substantially as nutrients are stripped out of surface waters and transferred to the deep ocean. On longer timescales,

declining macro-nutrient concentrations act to reduce export production outside nutrient-rich HNLC regions.

The effect of SO nutrient trapping is especially strong in the North Atlantic, and to a lesser degree in the West Pacific and Indian Ocean where rising nutrient deficiencies limit phytoplankton growth. In the nutrient-rich northern and eastern equatorial Pacific thermocline nutrients decline slightly but not enough to hinder biological production. Diatoms and small phytoplankton thrive in this generally nutrient-rich environment that is less dependent on SO thermocline nutrient export than the North Atlantic.

Increasing export production in the Southern and parts of the Pacific Ocean outweigh declines outside these HNLC regions, so that C export in LGM5i is about 4.6 % higher than in LGMstd, yielding an additional  $\sim 15$  ppm reduction of atmospheric CO<sub>2</sub>. This is in line with previous studies, but only about a quarter of the proposed 40 ppm by Watson et al. (2000). The observed effect of SO nutrient trapping under glacial iron fertilization suggests an upper bound to the estimates. Similar sensitivity tests of stimulated SO biological production report an additional CO<sub>2</sub> sequestration of 9 to 24 ppm, depending on the inclusion of a decreased sedimentary iron source (Muglia et al. 2017), and 15.6 ppm in Yamamoto et al. (2019). Even if glacial Fe fluxes to the SO were higher than assumed in the sensitivity experiments, global export production and thus CO<sub>2</sub> sequestration do neither increase linearly nor infinitely with increasing Fe fluxes, as they are limited by nutrient availability that is to a large degree set by the SO.

The performed simulations provide a good estimate of the magnitude of the iron fertilization effect at the LGM and elucidate the underlying mechanisms and interplay of marine biogeochemistry and ocean dynamics. Certain revisions of model parametrisation would further contribute to a deeper understanding of the glacial Fe cycle, such as the implementation of atmospheric Fe processing, variable solubility and dynamic ligand concentrations. The crucial importance of the first two has been shown in the sensitivity experiment LGM5i that develops nutrient trapping in response to enhanced SO export production as expected from theory and observations (Sarmiento et al. 2004, Costa et al. 2016). In simulations of the modern ocean, changes to ligand concentrations had a greater effect on atmospheric CO<sub>2</sub> sequestration than dust or hydrothermal sources (Tagliabue et al. 2014). What role did ligand dynamics play in the LGM ocean? How can sensitivity experiments be reconciled with their standard counterpart via inclusion of further essential Fe dynamics?

The implementation of additional and revision of existing parametrisations in all

---

concerned model components could maximise the potential arising from the use of a coupled, biogeochemistry-enabled ESM. CESM simulations of glacial iron fertilization go beyond previous approaches that run ocean-only models (Lambert et al. 2015) or incorporate simplified atmospheric modules and thus rely on external dust fields (Muglia et al. 2017). Modelling the interactions between atmosphere, ocean, land, ice, and biosphere and their combined role for phytoplankton iron fertilization comes with its own challenges but enables a holistic view of the underlying dynamics.

In his early formulation of the iron hypothesis Martin (1990) assigns “iron availability [...] to have been a player; [...] whether it had lead role or a bit part” (Martin 1990, p. 10). In line with previous research, the CESM simulations analysed in this thesis suggest that the magnitude of the effect of glacial iron fertilization is, if not a lead role, a substantial contributor to marine CO<sub>2</sub> sequestration at the LGM. Martin was right with his hypothesis that Fe enrichment in the SO could enhance phytoplankton growth markedly, leading to a greater use of upwelled nutrients, and that this productivity contributed to atmospheric CO<sub>2</sub> drawdown. However, he did not oversee the implications of enhanced SO biological production for phytoplankton growth north of it. In this line, it is fortunate that his wildest dream did not come true: “the ultimate enrichment experiment: [...] fertilization of the whole southern ocean with 430 000 tons of Fe”.

# Bibliography

- Abelmann, A., R. Gersonde, G. Knorr, X. Zhang, B. Chaplignin, E. Maier, O. Esper, H. Friedrichsen, G. Lohmann, H. Meyer and R. Tiedemann (2015). “The seasonal sea-ice zone in the glacial Southern Ocean as a carbon sink”. In: *Nature Communications* 6.1. DOI: 10.1038/ncomms9136.
- Adkins, J. F. (2013). “The role of deep ocean circulation in setting glacial climates”. In: *Paleoceanography* 28.3, pp. 539–561. DOI: 10.1002/palo.20046.
- Albani, S., N. M. Mahowald, L. N. Murphy, R. Raiswell, J. K. Moore, R. F. Anderson, D. McGee, L. I. Bradtmiller, B. Delmonte, P. P. Hesse and P. A. Mayewski (2016). “Paleodust variability since the Last Glacial Maximum and implications for iron inputs to the ocean”. In: *Geophysical Research Letters* 43.8, pp. 3944–3954. DOI: 10.1002/2016GL067911.
- Albani, S., N. M. Mahowald, A. T. Perry, R. A. Scanza, C. S. Zender, N. G. Heavens, V. Maggi, J. F. Kok and B. L. Otto-Bliesner (2014). “Improved dust representation in the Community Atmosphere Model”. In: *Journal of Advances in Modeling Earth Systems* 6.3, pp. 541–570. DOI: 10.1002/2013ms000279.
- Anderson, R. F., J. P. Sachs, M. Q. Fleisher, K. A. Allen, J. Yu, A. Koutavas and S. L. Jaccard (2019). “Deep-Sea Oxygen Depletion and Ocean Carbon Sequestration During the Last Ice Age”. In: *Global Biogeochemical Cycles* 33.3, pp. 301–317. DOI: 10.1029/2018gb006049.
- Annan, J. D. and J. C. Hargreaves (2013). “A new global reconstruction of temperature changes at the Last Glacial Maximum”. In: *Climate of the Past* 9.1, pp. 367–376. DOI: 10.5194/cp-9-367-2013.
- Archer, D. and E. Maier-Reimer (1994). “Effect of deep-sea sedimentary calcite preservation on atmospheric CO<sub>2</sub> concentration”. In: *Nature* 367.6460, pp. 260–263. DOI: 10.1038/367260a0.
- Archer, D. E. and K. Johnson (2000). “A model of the iron cycle in the ocean”. In: *Global Biogeochemical Cycles* 14.1, pp. 269–279. DOI: 10.1029/1999gb900053.
- Baines, S. B., X. Chen, B. S. Twining, N. S. Fisher and M. R. Landry (2015). “Factors affecting Fe and Zn contents of mesozooplankton from the Costa Rica Dome”. In: *Journal of Plankton Research* 38.2, pp. 331–347. DOI: 10.1093/plankt/fbv098.
- Baker, A. R. and P. L. Croot (2010). “Atmospheric and marine controls on aerosol iron solubility in seawater”. In: *Marine Chemistry* 120.1-4, pp. 4–13. DOI: 10.1016/j.marchem.2008.09.003.

## BIBLIOGRAPHY

---

- Beardall, J., D. Allen, J. Bragg, Z. V. Finkel, K. J. Flynn, A. Quigg, T. A. V. Rees, A. Richardson and J. A. Raven (2009). “Allometry and stoichiometry of unicellular, colonial and multicellular phytoplankton”. In: *New Phytologist* 181.2, pp. 295–309. DOI: <https://doi.org/10.1111/j.1469-8137.2008.02660.x>.
- Bereiter, B., S. Shackleton, D. Baggenstos, K. Kawamura and J. Severinghaus (2018). “Mean global ocean temperatures during the last glacial transition”. In: *Nature* 553.7686, pp. 39–44. DOI: [10.1038/nature25152](https://doi.org/10.1038/nature25152).
- Berger, A., M.-F. Loutre and C. Tricot (1993). “Insolation and Earth’s orbital periods”. In: *Journal of Geophysical Research* 98.D6, p. 10341. DOI: [10.1029/93jd00222](https://doi.org/10.1029/93jd00222).
- Binney, H., M. Edwards, M. Macias-Fauria, A. Lozhkin, P. Anderson, J. O. Kaplan, A. Andreev, E. Bezrukova, T. Blyakharchuk, V. Jankovska, I. Khazina, S. Krivonogov, K. Kremenetski, J. Nield, E. Novenko, N. Ryabogina, N. Solovieva, K. Willis and V. Zernitskaya (2017). “Vegetation of Eurasia from the last glacial maximum to present: Key biogeographic patterns”. In: *Quaternary Science Reviews* 157, pp. 80–97. ISSN: 0277-3791. DOI: <https://doi.org/10.1016/j.quascirev.2016.11.022>.
- Bopp, L., K. E. Kohfeld, C. L. Quéré and O. Aumont (2003). “Dust impact on marine biota and atmospheric CO<sub>2</sub> during glacial periods”. In: *Paleoceanography* 18.2. DOI: [10.1029/2002pa000810](https://doi.org/10.1029/2002pa000810).
- Bouttes, N., D. Paillard, D. M. Roche, V. Brovkin and L. Bopp (2011). “Last Glacial Maximum CO<sub>2</sub> and  $\delta^{13}\text{C}$  successfully reconciled”. In: *Geophysical Research Letters* 38.2. DOI: [10.1029/2010gl044499](https://doi.org/10.1029/2010gl044499).
- Boyd, P. W. and M. J. Ellwood (2010). “The biogeochemical cycle of iron in the ocean”. In: *Nature Geoscience* 3.10, pp. 675–682. DOI: [10.1038/ngeo964](https://doi.org/10.1038/ngeo964).
- Boyd, P. W., M. J. Ellwood, A. Tagliabue and B. S. Twining (2017). “Biotic and abiotic retention, recycling and remineralization of metals in the ocean”. In: *Nature Geoscience* 10.3, pp. 167–173. DOI: [10.1038/ngeo2876](https://doi.org/10.1038/ngeo2876).
- Bradt Miller, L. I., R. F. Anderson, M. Q. Fleisher and L. H. Burckle (2007). “Opal burial in the equatorial Atlantic Ocean over the last 30 ka: Implications for glacial-interglacial changes in the ocean silicon cycle”. In: *Paleoceanography* 22.4. DOI: [10.1029/2007pa001443](https://doi.org/10.1029/2007pa001443).
- Bradt Miller, L. I., D. McGee, M. Awalt, J. Evers, H. Yerxa, C. W. Kinsley and P. B. deMenocal (2016). “Changes in biological productivity along the northwest African margin over the past 20,000 years”. In: *Paleoceanography* 31.1, pp. 185–202. DOI: [10.1002/2015pa002862](https://doi.org/10.1002/2015pa002862).

## BIBLIOGRAPHY

---

- Briegleb, B., G. Danabasoglu and W. Large (2010). *An Overflow Parameterization for the ocean component of the Community Climate System Model*. Tech. rep. DOI: 10.5065/D69K4863.
- Brovkin, V., A. Ganopolski, D. Archer and S. Rahmstorf (2007). “Lowering of glacial atmospheric CO<sub>2</sub> in response to changes in oceanic circulation and marine biogeochemistry”. In: *Paleoceanography* 22.4. DOI: 10.1029/2006pa001380.
- Browning, T. J., I. Rapp, C. Schlosser, M. Gledhill, E. P. Achterberg, A. Bracher and F. A. C. L. Moigne (2018). “Influence of Iron, Cobalt, and Vitamin B12 Supply on Phytoplankton Growth in the Tropical East Pacific During the 2015 El Niño”. In: *Geophysical Research Letters* 45. DOI: 10.1029/2018GL07797.
- Browning, T. J., E. P. Achterberg, I. Rapp, A. Engel, E. M. Bertrand, A. Tagliabue and C. M. Moore (2017). “Nutrient co-limitation at the boundary of an oceanic gyre”. In: *Nature* 551.7679, pp. 242–246. DOI: 10.1038/nature24063.
- Bryan, K. and L. J. Lewis (1979). “A water mass model of the World Ocean”. In: *Journal of Geophysical Research* 84.C5, p. 2503. DOI: 10.1029/jc084ic05p02503.
- Brzezinski, M. A., C. J. Pride, V. M. Franck, D. M. Sigman, J. L. Sarmiento, K. Matsumoto, N. Gruber, G. H. Rau and K. H. Coale (2002). “A switch from Si(OH)<sub>4</sub> to NO<sub>3</sub>-depletion in the glacial Southern Ocean”. In: *Geophysical Research Letters* 29.12. DOI: 10.1029/2001gl1014349.
- Buchanan, P. J., R. J. Matear, A. Lenton, S. J. Phipps, Z. Chase and D. M. Etheridge (2016). “The simulated climate of the Last Glacial Maximum and insights into the global marine carbon cycle”. In: *Climate of the Past* 12.12, pp. 2271–2295. DOI: 10.5194/cp-12-2271-2016.
- Chen, X., N. S. Fisher and S. B. Baines (2014). “Influence of algal iron content on the assimilation and fate of iron and carbon in a marine copepod”. In: *Limnology and Oceanography* 59.1, pp. 129–140. DOI: 10.4319/lo.2014.59.1.0129.
- Chikamoto, M. O., A. Abe-Ouchi, A. Oka and S. L. Smith (2012). “Temperature-induced marine export production during glacial period”. In: *Geophysical Research Letters* 39.21. DOI: 10.1029/2012gl1053828.
- Clark, P. U., A. S. Dyke, J. D. Shakun, A. E. Carlson, J. Clark, B. Wohlfarth, J. X. Mitrovica, S. W. Hostetler and A. M. McCabe (2009). “The Last Glacial Maximum”. In: *Science* 325.5941, pp. 710–714. DOI: 10.1126/science.1172873.
- Clark, P. U. and A. C. Mix (2002). “Ice sheets and sea level of the Last Glacial Maximum”. In: *Quaternary Science Reviews* 21.1-3, pp. 1–7. DOI: 10.1016/S0277-3791(01)00118-4.

## BIBLIOGRAPHY

---

- Clayton, S., P. Gaube, T. Nagai, M. M. Omand and M. Honda (2017). “Fine-scale biophysical controls on nutrient supply, phytoplankton community structure, and carbon export in western boundary current regions”. en. In: *Frontiers in western boundary current research*. Ed. by K. Uhlenbrock. Vol. 15. 4. U.S. CLIVAR Project Office, pp. 17–21. DOI: 10.5065/D6SJ1JB2.
- Conway, T. M., E. W. Wolff, R. Röthlisberger, R. Mulvaney and H. E. Elderfield (2015). “Constraints on soluble aerosol iron flux to the Southern Ocean at the Last Glacial Maximum”. In: *Nature Communications* 6.1. DOI: 10.1038/ncomms8850.
- Costa, K. M., J. F. McManus, R. F. Anderson, H. Ren, D. M. Sigman, G. Winckler, M. Q. Fleisher, F. Marcantonio and A. C. Ravelo (2016). “No iron fertilization in the equatorial Pacific Ocean during the last ice age”. In: *Nature* 529.7587, pp. 519–522. DOI: 10.1038/nature16453.
- Danabasoglu, G., J.-F. Lamarque, J. Bacmeister, D. A. Bailey, A. K. DuVivier, J. Edwards, L. K. Emmons, J. Fasullo, R. Garcia, A. Gettelman, C. Hannay, M. M. Holland, W. G. Large, P. H. Lauritzen, D. M. Lawrence, J. T. M. Lenaerts, K. Lindsay, W. H. Lipscomb, M. J. Mills, R. Neale, K. W. Oleson, B. Otto-Bliesner, A. S. Phillips, W. Sacks, S. Tilmes, L. Kampenhout, M. Vertenstein, A. Bertini, J. Dennis, C. Deser, C. Fischer, B. Fox-Kemper, J. E. Kay, D. Kinnison, P. J. Kushner, V. E. Larson, M. C. Long, S. Mickelson, J. K. Moore, E. Nienhouse, L. Polvani, P. J. Rasch and W. G. Strand (2020). “The Community Earth System Model Version 2 (CESM2)”. In: *Journal of Advances in Modeling Earth Systems* 12.2. DOI: 10.1029/2019ms001916.
- Danabasoglu, G., S. C. Bates, B. P. Briegleb, S. R. Jayne, M. Jochum, W. G. Large, S. Peacock and S. G. Yeager (2012). “The CCSM4 Ocean Component”. In: *Journal of Climate* 25.5, pp. 1361–1389. DOI: 10.1175/jcli-d-11-00091.1.
- Danabasoglu, G., W. G. Large and B. P. Briegleb (2010). “Climate impacts of parameterized Nordic Sea overflows”. In: *Journal of Geophysical Research* 115.C11. DOI: 10.1029/2010jc006243.
- Delmas, R. J., J.-M. Ascencio and M. Legrand (1980). “Polar ice evidence that atmospheric CO<sub>2</sub> 20,000 yr BP was 50% of present”. In: *Nature* 284.5752, pp. 155–157. DOI: 10.1038/284155a0.
- Delmonte, B., J. Petit and V. Maggi (2002). “Glacial to Holocene implications of the new 27000-year dust record from the EPICA Dome C (East Antarctica) ice core”. In: *Climate Dynamics* 18.8, pp. 647–660. DOI: 10.1007/s00382-001-0193-9.

## BIBLIOGRAPHY

---

- Demina, Novichkova, Lisitzin and Kozina (2019). “Geochemical Signatures of Paleoclimate Changes in the Sediment Cores from the Gloria and Snorri Drifts (Northwest Atlantic) over the Holocene-Mid Pleistocene”. In: *Geosciences* 9.10, p. 432. DOI: 10.3390/geosciences9100432.
- Dezileau, L., J. L. Reyss and F. Lemoine (2003). “Late Quaternary changes in biogenic opal fluxes in the Southern Indian Ocean”. In: *Marine Geology* 202.3-4, pp. 143–158. DOI: 10.1016/s0025-3227(03)00283-4.
- Du, J., B. A. Haley and A. C. Mix (2020). “Evolution of the Global Overturning Circulation since the Last Glacial Maximum based on marine authigenic neodymium isotopes”. In: *Quaternary Science Reviews* 241, p. 106396. DOI: 10.1016/j.quascirev.2020.106396.
- Du, J., B. A. Haley, A. C. Mix, M. H. Walczak and S. K. Praetorius (2018). “Flushing of the deep Pacific Ocean and the deglacial rise of atmospheric CO<sub>2</sub> concentrations”. In: *Nature Geoscience* 11.10, pp. 749–755. DOI: 10.1038/s41561-018-0205-6.
- Durand, A., Z. Chase, T. L. Noble, H. Bostock, S. L. Jaccard, P. Kitchener, A. T. Townsend, N. Jansen, L. Kinsley, G. Jacobsen, S. Johnson and H. Neil (2017). “Export production in the New-Zealand region since the Last Glacial Maximum”. In: *Earth and Planetary Science Letters* 469, pp. 110–122. DOI: 10.1016/j.epsl.2017.03.035.
- Dutkiewicz, S., P. Cermeno, O. Jahn, M. J. Follows, A. E. Hickman, D. A. A. Taniguchi and B. A. Ward (2020). “Dimensions of marine phytoplankton diversity”. In: *Biogeosciences* 17.3, pp. 609–634. DOI: 10.5194/bg-17-609-2020.
- “Eighty years of Redfield” (2014). In: *Nature Geoscience* 7.12, pp. 849–849. DOI: 10.1038/ngeo2319.
- Emerson, D. (2019). “Biogenic Iron Dust: A Novel Approach to Ocean Iron Fertilization as a Means of Large Scale Removal of Carbon Dioxide From the Atmosphere”. In: *Frontiers in Marine Science* 6. DOI: 10.3389/fmars.2019.00022.
- Fasham, M. J. R., H. Ducklow and S. M. McKelvie (1990). “A nitrogen-based model of plankton dynamics in the oceanic mixed layer”. In: *Journal of Marine Research* 48, pp. 591–639. DOI: 10.1357/002224090784984678.
- Felip, M. and J. Catalan (2000). “The relationship between phytoplankton biovolume and chlorophyll in a deep oligotrophic lake: decoupling in their spatial and temporal maxima”. In: *Journal of Plankton Research* 22.1, pp. 91–106. DOI: 10.1093/plankt/22.1.91.

## BIBLIOGRAPHY

---

- Finkel, Z. V. (2014). “Marine Net Primary Production”. In: *Global Environmental Change*. Ed. by B. Freedman. Dordrecht: Springer Netherlands, pp. 117–124. ISBN: 978-94-007-5784-4. DOI: 10.1007/978-94-007-5784-4\_42.
- Fitzsimmons, K. E., S. B. Marković and U. Hambach (2012). “Pleistocene environmental dynamics recorded in the loess of the middle and lower Danube basin”. In: *Quaternary Science Reviews* 41, pp. 104–118. DOI: 10.1016/j.quascirev.2012.03.002.
- Freilich, M. A. and A. Mahadevan (2019). “Decomposition of Vertical Velocity for Nutrient Transport in the Upper Ocean”. In: *Journal of Physical Oceanography* 49.6, pp. 1561–1575. DOI: 10.1175/jpo-d-19-0002.1.
- Fuhrer, K., E. W. Wolff and S. J. Johnsen (1999). “Timescales for dust variability in the Greenland Ice Core Project (GRIP) ice core in the last 100,000 years”. In: *Journal of Geophysical Research: Atmospheres* 104.D24, pp. 31043–31052. DOI: 10.1029/1999jd900929.
- Fukuda, M., N. Harada, M. Sato, C. Lange, N. Ahagon, H. Kawakami, W. Miyashita, S. Pantoja, T. Matsumoto and I. Motoyama (2013). “<sup>230</sup>Th-normalized fluxes of biogenic components from the central and southernmost Chilean margin over the past 22,000 years”. In: *Geochemical Journal* 47, pp. 119–135.
- Fung, I. Y., S. K. Meyn, I. Tegen, S. C. Doney, J. G. John and J. K. B. Bishop (2000). “Iron supply and demand in the upper ocean”. In: *Global Biogeochemical Cycles* 14.1, pp. 281–295. DOI: 10.1029/1999gb900059.
- Galbraith, E. D. and A. C. Martiny (2015). “A simple nutrient-dependence mechanism for predicting the stoichiometry of marine ecosystems”. In: *Proceedings of the National Academy of Sciences* 112.27, pp. 8199–8204. DOI: 10.1073/pnas.1423917112.
- Galbraith, E. D. and L. C. Skinner (2020). “The Biological Pump During the Last Glacial Maximum”. In: *Annual Review of Marine Science* 12.1, pp. 559–586. DOI: 10.1146/annurev-marine-010419-010906.
- Ganeshram, R. S., T. F. Pedersen, S. Calvert and R. Francois (2002). “Reduced nitrogen fixation in the glacial ocean inferred from changes in marine nitrogen and phosphorus inventories”. In: *Nature* 415.6868, pp. 156–159. DOI: 10.1038/415156a.
- Ganopolski, A. and V. Brovkin (2017). “Simulation of climate, ice sheets and CO<sub>2</sub> evolution during the last four glacial cycles with an Earth system model of intermediate complexity”. In: *Climate of the Past* 13.12, pp. 1695–1716. DOI: 10.5194/cp-13-1695-2017.

## BIBLIOGRAPHY

---

- Gebhardt, H., M. Sarnthein, P. M. Grootes, T. Kiefer, H. Kuehn, F. Schmieder and U. Röhl (2008). “Paleonutrient and productivity records from the subarctic North Pacific for Pleistocene glacial terminations I to V”. In: *Paleoceanography* 23.4. DOI: 10.1029/2007pa001513.
- Gent, P. R., G. Danabasoglu, L. J. Donner, M. M. Holland, E. C. Hunke, S. R. Jayne, D. M. Lawrence, R. B. Neale, P. J. Rasch, M. Vertenstein, P. H. Worley, Z.-L. Yang and M. Zhang (2011). “The Community Climate System Model Version 4”. In: *Journal of Climate* 24.19, pp. 4973–4991. DOI: 10.1175/2011jcli4083.1.
- Gledhill, M. and K. N. Buck (2012). “The organic complexation of iron in the marine environment: a review”. In: *Frontiers in Microbiology* 3. DOI: 10.3389/fmicb.2012.00069.
- Glock, N., Z. Erdem, K. Wallmann, C. J. Somes, V. Liebetrau, J. Schönfeld, S. Gorb and A. Eisenhauer (2018). “Coupling of oceanic carbon and nitrogen facilitates spatially resolved quantitative reconstruction of nitrate inventories”. In: *Nature Communications* 9.1. DOI: 10.1038/s41467-018-03647-5.
- Gruber, N. (2008). “The Marine Nitrogen Cycle: Overview and Challenges”. In: *Nitrogen in the Marine Environment (Second Edition)*. Ed. by D. G. Capone, D. A. Bronk, M. R. Mulholland and E. J. Carpenter. Second Edition. San Diego: Academic Press, pp. 1–50. ISBN: 978-0-12-372522-6. DOI: 10.1016/B978-0-12-372522-6.00001-3. URL: <http://www.sciencedirect.com/science/article/pii/B9780123725226000013>.
- Gu, S., Z. Liu, D. W. Oppo, J. Lynch-Stieglitz, A. Jahn, J. Zhang and L. Wu (2020). “Assessing the potential capability of reconstructing glacial Atlantic water masses and AMOC using multiple proxies in CESM”. In: *Earth and Planetary Science Letters* 541, p. 116294. DOI: 10.1016/j.epsl.2020.116294.
- Hain, M. P., D. M. Sigman and G. H. Haug (2014). “The Biological Pump in the Past”. In: *Treatise on Geochemistry*. Elsevier, pp. 485–517. DOI: 10.1016/b978-0-08-095975-7.00618-5.
- Hain, M. P., D. M. Sigman and G. H. Haug (2010). “Carbon dioxide effects of Antarctic stratification, North Atlantic Intermediate Water formation, and sub-antarctic nutrient drawdown during the last ice age: Diagnosis and synthesis in a geochemical box model”. In: *Global Biogeochemical Cycles* 24.4. DOI: 10.1029/2010gb003790.
- Hamilton, D. S., R. A. Scanza, Y. Feng, J. Guinness, J. F. Kok, L. Li, X. Liu, S. D. Rathod, J. S. Wan, M. Wu and N. M. Mahowald (2019). “Improved methodologies for Earth system modelling of atmospheric soluble iron and observation

## BIBLIOGRAPHY

---

- comparisons using the Mechanism of Intermediate complexity for Modelling Iron (MIMI v1.0)". In: *Geoscientific Model Development* 12.9, pp. 3835–3862. DOI: 10.5194/gmd-12-3835-2019.
- Hammer, C. U., H. B. Clausen, W. Dansgaard, A. Neftel, P. Kristinsdottir and E. Johnson (1985). "Continuous impurity analysis along the Dye 3 deep core". In: *Greenland Ice Core: Geophysics, Geochemistry, and the Environment*. American Geophysical Union, pp. 90–94. DOI: 10.1029/gm033p0090.
- Harrison, D. P. (2017). "Global negative emissions capacity of ocean macronutrient fertilization". In: *Environmental Research Letters* 12.3, p. 035001. DOI: 10.1088/1748-9326/aa5ef5.
- Harrison, S. P., K. E. Kohfeld, C. Roelandt and T. Claquin (2001). "The role of dust in climate changes today, at the last glacial maximum and in the future". In: *Earth-Science Reviews* 54.1-3, pp. 43–80. DOI: 10.1016/s0012-8252(01)00041-1.
- Harrisson, S. P. and C. I. Prentice (2003). "Climate and CO<sub>2</sub> controls on global vegetation distribution at the last glacial maximum: analysis based on palaeovegetation data, biome modelling and palaeoclimate simulations". In: *Global Change Biology* 9.7, pp. 983–1004. DOI: 10.1046/j.1365-2486.2003.00640.x.
- Hartin, C. A., R. A. Fine, B. M. Sloyan, L. D. Talley, T. K. Chereskin and J. Happell (2011). "Formation rates of Subantarctic mode water and Antarctic intermediate water within the South Pacific". In: *Deep Sea Research Part I: Oceanographic Research Papers* 58.5, pp. 524–534. DOI: 10.1016/j.dsr.2011.02.010.
- Heine, K. B., A. Abebe, A. E. Wilson and W. R. Hood (2019). "Copepod respiration increases by 7% per °C increase in temperature: A meta-analysis". In: *Limnology and Oceanography Letters* 4.3, pp. 53–61. DOI: 10.1002/lol2.10106.
- Heinemann, M., J. Segschneider and B. Schneider (2019). "CO<sub>2</sub> drawdown due to particle ballasting by glacial aeolian dust: an estimate based on the ocean carbon cycle model MPIOM/HAMOCC version 1.6.2p3". In: *Geoscientific Model Development* 12.5, pp. 1869–1883. DOI: 10.5194/gmd-12-1869-2019.
- Hendry, K., O. Romero and V. Pashley (2020). "Nutrient utilization and diatom productivity changes in the low-latitude SE Atlantic over the past 70 kyr: Response to Southern Ocean leakage". In: *Climate of the Past*. DOI: 10.5194/cp-2020-115.
- Hendry, K. R., X. Gong, G. Knorr, J. Pike and I. R. Hall (2016). "Deglacial diatom production in the tropical North Atlantic driven by enhanced silicic acid supply". In: *Earth and Planetary Science Letters* 438, pp. 122–129. DOI: 10.1016/j.epsl.2016.01.016.

## BIBLIOGRAPHY

---

- Howe, J. N. W., A. M. Piotrowski, T. L. Noble, S. Mulitza, C. M. Chiessi and G. Bayon (2016). “North Atlantic Deep Water Production during the Last Glacial Maximum”. In: *Nature Communications* 7.1. DOI: 10.1038/ncomms11765.
- Huang, H., M. Gutjahr, A. Eisenhauer and G. Kuhn (2020). “No detectable Weddell Sea Antarctic Bottom Water export during the Last and Penultimate Glacial Maximum”. In: *Nature Communications* 11.1. DOI: 10.1038/s41467-020-14302-3.
- Hughes, P. D., P. L. Gibbard and J. Ehlers (2013). “Timing of glaciation during the last glacial cycle: evaluating the concept of a global ‘Last Glacial Maximum’ (LGM)”. In: *Earth-Science Reviews* 125, pp. 171–198. DOI: 10.1016/j.earscirev.2013.07.003.
- Huot, Y., M. Babin, F. Bruyant, C. Grob, M. S. Twardowski and H. Claustre (2007). “Does chlorophyll a provide the best index of phytoplankton biomass for primary productivity studies?” In: *Biogeosciences Discussions, European Geosciences Union* 4.2, pp. 707–745.
- Hurrell, J. W., M. M. Holland, P. R. Gent, S. Ghan, J. E. Kay, P. J. Kushner, J.-F. Lamarque, W. G. Large, D. Lawrence, K. Lindsay, W. H. Lipscomb, M. C. Long, N. Mahowald, D. R. Marsh, R. B. Neale, P. Rasch, S. Vavrus, M. Vertenstein, D. Bader, W. D. Collins, J. J. Hack, J. Kiehl and S. Marshall (2013). “The Community Earth System Model: A Framework for Collaborative Research”. In: *Bulletin of the American Meteorological Society* 94.9, pp. 1339–1360. DOI: 10.1175/bams-d-12-00121.1.
- Ilyina, T., K. D. Six, J. Segschneider, E. Maier-Reimer, H. Li and I. Nunez-Riboni (2013). “Global ocean biogeochemistry model HAMOCC: Model architecture and performance as component of the MPI-Earth system model in different CMIP5 experimental realizations”. In: *Journal of Advances in Modeling Earth Systems* 5.2, pp. 287–315. DOI: 10.1029/2012ms000178.
- Jayne, S. R. (2009). “The Impact of Abyssal Mixing Parameterizations in an Ocean General Circulation Model”. In: *Journal of Physical Oceanography* 39.7, pp. 1756–1775. DOI: 10.1175/2009jpo4085.1.
- Jickells, T. and L. Spokes (2001). “Atmospheric iron inputs to the oceans”. In: *Biogeochemistry of Iron in Seawater*. Ed. by D. R. Turner and K. A. Hunter. John Wiley, Hoboken, N. J., pp. 85–121.
- Jochum, M., G. Vettoretti, R. Nuterman and Z. Chase (submitted). “Carbon pools in a Last Glacial Maximum integration of a fully coupled Earth system model”. In: *Paleoceanography and Paleoclimatology*.

## BIBLIOGRAPHY

---

- Johnson, K. S., R. M. Gordon and K. H. Coale (1997). “What controls dissolved iron concentrations in the world ocean?” In: *Marine Chemistry* 57.3-4, pp. 137–161. DOI: 10.1016/s0304-4203(97)00043-1.
- Üjvári, G., T. Stevens, M. Molnár, A. Demény, F. Lambert, G. Varga, A. J. T. Jull, B. Páll-Gergely, J.-P. Buylaert and J. Kovács (2017). “Coupled European and Greenland last glacial dust activity driven by North Atlantic climate”. In: *Proceedings of the National Academy of Sciences* 114.50, E10632–E10638. DOI: 10.1073/pnas.1712651114.
- Kienast, S. S., M. Kienast, S. Jaccard, S. E. Calvert and R. François (2006). “Testing the silica leakage hypothesis with sedimentary opal records from the eastern equatorial Pacific over the last 150 kyrs”. In: *Geophysical Research Letters* 33.15. DOI: 10.1029/2006gl026651.
- Kienast, S. S., I. L. Hendy, J. Crusius, T. F. Pedersen and S. E. Calvert (2004). “Export Production in the Subarctic North Pacific over the Last 800 kyrs: No Evidence for Iron Fertilization?” In: *Journal of Oceanography* 60.1, pp. 189–203. DOI: 10.1023/b:joce.0000038326.73943.aa.
- Kim, S.-J. and Y.-G. Park (2008). “Glacial ocean circulation and property changes in the North Pacific”. In: *Atmosphere-Ocean* 46.2, pp. 257–275. DOI: 10.3137/ao.460205.
- Koch, F. and S. Trimborn (2019). “Limitation by Fe, Zn, Co, and B12 Results in Similar Physiological Responses in Two Antarctic Phytoplankton Species”. In: *Frontiers in Marine Science* 6. DOI: 10.3389/fmars.2019.00514.
- Kohfeld, K. and S. P. Harrison (2003). “Glacial-interglacial changes in dust deposition on the Chinese Loess Plateau”. In: *Quaternary Science Reviews* 22.18-19, pp. 1859–1878. DOI: 10.1016/s0277-3791(03)00166-5.
- Kohfeld, K. E., R. M. Graham, A. M. de Boer, L. C. Sime, E. W. Wolff, C. L. Quéré and L. Bopp (2013). “Southern Hemisphere westerly wind changes during the Last Glacial Maximum: paleo-data synthesis”. In: *Quaternary Science Reviews* 68, pp. 76–95. DOI: 10.1016/j.quascirev.2013.01.017.
- Kohfeld, K. E. and A. Ridgwell (2009). “Glacial-interglacial variability in atmospheric CO<sub>2</sub>”. In: *Surface Ocean-Atmosphere Processes*. American Geophysical Union, pp. 251–286. DOI: 10.1029/2008gm000845.
- Kok, J. F., S. Albani, N. M. Mahowald and D. S. Ward (2014). “An improved dust emission model – Part 2: Evaluation in the Community Earth System Model, with implications for the use of dust source functions”. In: *Atmospheric Chemistry and Physics* 14.23, pp. 13043–13061. DOI: 10.5194/acp-14-13043-2014.

## BIBLIOGRAPHY

---

- Kowalski, E. A. and P. A. Meyers (1997). “Glacial-interglacial variations in Quaternary production of marine organic matter at DSDP Site 594, Chatham Rise, southeastern New Zealand margin”. In: *Marine Geology* 140.3-4, pp. 249–263. DOI: 10.1016/S0025-3227(97)00044-3.
- Krachler, R., R. Krachler, A. Valda and B. K. Keppler (2019). “Natural iron fertilization of the coastal ocean by “blackwater rivers””. In: *Science of The Total Environment* 656, pp. 952–958. DOI: 10.1016/j.scitotenv.2018.11.423.
- Kremer, C. T., M. K. Thomas and E. Litchman (2017). “Temperature- and size-scaling of phytoplankton population growth rates: Reconciling the Eppley curve and the metabolic theory of ecology”. In: *Limnology and Oceanography* 62.4, pp. 1658–1670. DOI: 10.1002/lno.10523.
- Kriest, I. and A. Oschlies (2008). “On the treatment of particulate organic matter sinking in large-scale models of marine biogeochemical cycles”. In: *Biogeosciences* 5.1, pp. 55–72. DOI: 10.5194/bg-5-55-2008.
- Lamarque, J.-F., T. C. Bond, V. Eyering, C. Granier, A. Heil, Z. Klimont, D. Lee, C. Liousse, A. Mieville, B. Owen, M. G. Schultz, D. Shindell, S. J. Smith, E. Stehfest, J. V. Aardenne, O. R. Cooper, M. Kainuma, N. Mahowald, J. R. McConnell, V. Naik, K. Riahi and D. P. van Vuuren (2010). “Historical (1850–2000) gridded anthropogenic and biomass burning emissions of reactive gases and aerosols: methodology and application”. In: *Atmospheric Chemistry and Physics* 10.15, pp. 7017–7039. DOI: 10.5194/acp-10-7017-2010.
- Lambert, F., B. Delmonte, J. R. Petit, M. Bigler, P. R. Kaufmann, M. A. Hutterli, T. F. Stocker, U. Ruth, J. P. Steffensen and V. Maggi (2008). “Dust-climate couplings over the past 800,000 years from the EPICA Dome C ice core”. In: *Nature* 452.7187, pp. 616–619. DOI: 10.1038/nature06763.
- Lambert, F., A. Tagliabue, G. Shaffer, F. Lamy, G. Winckler, L. Farias, L. Gallardo and R. D. Pol-Holz (2015). “Dust fluxes and iron fertilization in Holocene and Last Glacial Maximum climates”. In: *Geophysical Research Letters* 42.14, pp. 6014–6023. DOI: 10.1002/2015gl064250.
- Lannuzel, D., M. Vancoppenolle, P. van der Merwe, J. de Jong, K. M. Meiners, M. Grotti, J. Nishioka and V. Schoemann (2016). “Iron in sea ice: Review and new insights”. In: *Elementa: Science of the Anthropocene* 4, p. 000130. DOI: 10.12952/journal.elementa.000130.
- Lauderdale, J. M., R. Braakman, G. Forget, S. Dutkiewicz and M. J. Follows (2020). “Microbial feedbacks optimize ocean iron availability”. In: *Proceedings of the*

## BIBLIOGRAPHY

---

- National Academy of Sciences* 117.9, pp. 4842–4849. DOI: 10.1073/pnas.1917277117.
- Laufkötter, C., J. G. John, C. A. Stock and J. P. Dunne (2017). “Temperature and oxygen dependence of the remineralization of organic matter”. In: *Global Biogeochemical Cycles* 31.7, pp. 1038–1050. DOI: 10.1002/2017gb005643.
- Lefèvre, N. and A. J. Watson (1999). “Modeling the geochemical cycle of iron in the oceans and its impact on atmospheric CO<sub>2</sub> concentrations”. In: *Global Biogeochemical Cycles* 13.3, pp. 727–736. DOI: 10.1029/1999gb900034.
- Legrand, M. R., C. Lorius, N. I. Barkov and V. N. Petrov (1988). “Vostok (Antarctica) ice core: Atmospheric chemistry changes over the last climatic cycle (160,000 years)”. In: *Atmospheric Environment (1967)* 22.2, pp. 317–331. DOI: 10.1016/0004-6981(88)90037-6.
- Letscher, R. T., J. K. Moore, Y.-C. Teng and F. Primeau (2015). “Variable C : N : P stoichiometry of dissolved organic matter cycling in the Community Earth System Model”. In: *Biogeosciences* 12.1, pp. 209–221. DOI: 10.5194/bg-12-209-2015.
- Letscher, R. T., F. Primeau and J. K. Moore (2016). “Nutrient budgets in the subtropical ocean gyres dominated by lateral transport”. In: *Nature Geoscience* 9.11, pp. 815–819. DOI: 10.1038/ngeo2812.
- Leynaert, A., E. Bucciarelli, P. Claquin, R. C. Dugdale, V. Martin-Jézéquel, P. Pondaven and O. Ragueneau (2004). “Effect of iron deficiency on diatom cell size and silicic acid uptake kinetics”. In: *Limnology and Oceanography* 49.4, pp. 1134–1143. DOI: 10.4319/lo.2004.49.4.1134.
- Lindsay, K., G. B. Bonan, S. C. Doney, F. M. Hoffman, D. M. Lawrence, M. C. Long, N. M. Mahowald, J. K. Moore, J. T. Randerson and P. E. Thornton (2014). “Preindustrial-Control and Twentieth-Century Carbon Cycle Experiments with the Earth System Model CESM1(BGC)”. In: *Journal of Climate* 27.24, pp. 8981–9005. DOI: 10.1175/jcli-d-12-00565.1.
- Loubere, P., F. Mekik, R. Francois and S. Pichat (2004). “Export fluxes of calcite in the eastern equatorial Pacific from the Last Glacial Maximum to present”. In: *Paleoceanography* 19.2. DOI: 10.1029/2003pa000986.
- Lu, H., S. Yi, Z. Xu, Y. Zhou, L. Zeng, F. Zhu, H. Feng, L. Dong, H. Zhuo, K. Yu, J. Mason, X. Wang, Y. Chen, Q. Lu, B. Wu, Z. Dong, J. Qu, X. Wang and Z. Guo (2013). “Chinese deserts and sand fields in Last Glacial Maximum and Holocene Optimum”. In: *Chinese Science Bulletin* 58.23, pp. 2775–2783. DOI: 10.1007/s11434-013-5919-7.

## BIBLIOGRAPHY

---

- Luo, C., N. M. Mahowald and J. del Corral (2003). “Sensitivity study of meteorological parameters on mineral aerosol mobilization, transport, and distribution”. In: *Journal of Geophysical Research: Atmospheres* 108.D15. DOI: 10.1029/2003JD003483.
- Mahowald, N., K. Kohfeld, M. Hansson, Y. Balkanski, S. P. Harrison, I. C. Prentice, M. Schulz and H. Rodhe (1999). “Dust sources and deposition during the last glacial maximum and current climate: A comparison of model results with paleodata from ice cores and marine sediments”. In: *Journal of Geophysical Research: Atmospheres* 104.D13, pp. 15895–15916. DOI: 10.1029/1999jd900084.
- Mahowald, N. M., D. R. Muhs, S. Levis, P. J. Rasch, M. Yoshioka, C. S. Zender and C. Luo (2006). “Change in atmospheric mineral aerosols in response to climate: Last glacial period, preindustrial, modern, and doubled carbon dioxide climates”. In: *Journal of Geophysical Research: Atmospheres* 111.D10. DOI: 10.1029/2005jd006653.
- Marchant, R., A. Cleef, S. P. Harrison, H. Hooghiemstra, V. Markgraf, J. van Boxel, T. Ager, L. Almeida, R. Anderson, C. Baied, H. Behling, J. C. Berrio, R. Burbridge, S. Björck, R. Byrne, M. Bush, J. Duivenvoorden, J. Flenley, P. D. Oliveira, B. van Geel, K. Graf, W. D. Gosling, S. Harbele, T. van der Hammen, B. Hansen, S. Horn, P. Kuhry, M.-P. Ledru, F. Mayle, B. Leyden, S. Lozano-Garcia, A. M. Melief, P. Moreno, N. T. Moar, A. Prieto, G. van Reenen, M. Salgado-Labouriau, F. Schäbitz, E. J. Schreve-Brinkman and M. Wille (2009). “Pollen-based biome reconstructions for Latin America at 0, 6000 and 18 000 radiocarbon years ago”. In: *Climate of the Past* 5.4, pp. 725–767. DOI: 10.5194/cp-5-725-2009.
- Martin, J. H. (1990). “Glacial-interglacial CO<sub>2</sub> change: The Iron Hypothesis”. In: *Paleoceanography* 5.1, pp. 1–13. DOI: 10.1029/pa005i001p00001.
- Martin, J. H. and S. E. Fitzwater (1988). “Iron deficiency limits phytoplankton growth in the north-east Pacific subarctic”. In: *Nature* 331.6154, pp. 341–343. DOI: 10.1038/331341a0.
- Martin, J. H., S. E. Fitzwater and R. M. Gordon (1990). “Iron deficiency limits phytoplankton growth in Antarctic waters”. In: *Global Biogeochemical Cycles* 4.1, pp. 5–12. DOI: 10.1029/gb004i001p00005.
- Martin, J. H., M. Gordon and S. E. Fitzwater (1991). “The case for iron”. In: *Limnology and Oceanography* 36.8, pp. 1793–1802. DOI: <https://doi.org/10.4319/10.1991.36.8.1793>.

## BIBLIOGRAPHY

---

- Martinez-Garcia, A., D. M. Sigman, H. Ren, R. F. Anderson, M. Straub, D. A. Hodell, S. L. Jaccard, T. I. Eglinton and G. H. Haug (2014). “Iron Fertilization of the Subantarctic Ocean During the Last Ice Age”. In: *Science* 343.6177, pp. 1347–1350. DOI: 10.1126/science.1246848.
- Matsumoto, K. (2007). “Biology-mediated temperature control on atmospheric pCO<sub>2</sub> and ocean biogeochemistry”. In: *Geophysical Research Letters* 34.20. DOI: 10.1029/2007g1031301.
- Matsumoto, K., J. L. Sarmiento and M. A. Brzezinski (2002). “Silicic acid leakage from the Southern Ocean: A possible explanation for glacial atmospheric pCO<sub>2</sub>”. In: *Global Biogeochemical Cycles* 16.3. DOI: <https://doi.org/10.1029/2001GB001442>.
- Matsumoto, K., T. Tanioka and R. Rickaby (2020). “Linkages Between Dynamic Phytoplankton C:N:P and the Ocean Carbon Cycle Under Climate Change”. In: *Oceanography* 33.2. DOI: 10.5670/oceanog.2020.203.
- Menviel, L., F. Joos and S. P. Ritz (2012). “Simulating atmospheric CO<sub>2</sub>,  $\delta^{13}\text{C}$  and the marine carbon cycle during the Last Glacial-Interglacial cycle: possible role for a deepening of the mean remineralization depth and an increase in the oceanic nutrient inventory”. In: *Quaternary Science Reviews* 56, pp. 46–68. DOI: 10.1016/j.quascirev.2012.09.012.
- Menviel, L., J. Yu, F. Joos, A. Mouchet, K. J. Meissner and M. H. England (2017). “Poorly ventilated deep ocean at the Last Glacial Maximum inferred from carbon isotopes: A data-model comparison study”. In: *Paleoceanography* 32.1, pp. 2–17. DOI: 10.1002/2016pa003024.
- Mix, A. C., E. Bard and R. Schneider (2001). “Environmental processes of the ice age: land, oceans, glaciers (EPILOG)”. In: *Quaternary Science Reviews* 20.4, pp. 627–657. DOI: 10.1016/s0277-3791(00)00145-1.
- Moore, C. M., M. M. Mills, K. R. Arrigo, I. Berman-Frank, L. Bopp, P. W. Boyd, E. D. Galbraith, R. J. Geider, C. Guieu, S. L. Jaccard, T. D. Jickells, J. L. Roche, T. M. Lenton, N. M. Mahowald, E. Maraón, I. Marinov, J. K. Moore, T. Nakatsuka, A. Oschlies, M. A. Saito, T. F. Thingstad, A. Tsuda and O. Ulloa (2013b). “Processes and patterns of oceanic nutrient limitation”. In: *Nature Geoscience* 6.9, pp. 701–710. DOI: 10.1038/ngeo1765.
- Moore, J. K. and O. Braucher (2008). “Sedimentary and mineral dust sources of dissolved iron to the world ocean”. In: *Biogeosciences* 5.3, pp. 631–656. DOI: 10.5194/bg-5-631-2008.

## BIBLIOGRAPHY

---

- Moore, J. K. and S. C. Doney (2007). “Iron availability limits the ocean nitrogen inventory stabilizing feedbacks between marine denitrification and nitrogen fixation”. In: *Global Biogeochemical Cycles* 21.2. DOI: 10.1029/2006gb002762.
- Moore, J. K., S. C. Doney, D. M. Glover and I. Y. Fung (2002a). “Iron cycling and nutrient-limitation patterns in surface waters of the World Ocean”. In: *Deep Sea Research Part II: Topical Studies in Oceanography* 49.1-3, pp. 463–507. DOI: 10.1016/s0967-0645(01)00109-6.
- Moore, J. K., S. C. Doney, J. A. Kleypas, D. M. Glover and I. Y. Fung (2002b). “An intermediate complexity marine ecosystem model for the global domain”. In: *Deep Sea Research Part II: Topical Studies in Oceanography* 49.1-3, pp. 403–462. DOI: 10.1016/s0967-0645(01)00108-4.
- Moore, J. K., S. C. Doney and K. Lindsay (2004). “Upper ocean ecosystem dynamics and iron cycling in a global three-dimensional model”. In: *Global Biogeochemical Cycles* 18.4. DOI: 10.1029/2004gb002220.
- Moore, J. K., W. Fu, F. Primeau, G. L. Britten, K. Lindsay, M. Long, S. C. Doney, N. Mahowald, F. Hoffman and J. T. Randerson (2018). “Sustained climate warming drives declining marine biological productivity”. In: *Science* 359.6380, pp. 1139–1143. DOI: 10.1126/science.aao6379.
- Moore, J. K., K. Lindsay, S. C. Doney, M. C. Long and K. Misumi (2013a). “Marine Ecosystem Dynamics and Biogeochemical Cycling in the Community Earth System Model [CESM1(BGC)]: Comparison of the 1990s with the 2090s under the RCP4.5 and RCP8.5 Scenarios”. In: *Journal of Climate* 26.23, pp. 9291–9312. DOI: 10.1175/jcli-d-12-00566.1.
- Moran, M. A., E. B. Kujawinski, A. Stubbins, R. Fatland, L. I. Aluwihare, A. Buchan, B. C. Crump, P. C. Dorrestein, S. T. Dyhrman, N. J. Hess, B. Howe, K. Longnecker, P. M. Medeiros, J. Niggemann, I. Obernosterer, D. J. Repeta and J. R. Waldbauer (2016). “Deciphering ocean carbon in a changing world”. In: *Proceedings of the National Academy of Sciences* 113.12, pp. 3143–3151. DOI: 10.1073/pnas.1514645113.
- Moreno, A. R. and A. C. Martiny (2018). “Ecological Stoichiometry of Ocean Plankton”. In: *Annual Review of Marine Science* 10.1, pp. 43–69. DOI: 10.1146/annurev-marine-121916-063126.
- Mortlock, R. A., C. D. Charles, P. N. Froelich, M. A. Zibello, J. Saltzman, J. D. Hays and L. H. Burckle (1991). “Evidence for lower productivity in the Antarctic Ocean during the last glaciation”. In: *Nature* 351.6323, pp. 220–223. DOI: 10.1038/351220a0.

## BIBLIOGRAPHY

---

- Muglia, J., C. J. Somes, L. Nickelsen and A. Schmittner (2017). “Combined Effects of Atmospheric and Seafloor Iron Fluxes to the Glacial Ocean”. In: *Paleoceanography* 32.11, pp. 1204–1218. DOI: 10.1002/2016pa003077.
- Muhs, D. R., M. A. Prins and B. Machalett (2014). “Loess as a Quaternary paleoenvironmental indicator”. In: *Past Global Changes Magazine* 22.2, pp. 84–85. DOI: 10.22498/pages.22.2.84.
- Neftel, A., H. Oeschger, J. Schwander, B. Stauffer and R. Zimbrunn (1982). “Ice core sample measurements give atmospheric CO<sub>2</sub> content during the past 40,000 yr”. In: *Nature* 295.5846, pp. 220–223. DOI: 10.1038/295220a0.
- Nickelsen, L. and A. Oschlies (2015). “Enhanced sensitivity of oceanic CO<sub>2</sub> uptake to dust deposition by iron-light colimitation”. In: *Geophysical Research Letters* 42.2, pp. 492–499. DOI: 10.1002/2014g1062969.
- Nielsen, S. B., M. Jochum, J. B. Pedro, C. Eden and R. Nuterman (2019). “Two-Timescale Carbon Cycle Response to an AMOC Collapse”. In: *Paleoceanography and Paleoclimatology* 34.4, pp. 511–523. DOI: 10.1029/2018pa003481.
- Nishioka, J., H. Obata, H. Ogawa, K. Ono, Y. Yamashita, K. Lee, S. Takeda and I. Yasuda (2020). “Subpolar marginal seas fuel the North Pacific through the intermediate water at the termination of the global ocean circulation”. In: *Proceedings of the National Academy of Sciences* 117.23, pp. 12665–12673. DOI: 10.1073/pnas.2000658117.
- North, R. L., S. J. Guildford, R. E. H. Smith, S. M. Havens and M. R. Twiss (2007). “Evidence for phosphorus, nitrogen, and iron colimitation of phytoplankton communities in Lake Erie”. In: *Limnology and Oceanography* 52.1, pp. 315–328. DOI: 10.4319/lo.2007.52.1.0315.
- Ohgaito, R., A. Abe-Ouchi, R. Oishi, T. Takemura, A. Ito, T. Hajima, S. Watanabe and M. Kawamiya (2018). “Effect of high dust amount on surface temperature during the Last Glacial Maximum: a modelling study using MIROC-ESM”. In: *Climate of the Past* 14.11, pp. 1565–1581. DOI: 10.5194/cp-14-1565-2018.
- Oka, A., A. Abe-Ouchi, M. O. Chikamoto and T. Ide (2011). “Mechanisms controlling export production at the LGM: Effects of changes in oceanic physical fields and atmospheric dust deposition”. In: *Global Biogeochemical Cycles* 25.2. DOI: 10.1029/2009gb003628.
- Okazaki, Y., A. Timmermann, L. Menviel, M. O. Chikamoto, N. Harada and A. Abe-Ouchi (2012). “Ocean circulation in the North Pacific during the last glacial termination”. In: *PAGES news* 20.2, pp. 60–61. DOI: 10.22498/pages.20.2.60.

## BIBLIOGRAPHY

---

- Oppo, D. W., G. Gebbie, K.-F. Huang, W. B. Curry, T. M. Marchitto and K. R. Pietro (2018). “Data Constraints on Glacial Atlantic Water Mass Geometry and Properties”. In: *Paleoceanography and Paleoclimatology* 33.9, pp. 1013–1034. DOI: 10.1029/2018pa003408.
- Pajares, S. and R. Ramos (2019). “Processes and Microorganisms Involved in the Marine Nitrogen Cycle: Knowledge and Gaps”. In: *Frontiers in Marine Science* 6. DOI: 10.3389/fmars.2019.00739.
- Parekh, P., M. J. Follows, S. Dutkiewicz and T. Ito (2006). “Physical and biological regulation of the soft tissue carbon pump”. In: *Paleoceanography* 21.3. DOI: 10.1029/2005pa001258.
- Parekh, P., F. Joos and S. A. Müller (2008). “A modeling assessment of the interplay between aeolian iron fluxes and iron-binding ligands in controlling carbon dioxide fluctuations during Antarctic warm events”. In: *Paleoceanography* 23.4. DOI: 10.1029/2007pa001531.
- Pausch, F., K. Bischof and S. Trimborn (2019). “Iron and manganese co-limit growth of the Southern Ocean diatom *Chaetoceros debilis*”. In: *PLOS ONE* 14.9. Ed. by B. Jesus. DOI: 10.1371/journal.pone.0221959.
- Paytan, A. and K. McLaughlin (2007). “The Oceanic Phosphorus Cycle”. In: *Chemical Reviews* 107.2, pp. 563–576. DOI: 10.1021/cr0503613.
- Pedro, J. B., M. Jochum, C. Buizert, F. He, S. Barker and S. O. Rasmussen (2018). “Beyond the bipolar seesaw: Toward a process understanding of interhemispheric coupling”. In: *Quaternary Science Reviews* 192, pp. 27–46. DOI: 10.1016/j.quascirev.2018.05.005.
- Peltier, W. R., D. F. Argus and R. Drummond (2015). “Space geodesy constrains ice age terminal deglaciation: The global ICE-6G C (VM5a) model”. In: *Journal of Geophysical Research: Solid Earth* 120.1, pp. 450–487. DOI: 10.1002/2014JB011176.
- Petit, J.-R., M. Briat and A. Royer (1981). “Ice age aerosol content from East Antarctic ice core samples and past wind strength”. In: *Nature* 293.5831, pp. 391–394. DOI: 10.1038/293391a0.
- Pianosi, F., K. Beven, J. Freer, J. W. Hall, J. Rougier, D. B. Stephenson and T. Wagener (2016). “Sensitivity analysis of environmental models: A systematic review with practical workflow”. In: *Environmental Modelling & Software* 79, pp. 214–232. DOI: 10.1016/j.envsoft.2016.02.008.
- Prentice, I. C. and D. Jolly (2000). “Mid-Holocene and glacial-maximum vegetation geography of the northern continents and Africa”. In: *Journal of Biogeography* 27.3, pp. 507–519. DOI: 10.1046/j.1365-2699.2000.00425.x.

## BIBLIOGRAPHY

---

- Rahmstorf, S. (2013). "GLACIAL CLIMATES Thermohaline Circulation". In: *Encyclopedia of Quaternary Science*. Elsevier, pp. 737–747. DOI: 10.1016/b978-0-444-53643-3.00020-0.
- Redfield, A. C. (1958). "THE BIOLOGICAL CONTROL OF CHEMICAL FACTORS IN THE ENVIRONMENT". In: *American Scientist* 46.3, 230A–221. ISSN: 00030996.
- Redfield, A. C. (1934). "On the proportions of organic derivatives in sea water and their relation to the composition of plankton". In: *James Johnstone memorial volume*, pp. 176–192.
- Rijkenberg, M. J. A., R. Middag, P. Laan, L. J. A. Gerringa, H. M. van Aken, V. Schoemann, J. T. M. de Jong and H. J. W. de Baar (2014). "The Distribution of Dissolved Iron in the West Atlantic Ocean". In: *PLoS ONE* 9.6. Ed. by F. Missirlis, e101323. DOI: 10.1371/journal.pone.0101323.
- Roberts, H. M., D. R. Muhs, A. G. Wintle, G. A. T. Duller and E. A. Bettis (2003). "Unprecedented last-glacial mass accumulation rates determined by luminescence dating of loess from western Nebraska". In: *Quaternary Research* 59.3, pp. 411–419. DOI: 10.1016/s0033-5894(03)00040-1.
- Rocha, C. L. D. L. (2007). "The Biological Pump". In: *Treatise on Geochemistry*. Elsevier, pp. 1–29. DOI: 10.1016/b0-08-043751-6/06107-7.
- Rocha, C. L. D. L., D. A. Hutchins, M. A. Brzezinski and Y. Zhang (2000). "Effects of iron and zinc deficiency on elemental composition and silica production by diatoms". In: *Marine Ecology Progress Series* 195, pp. 71–79. DOI: 10.3354/meps195071.
- Royer, A., M. D. Angelis and J. R. Petit (1983). "A 30000 year record of physical and optical properties of microparticles from an East Antarctic ice core and implications for paleoclimate reconstruction models". In: *Climatic Change* 5.4, pp. 381–412. DOI: 10.1007/bf00140802.
- Ruth, U., D. Wagenbach, J. P. Steffensen and M. Bigler (2003). "Continuous record of microparticle concentration and size distribution in the central Greenland NGRIP ice core during the last glacial period". In: *Journal of Geophysical Research: Atmospheres* 108.D3, n/a–n/a. DOI: 10.1029/2002jd002376.
- Sarmiento, J. L., N. Gruber, M. A. Brzezinski and J. P. Dunne (2004). "High-latitude controls of thermocline nutrients and low latitude biological productivity". In: *Nature* 427, pp. 56–60. DOI: 10.1038/nature02127.
- Schmitt, J., R. Schneider, J. Elsig, D. Leuenberger, A. Laurantou, J. Chappellaz, P. Kohler, F. Joos, T. F. Stocker, M. Leuenberger and H. Fischer (2012). "Car-

## BIBLIOGRAPHY

---

- bon Isotope Constraints on the Deglacial CO<sub>2</sub> Rise from Ice Cores”. In: *Science* 336.6082, pp. 711–714. DOI: 10.1126/science.1217161.
- Schmittner, A. and C. J. Somes (2016). “Complementary constraints from carbon  $\delta^{13}\text{C}$  and nitrogen  $\delta^{15}\text{N}$  isotopes on the glacial ocean’s soft-tissue biological pump”. In: *Paleoceanography* 31.6, pp. 669–693. DOI: 10.1002/2015pa002905.
- Schroth, A. W., J. Crusius, E. R. Sholkovitz and B. C. Bostick (2009). “Iron solubility driven by speciation in dust sources to the ocean”. In: *Nature Geoscience* 2.5, pp. 337–340. DOI: 10.1038/ngeo501.
- Shields, C. A., D. A. Bailey, G. Danabasoglu, M. Jochum, J. T. Kiehl, S. Levis and S. Park (2012). “The Low-Resolution CCSM4”. In: *Journal of Climate* 25.12, pp. 3993–4014. DOI: 10.1175/jcli-d-11-00260.1.
- Shoenfelt, E. M., G. Winckler, F. Lamy, R. F. Anderson and B. C. Bostick (2018). “Highly bioavailable dust-borne iron delivered to the Southern Ocean during glacial periods”. In: *Proceedings of the National Academy of Sciences* 115.44, pp. 11180–11185. DOI: 10.1073/pnas.1809755115.
- Sholkovitz, E. R., P. N. Sedwick, T. M. Church, A. R. Baker and C. F. Powell (2012). “Fractional solubility of aerosol iron: Synthesis of a global-scale data set”. In: *Geochimica et Cosmochimica Acta* 89, pp. 173–189. DOI: 10.1016/j.gca.2012.04.022.
- Sigman, D. and M. Hain (2012). “The Biological Productivity of the Ocean”. In: *Nature Education* 3, pp. 1–16.
- Simonsen, M. F., G. Baccolo, T. Blunier, A. Borunda, B. Delmonte, R. Frei, S. Goldstein, A. Grinsted, H. A. Kjaer, T. Sowers, A. Svensson, B. Vinther, D. Vladimirova, G. Winckler, M. Winstrup and P. Vallelonga (2019). “East Greenland ice core dust record reveals timing of Greenland ice sheet advance and retreat”. In: *Nature Communications* 10.1. DOI: 10.1038/s41467-019-12546-2.
- Smith, R., P. Jones, B. Briegleb, F. Bryan, G. D. and J. Dennis, J. Dukowicz, C. Eden, B. Fox-Kemper, P. Gent, M. Hecht, S. Jayne, M. Jochum, W. Large, K. Lindsay, M. Maltrud, N. Norton, S. Peacock, M. Vertenstein and S. Yeager (2010). “The Parallel Ocean Program (POP) reference manual”. In: *Los Alamos Unclassified Report LA-UR-02-2484*.
- Somes, C. J., A. Schmittner, J. Muglia and A. Oeschies (2017). “A Three-Dimensional Model of the Marine Nitrogen Cycle during the Last Glacial Maximum Constrained by Sedimentary Isotopes”. In: *Frontiers in Marine Science* 4. DOI: 10.3389/fmars.2017.00108.

## BIBLIOGRAPHY

---

- Spolaor, A., P. Vallelonga, G. Cozzi, J. Gabrieli, C. Varin, N. Kehrwald, P. Zennaro, C. Boutron and C. Barbante (2013). “Iron speciation in aerosol dust influences iron bioavailability over glacial-interglacial timescales”. In: *Geophysical Research Letters* 40.8, pp. 1618–1623. DOI: 10.1002/grl.50296.
- Steffensen, J. P. (1997). “The size distribution of microparticles from selected segments of the Greenland Ice Core Project ice core representing different climatic periods”. In: *Journal of Geophysical Research: Oceans* 102.C12, pp. 26755–26763. DOI: 10.1029/97jc01490.
- Stock, C. A., J. P. Dunne and J. G. John (2014). “Global-scale carbon and energy flows through the marine planktonic food web: An analysis with a coupled physical-biological model”. In: *Progress in Oceanography* 120, pp. 1–28. DOI: 10.1016/j.pocean.2013.07.001.
- Strzepek, R. F., M. T. Maldonado, K. A. Hunter, R. D. Frew and P. W. Boyd (2011). “Adaptive strategies by Southern Ocean phytoplankton to lessen iron limitation: Uptake of organically complexed iron and reduced cellular iron requirements”. In: *Limnology and Oceanography* 56.6, pp. 1983–2002. DOI: 10.4319/lo.2011.56.6.1983.
- Studer, A. S., D. M. Sigman, A. Martinez-Garcia, V. Benz, G. Winckler, G. Kuhn, O. Esper, F. Lamy, S. L. Jaccard, L. Wacker, S. Oleynik, R. Gersonde and G. H. Haug (2015). “Antarctic Zone nutrient conditions during the last two glacial cycles”. In: *Paleoceanography* 30.7, pp. 845–862. DOI: 10.1002/2014pa002745.
- Sunda, W. G. and S. A. Huntsman (1997). “Interrelated influence of iron, light and cell size on marine phytoplankton growth”. In: *Nature* 390.6658, pp. 389–392. DOI: 10.1038/37093.
- Tagliabue, A., L. Bopp, D. M. Roche, N. Bouttes, J.-C. Dutay, R. Alkama, M. Kageyama, E. Michel and D. Paillard (2009). “Quantifying the roles of ocean circulation and biogeochemistry in governing ocean carbon-13 and atmospheric carbon dioxide at the last glacial maximum”. In: *Climate of the Past* 5.4, pp. 695–706. DOI: 10.5194/cp-5-695-2009.
- Tagliabue, A., O. Aumont and L. Bopp (2014). “The impact of different external sources of iron on the global carbon cycle”. In: *Geophysical Research Letters* 41.3, pp. 920–926. DOI: 10.1002/2013gl1059059.
- Tagliabue, A., L. Bopp, J.-C. Dutay, A. R. Bowie, F. Chever, P. Jean-Baptiste, E. Bucciarelli, D. Lannuzel, T. Remenyi, G. Sarthou, O. Aumont, M. Gehlen and C. Jeandel (2010). “Hydrothermal contribution to the oceanic dissolved iron inventory”. In: *Nature Geoscience* 3.4, pp. 252–256. DOI: 10.1038/ngeo818.

## BIBLIOGRAPHY

---

- Tagliabue, A., A. R. Bowie, P. W. Boyd, K. N. Buck, K. S. Johnson and M. A. Saito (2017). “The integral role of iron in ocean biogeochemistry”. In: *Nature* 543.7643, pp. 51–59. DOI: 10.1038/nature21058.
- Takemura, T., M. Egashira, K. Matsuzawa, H. Ichijo, R. O'ishi and A. Abe-Ouchi (2009). “A simulation of the global distribution and radiative forcing of soil dust aerosols at the Last Glacial Maximum”. In: *Atmospheric Chemistry and Physics* 9.9, pp. 3061–3073. DOI: 10.5194/acp-9-3061-2009.
- Talley, L. D. (2013). “Closure of the Global Overturning Circulation Through the Indian, Pacific, and Southern Oceans: Schematics and Transports”. In: *Oceanography* 26.1, pp. 80–97. DOI: 10.5670/oceanog.2013.07.
- Thöle, L. M., H. E. Amsler, S. Moretti, A. Auderset, J. Gilgannon, J. Lippold, H. Vogel, X. Crosta, A. Mazaud, E. Michel, A. Martínez-García and S. L. Jaccard (2019). “Glacial-interglacial dust and export production records from the Southern Indian Ocean”. In: *Earth and Planetary Science Letters* 525, p. 115716. DOI: 10.1016/j.epsl.2019.115716.
- Thompson, L., M. Davis, E. Mosley-Thompson, E. Sowers, K. Henderson, V. Zagorodnov, P.-N. Lin, V. Mikhalenko, R. Campen, J. Bolzan, D. Cole and B. Francou (1998). “A 25,000-year tropical climate history from Bolivian ice cores”. In: *Science*.
- Thompson, L. G., E. Mosley-Thompson, M. E. Davis, P.-N. Lin, K. A. Henderson, J. Cole-Dai, J. F. Bolzan and K.-B. Liu (1995). “Late Glacial Stage and Holocene Tropical Ice Core Records from Huascarán, Peru”. In: *Science* 269.5220, pp. 46–50. DOI: 10.1126/science.269.5220.46.
- Tréguer, P. J. and C. L. D. L. Rocha (2013). “The World Ocean Silica Cycle”. In: *Annual Review of Marine Science* 5.1, pp. 477–501. DOI: 10.1146/annurev-marine-121211-172346.
- Twining, B. S. and S. B. Baines (2013). “The Trace Metal Composition of Marine Phytoplankton”. In: *Annual Review of Marine Science* 5.1, pp. 191–215. DOI: 10.1146/annurev-marine-121211-172322.
- Volk, T. and M. I. Hoffert (1985). “Ocean carbon pumps: Analysis of relative strengths and efficiencies in ocean-driven atmospheric CO<sub>2</sub> changes”. In: *The carbon cycle and atmospheric CO<sub>2</sub>: natural variations Archean to present* 32, pp. 99–110.
- Wallmann, K., B. Schneider and M. Sarnthein (2016). “Effects of eustatic sea-level change, ocean dynamics, and nutrient utilization on atmospheric pCO<sub>2</sub> and seawater composition over the last 130,000 years: a model study”. In: *Climate of the Past* 12.2, pp. 339–375. DOI: 10.5194/cp-12-339-2016.

## BIBLIOGRAPHY

---

- Wang, S., D. Bailey, K. Lindsay, J. K. Moore and M. Holland (2014). “Impact of sea ice on the marine iron cycle and phytoplankton productivity”. In: *Biogeosciences* 11.17, pp. 4713–4731. DOI: 10.5194/bg-11-4713-2014.
- Watson, A. J., D. C. E. Bakker, A. J. Ridgwell, P. W. Boyd and C. S. Law (2000). “Effect of iron supply on Southern Ocean CO<sub>2</sub> uptake and implications for glacial atmospheric CO<sub>2</sub>”. In: *Nature* 407.6805, pp. 730–733. DOI: 10.1038/35037561.
- Weber, T. S. and C. Deutsch (2010). “Ocean nutrient ratios governed by plankton biogeography”. In: *Nature* 467.7315, pp. 550–554. DOI: 10.1038/nature09403.
- Williams, R. G. and M. J. Follows (2003). “Ocean biogeochemistry: a synthesis of the Joint Global Ocean Flux Study (JGOFS)”. In: ed. by M. J. R. Fasham. Springer. Chap. Physical Transport of Nutrients and the Maintenance of Biological Production, pp. 19–51. ISBN: 978-3-642-62691-3. DOI: 10.1007/978-3-642-55844-3.
- Winckler, G., R. F. Anderson, M. Q. Fleisher, D. McGee and N. Mahowald (2008). “Covariant Glacial-Interglacial Dust Fluxes in the Equatorial Pacific and Antarctica”. In: *Science* 320.5872, pp. 93–96. DOI: 10.1126/science.1150595.
- Wu, G., T. Yao, L. G. Thompson and Z. Li (2004). “Microparticle record in the Guliya ice core and its comparison with polar records since the last interglacial”. In: *Chinese Science Bulletin* 49.6, p. 607. DOI: 10.1360/03wd0419.
- Wu, J., E. Boyle, W. Sunda and L.-S. Wen (2001). “Soluble and Colloidal Iron in the Oligotrophic North Atlantic and North Pacific”. In: *Science* 293.5531, pp. 847–849. DOI: 10.1126/science.1059251.
- Yamamoto, A., A. Abe-Ouchi, R. Ohgaito, A. Ito and A. Oka (2019). “Glacial CO<sub>2</sub> decrease and deep-water deoxygenation by iron fertilization from glaciogenic dust”. In: *Climate of the Past* 15.3, pp. 981–996. DOI: 10.5194/cp-15-981-2019.
- Yoon, J.-E., K.-C. Yoo, A. M. Macdonald, H.-I. Yoon, K.-T. Park, E. J. Yang, H.-C. Kim, J. I. Lee, M. K. Lee, J. Jung, J. Park, J. Lee, S. Kim, S.-S. Kim, K. Kim and I.-N. Kim (2018). “Reviews and syntheses: Ocean iron fertilization experiments – past, present, and future looking to a future Korean Iron Fertilization Experiment in the Southern Ocean (KIFES) project”. In: *Biogeosciences* 15.19, pp. 5847–5889. DOI: 10.5194/bg-15-5847-2018.
- Zehr, J. P. and R. M. Kudela (2011). “Nitrogen Cycle of the Open Ocean: From Genes to Ecosystems”. In: *Annual Review of Marine Science* 3.1, pp. 197–225. DOI: 10.1146/annurev-marine-120709-142819.

## BIBLIOGRAPHY

---

Zender, C. S., H. Bian and D. Newman (2003). "Mineral Dust Entrainment and Deposition (DEAD) model: Description and 1990s dust climatology". In: *Journal of Geophysical Research: Atmospheres* 108.D14. DOI: 10.1029/2002JD002775.

# Appendix

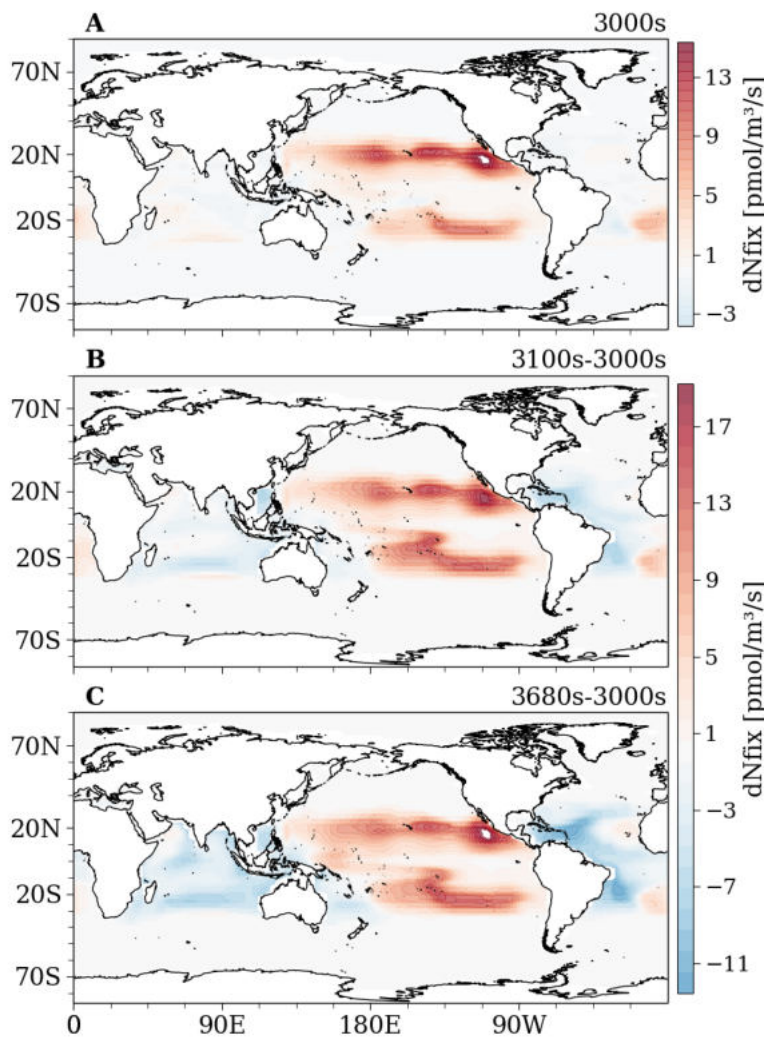


**Figure A.1:** Global map of 10-year-mean diazotroph  $N_2$  fixation anomaly ( $dN_{fix}$ ), averaged over the upper 150 m depth in the 3000s (A), difference of 3100s-3000s (B) and 3680s-3000s (C).

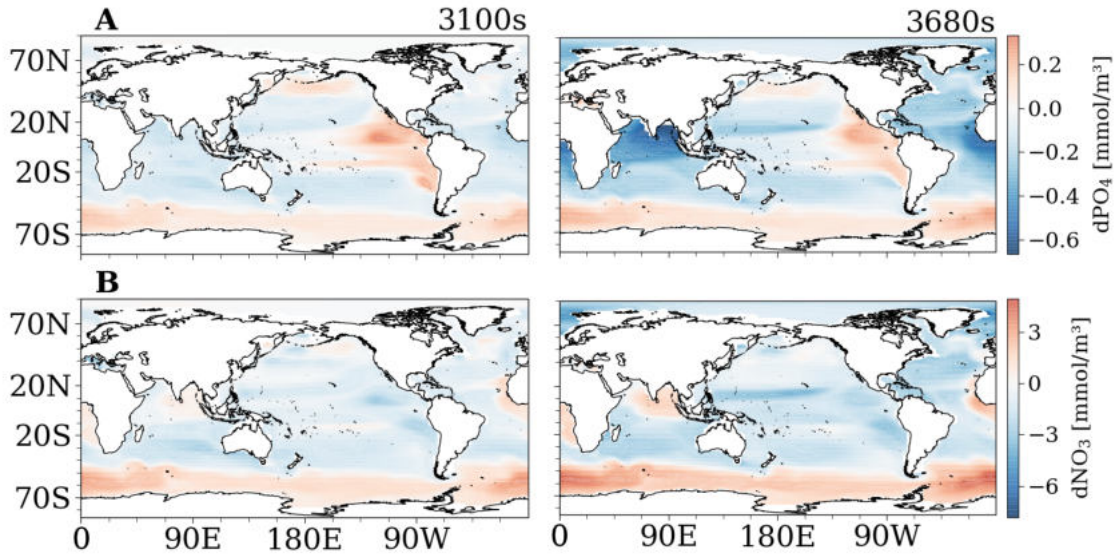


**Figure A.2:** Global map of 10-year-mean  $\text{PO}_4$  (A) and  $\text{NO}_3$  (B) concentration anomaly, averaged over 200 to 1000 m depth in the 3100s (left) and 3680s (right).

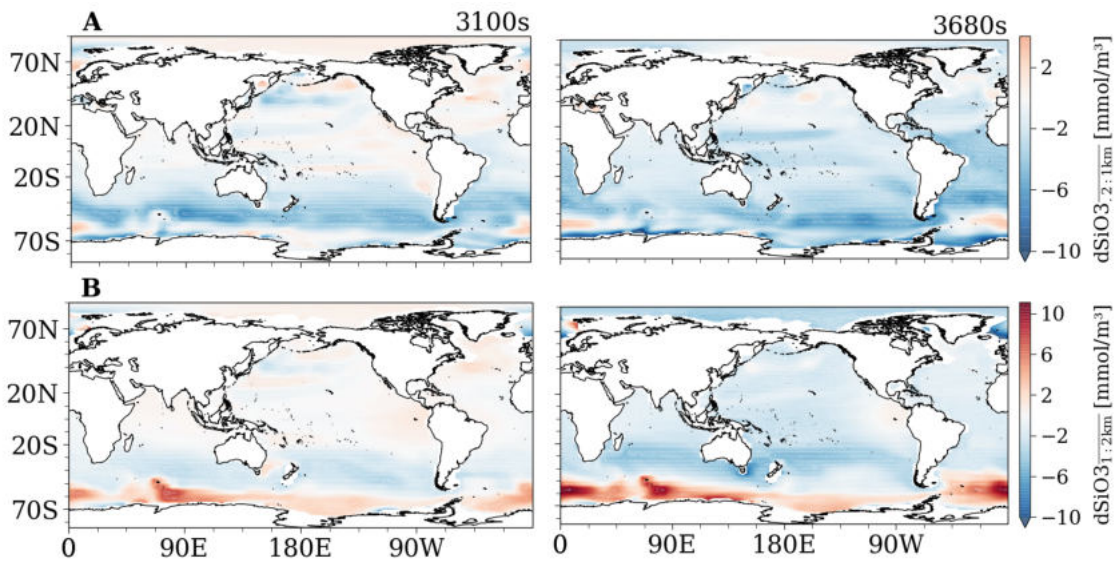


**Figure A.3:** Global map of 10-year-mean  $\text{SiO}_3$  concentration anomaly, averaged over 200 to 1000 m depth (A) and 1000 to 2000 m depth (B), in the 3100s (left) and 3680s (right).

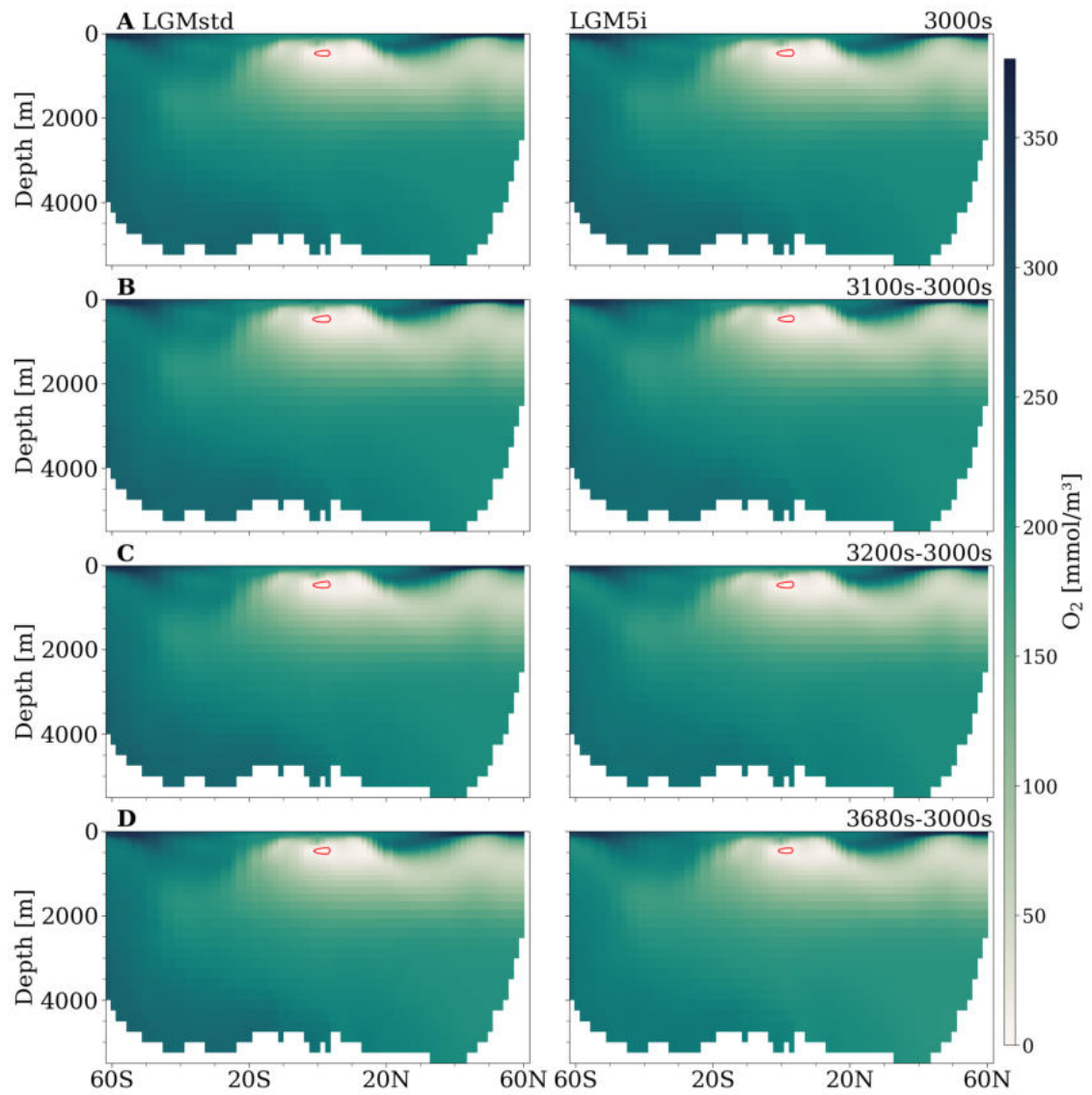


**Figure A.4:** Zonal mean  $O_2$  in the Pacific (averaged over longitudes  $168\text{--}133^\circ\text{W}$ ) in LGMstd (left) and LGM5i (right). 10-year-mean over the 3000s (A), and difference of 3100s-3000s (B), 3200s-3000s (C) and 3680s-3000s (D). Red contour line at  $O_2$  values of  $4\text{ mmol/m}^3$ .

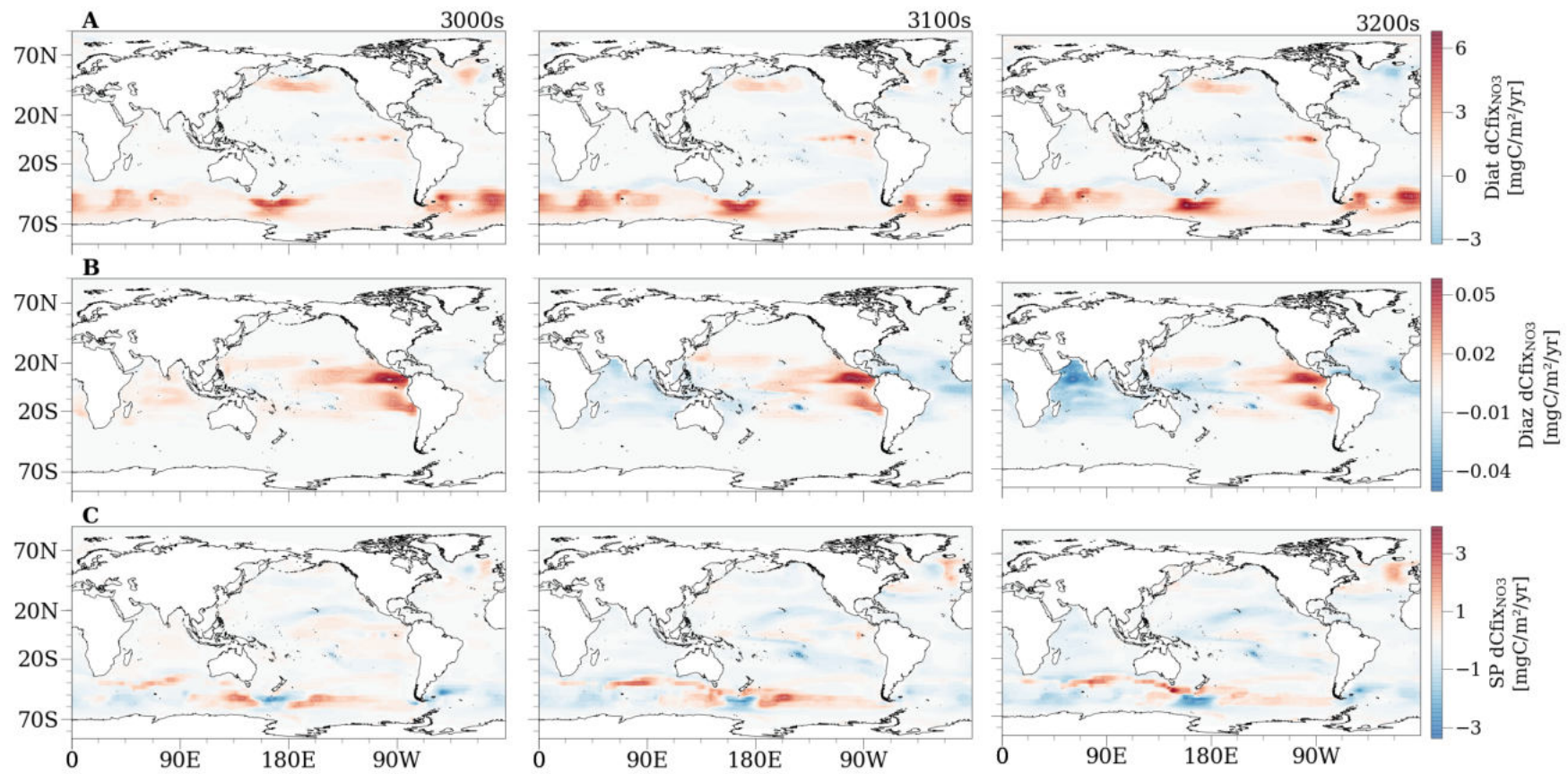


**Figure A.5:** Global map of upper ocean mean phytoplankton C fixation from  $\text{NO}_3$  ( $\text{Cfix}_{\text{NO}_3}$ ) by diatoms (Diat, row A), diazotrophs (Diaz, row B) and small phytoplankton (SP, row C) in LGM5i. 10-year-mean over the 3000s, 3100s and 3200s, averaged over the upper 150 m depth.

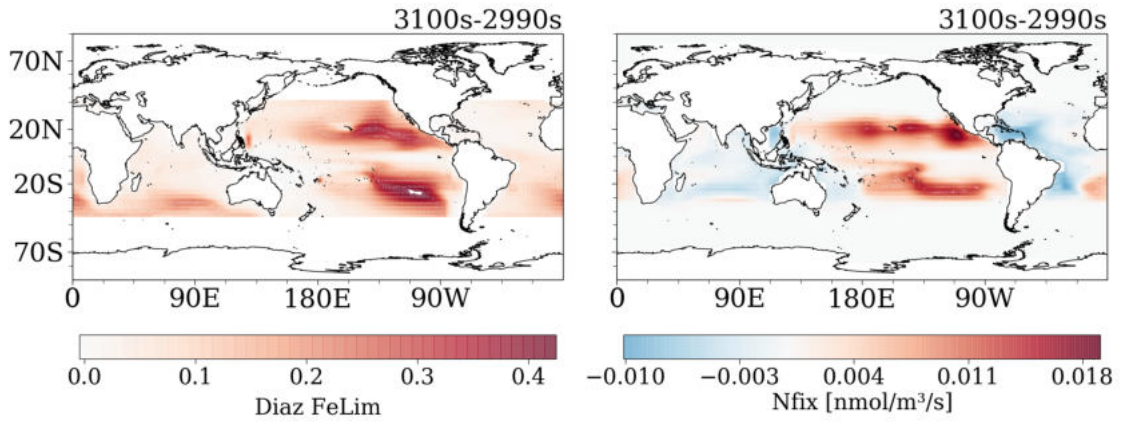


**Figure A.6:** Global map of upper ocean mean diazotroph Fe limitation (left) and  $N_2$  fixation (Nfix) (right). Difference of 10-year-mean LGM5i in the 3100s to LGMstd in the 2990s, averaged over the upper 150 m depth.

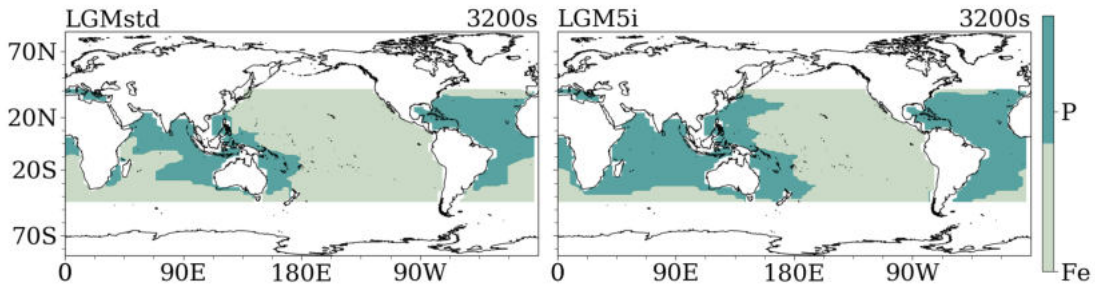


**Figure A.7:** Most limiting nutrient to diazotroph growth in LGMstd (left) and LGM5i (right). 10-year-mean over the 3200s.

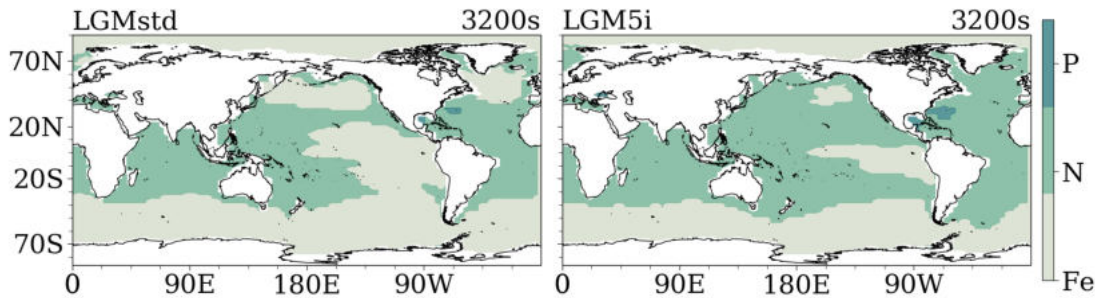


**Figure A.8:** Most limiting nutrient to small phytoplankton growth in LGMstd (left) and LGM5i (right). 10-year-mean over the 3200s.

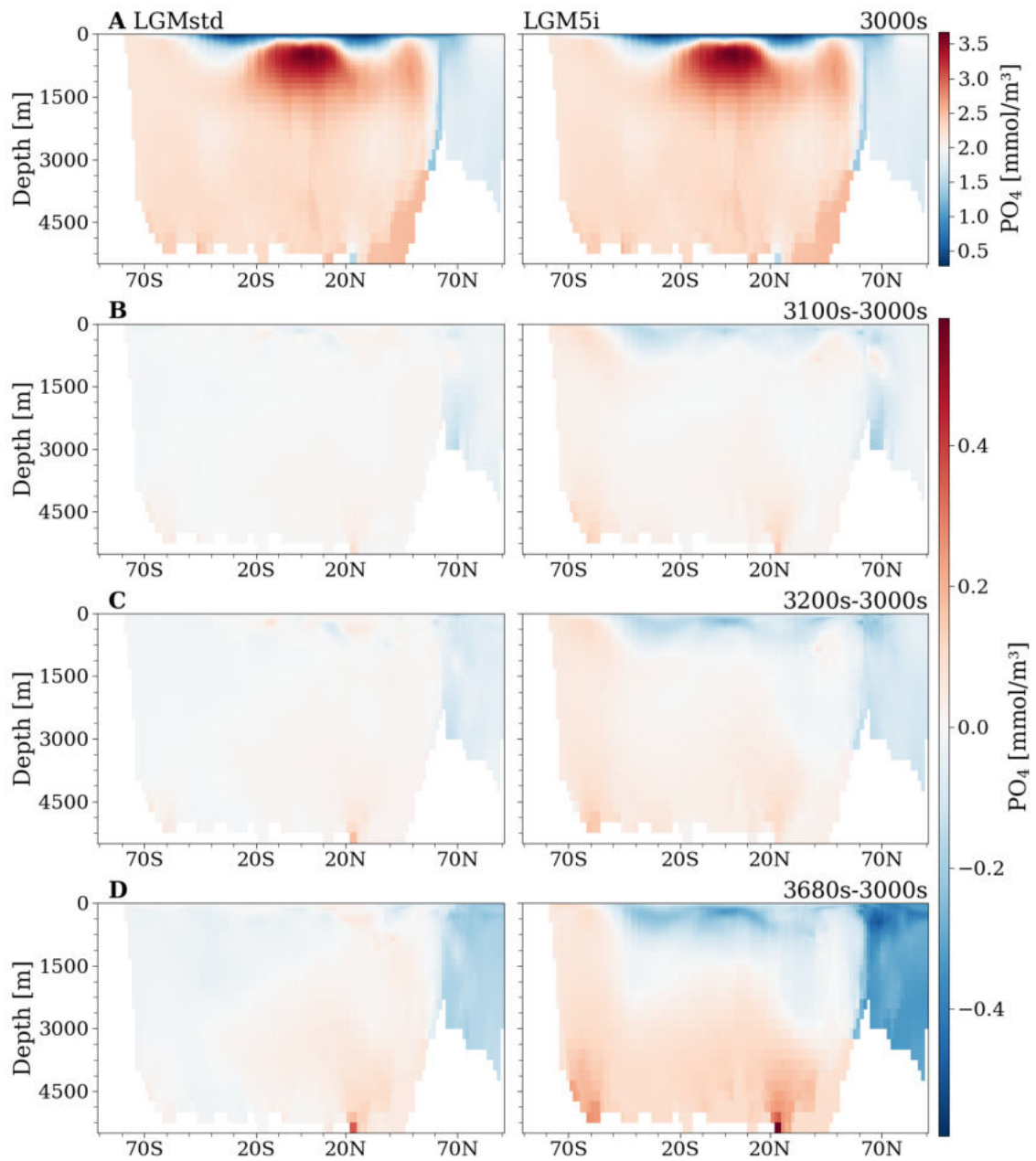


**Figure A.9:** Zonal mean  $\text{PO}_4$  concentration in LGMstd (left) and LGM5i (right). 10-year-mean over the 3000s (A) and difference of 3100s-3000s (B), 3200s-3000s (C) and 3680s-3000s (D).

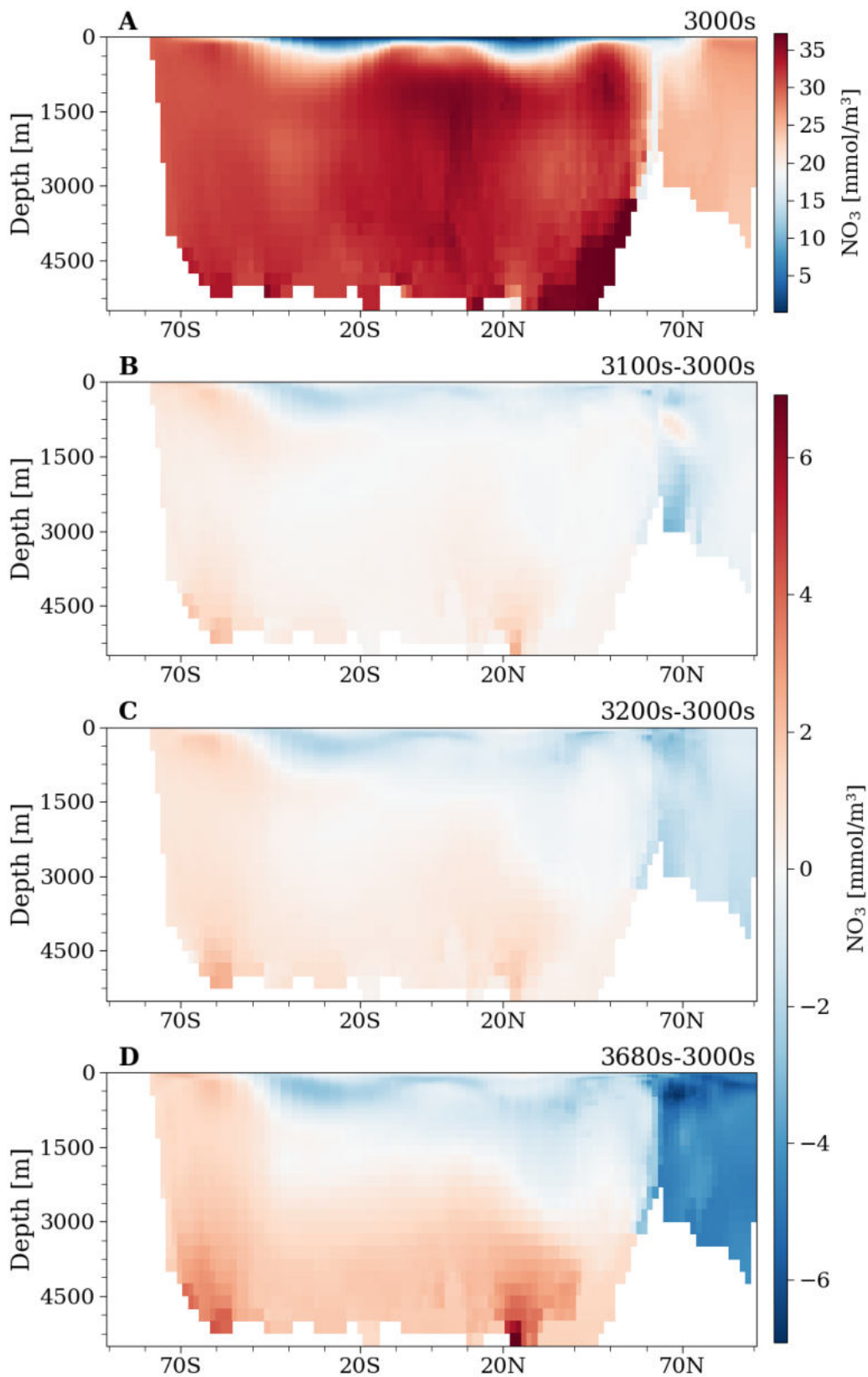


**Figure A.10:** Zonal mean  $\text{NO}_3$  concentration in LGM5i. 10-year-mean over the 3000s (A), and difference 3100s-3000s (B), 3200s-3000s (C) and 3680s-3000s (D).

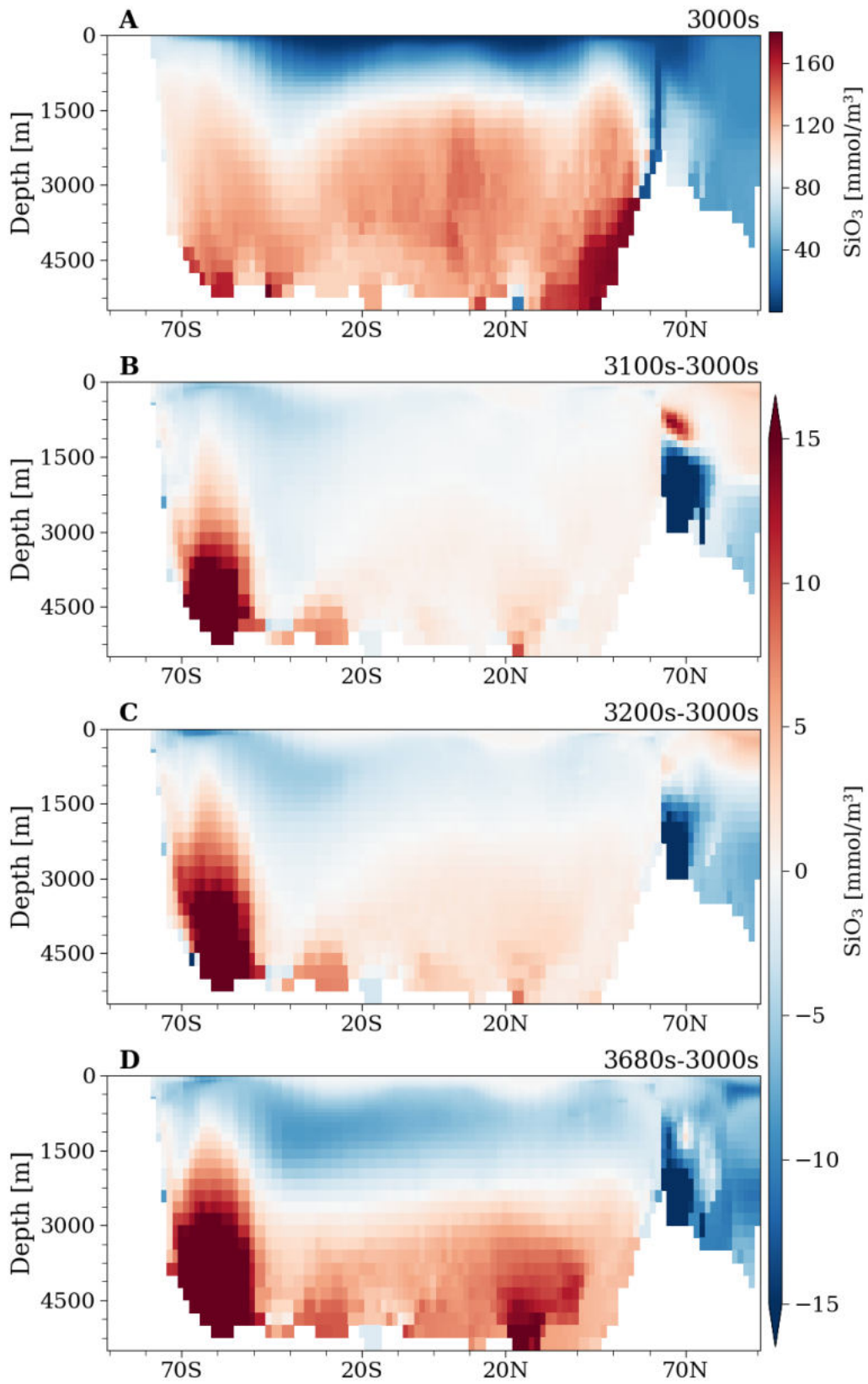


**Figure A.11:** Zonal mean  $\text{SiO}_3$  concentration in LGM5i. 10-year-mean over the 3000s (A), and difference 3100s-3000s (B), 3200s-3000s (C) and 3680s-3000s (D).

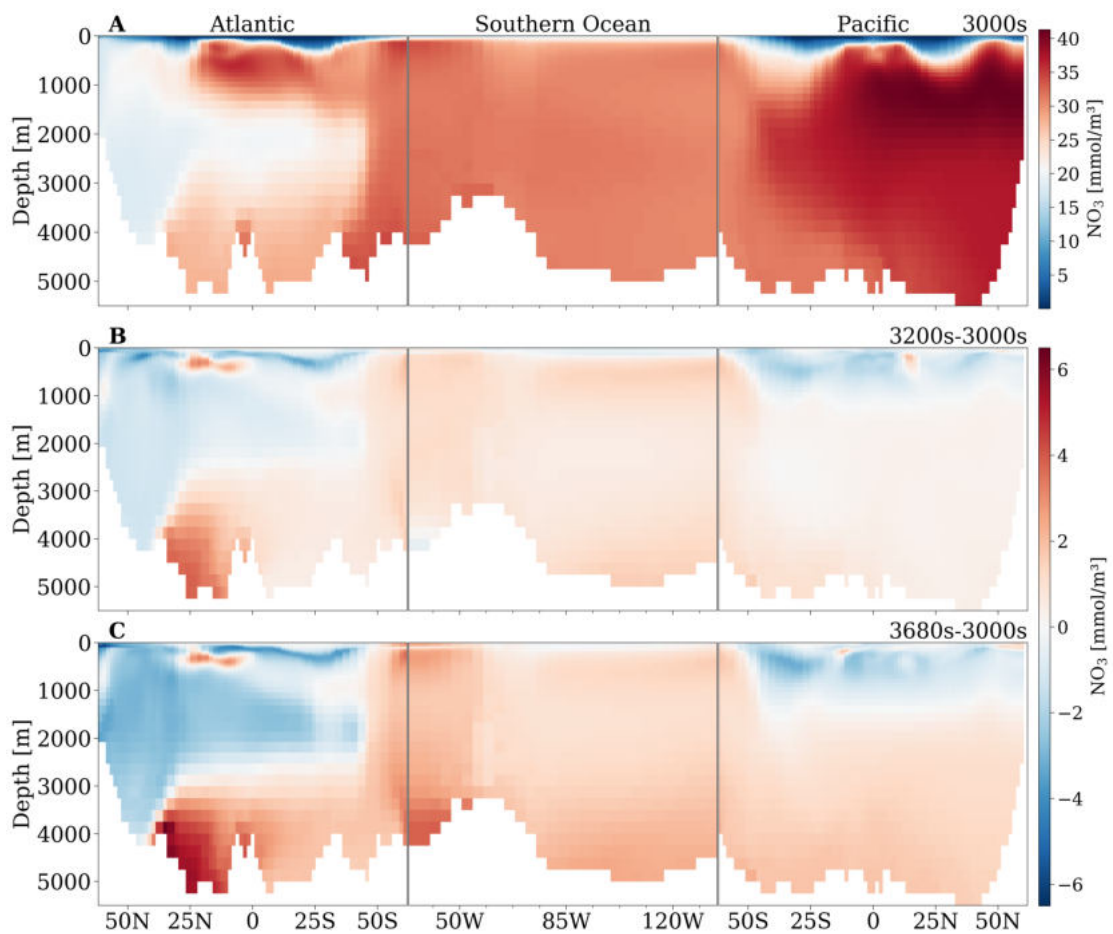


**Figure A.12:**  $\text{NO}_3$  concentrations in depth transects of the Atlantic (mean over 328–346 °E), Southern (mean over 64–56 °S) and Pacific Ocean (mean over 168–133 °W). LGM5i 10-year-mean over the 3000s (A), difference 3200s-3000s (B), and 3680s-3000s (C).

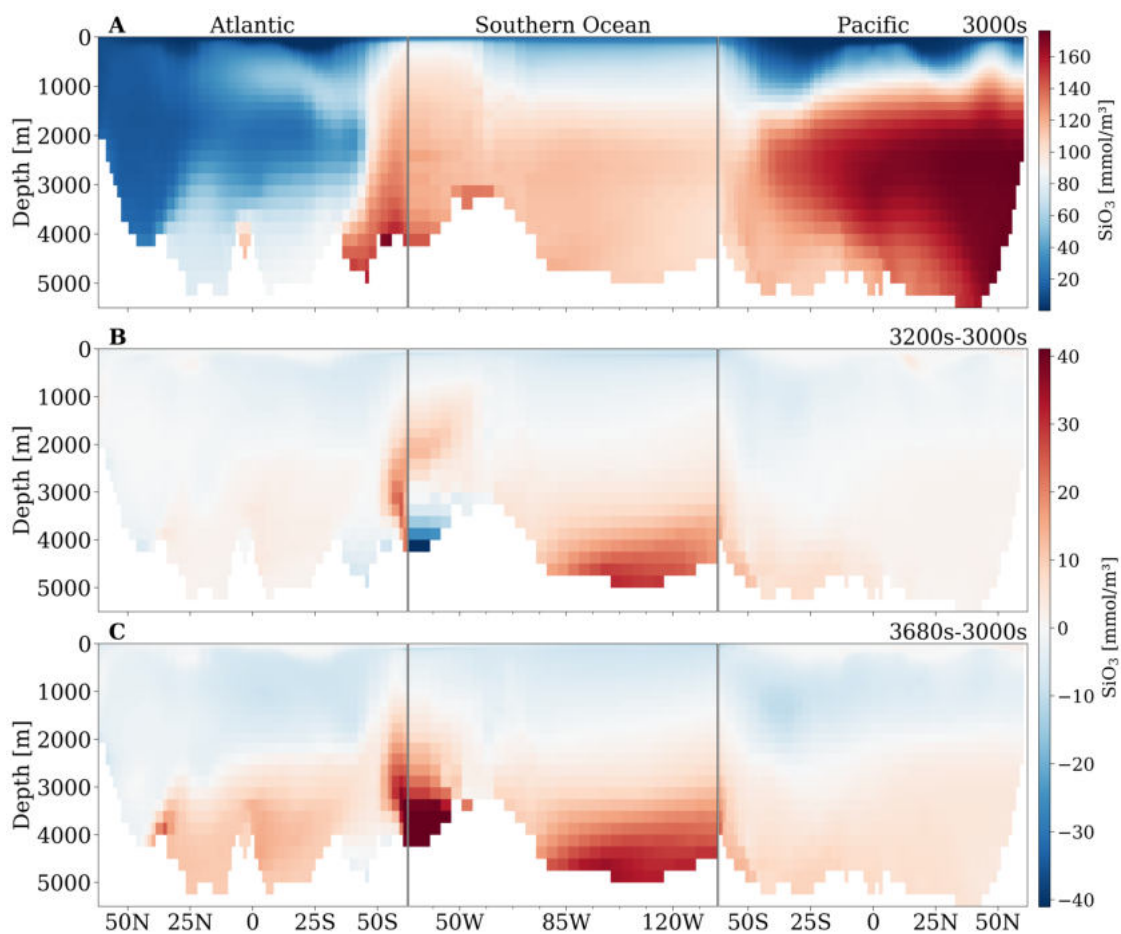


**Figure A.13:**  $\text{SiO}_3$  concentrations in depth transects of the Atlantic (mean over 328–346 °E), Southern (mean over 64–56 °S) and Pacific Ocean (mean over 168–133 °W). LGM5i 10-year-mean over the 3000s (A), difference 3200s-3000s (B), and 3680s-3000s (C).

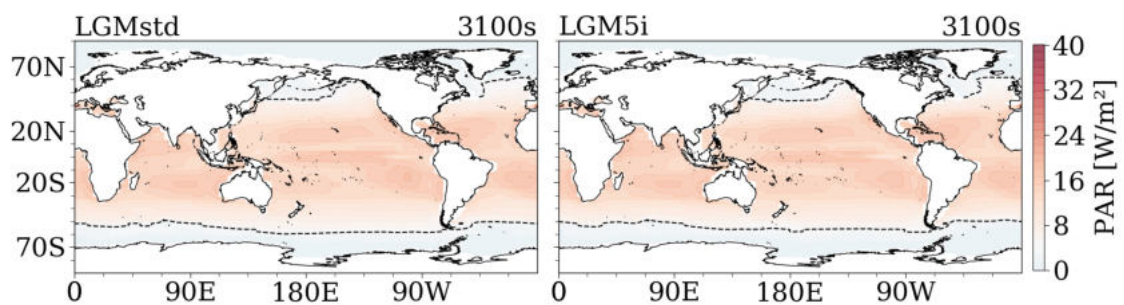


**Figure A.14:** Global map of 10-year-mean PAR in LGMstd (left) and LGM5i (right) in the 3100s. Mean over the upper 150 m depth. Dashed line indicates 4 W/m<sup>2</sup> contour line.

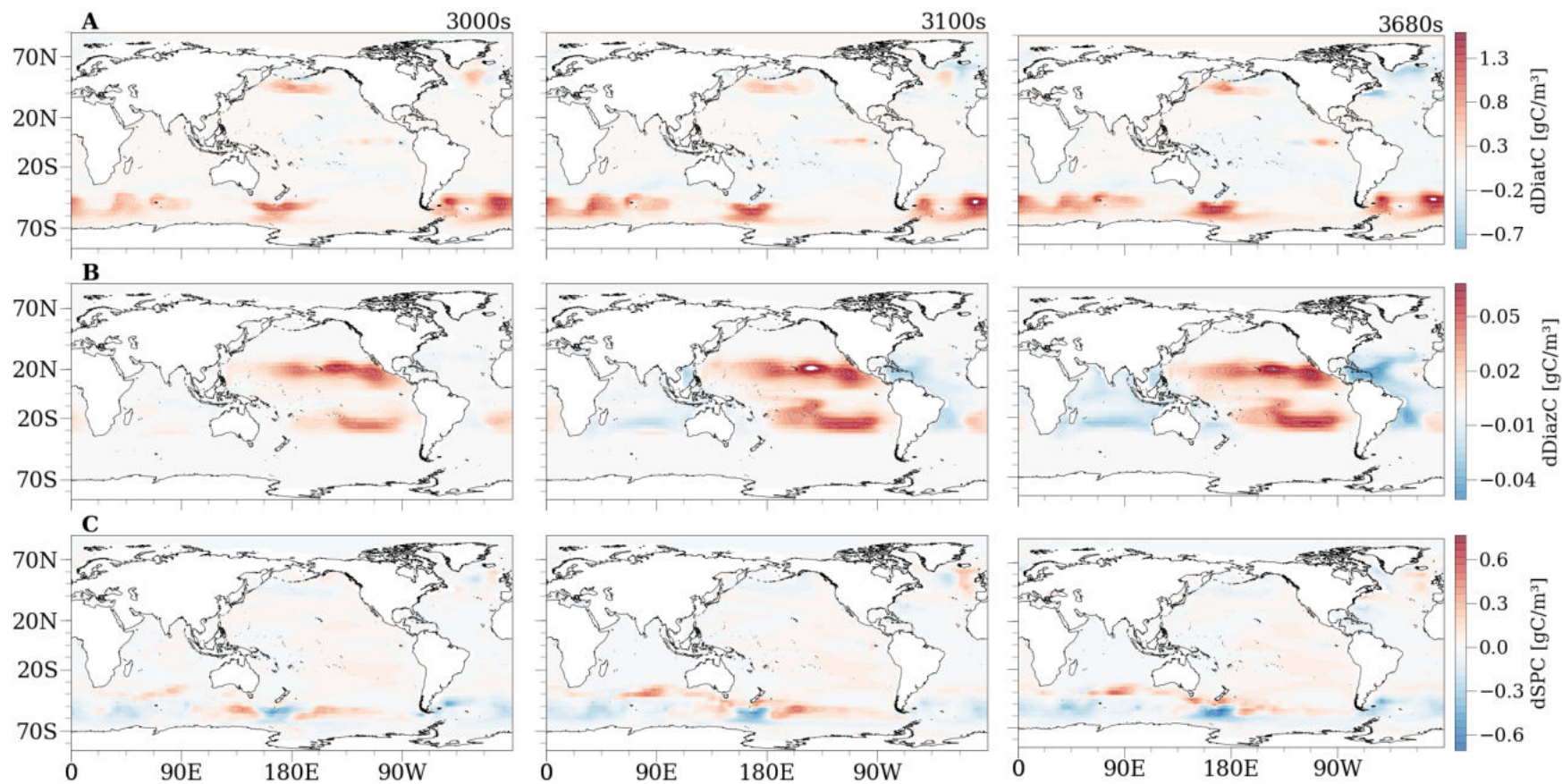


**Figure A.15:** Global map of upper ocean mean phytoplankton C biomass anomaly of diatoms (dDiatC, row A), diazotrophs (dDiazC, row B) and small phytoplankton (dSPC, row C). 10-year-mean over the 3000s, 3100s and 3680s, averaged over the upper 150 m depth.

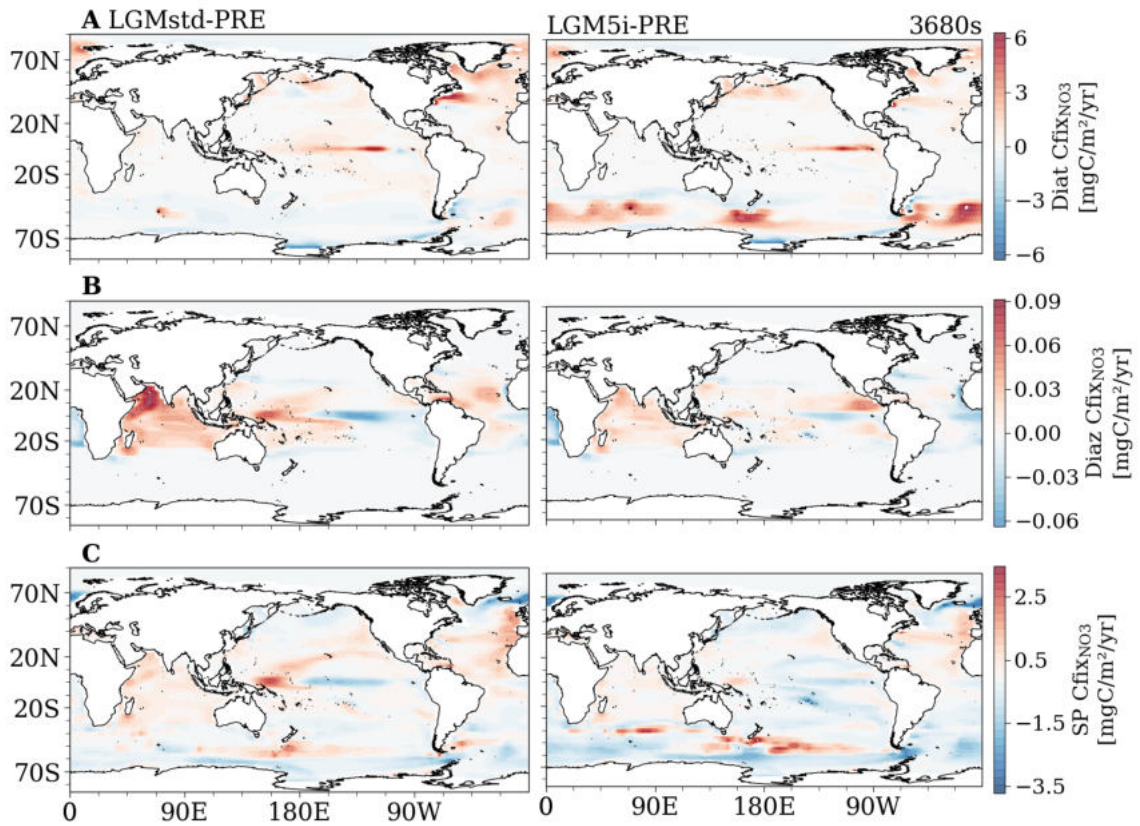


**Figure A.16:** Global map of upper ocean mean phytoplankton C fixation from  $\text{NO}_3$  ( $\text{Cfix}_{\text{NO}_3}$ ) by diatoms (Diat, row A), diazotrophs (Diaz, row B) and small phytoplankton (SP, row C). 10-year-mean over the 3680s, averaged over the upper 150 m depth. Difference of LGMstd (left) and LGM5i (right) to PRE.

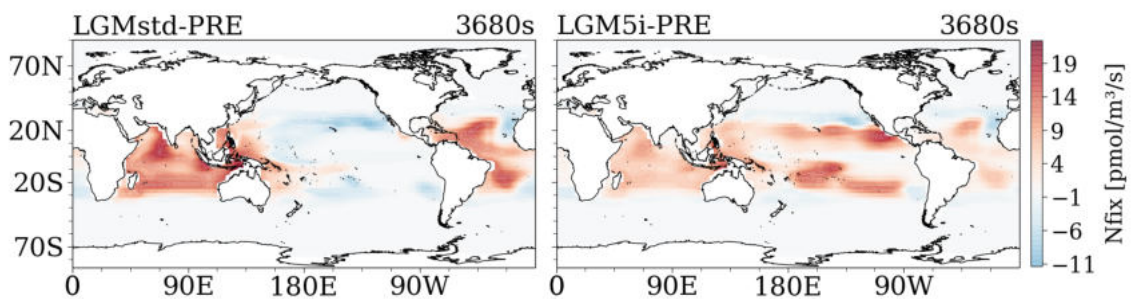


**Figure A.17:** Global map of changes in diazotrophic N fixation ( $\text{Nfix}$ ), mean over the upper 150 m depth from pre-industrial CESM simulation (PRE) to LGMstd (left) and to LGM5i (right) in 10-year-mean over the 3680s.

# Versicherung an Eides statt

Ich versichere an Eides statt, dass ich die vorliegende Arbeit im Studiengang M.Sc. Meteorologie selbstständig verfasst und keine anderen als die angegebenen Hilfsmittel – insbesondere keine im Quellenverzeichnis nicht benannten Internet-Quellen – benutzt habe. Alle Stellen, die wörtlich oder sinngemäß aus Veröffentlichungen entnommen wurden, sind als solche kenntlich gemacht. Ich versichere weiterhin, dass ich die Arbeit vorher nicht in einem anderen Prüfungsverfahren eingereicht habe und die eingereichte schriftliche Fassung der auf dem elektronischen Speichermedium entspricht. Ich bin damit einverstanden, dass die Arbeit in der Fachbibliothek ausgestellt wird.

Solingen, d. 21.12.2020  
Ort und Datum

Lara Möllney  
Unterschrift